Published in final edited form as:

*Adv Heat Transf*. 2019 ; 51: 55–129. doi:10.1016/bs.aiht.2019.08.002.

# Nanoparticle transport phenomena in confined flows

**Ravi Radhakrishnan**[a,b,*], **Samaneh Farokhirad**[b], **David M. Eckmann**[a,c], **Portonovo S. Ayyaswamy**[d,e]

[a]Department of Bioengineering, University of Pennsylvania, Philadelphia, PA, United States

[b]Department of Chemical and Biomolecular Engineering, University of Pennsylvania, Philadelphia, PA, United States

[c]Department of Anesthesiology and Critical Care, University of Pennsylvania, Philadelphia, PA, United States

[d]Department of Mechanical Engineering and Applied Mechanics, University of Pennsylvania, Philadelphia, PA, United States

[e]Mechanical and Aerospace Engineering Department, University of California, Los Angeles, CA, United States

## Abstract

Nanoparticles submerged in confined flow fields occur in several technological applications involving heat and mass transfer in nanoscale systems. Describing the transport with nanoparticles in confined flows poses additional challenges due to the coupling between the thermal effects and fluid forces. Here, we focus on the relevant literature related to Brownian motion, hydrodynamic interactions and transport associated with nanoparticles in confined flows. We review the literature on the several techniques that are based on the principles of non-equilibrium statistical mechanics and computational fluid dynamics in order to simultaneously preserve the fluctuation-dissipation relationship and the prevailing hydrodynamic correlations. Through a review of select examples, we discuss the treatments of the temporal dynamics from the colloidal scales to the molecular scales pertaining to nanoscale fluid dynamics and heat transfer. As evident from this review, there, indeed has been little progress made in regard to the accurate modeling of heat transport in nanofluids flowing in confined geometries such as tubes. Therefore the associated mechanisms with such processes remain unexplained. This review has revealed that the information available in open literature on the transport properties of nanofluids is often contradictory and confusing. It has been very difficult to draw definitive conclusions. The quality of work reported on this topic is non-uniform. A significant portion of this review pertains to the treatment of the fluid dynamic aspects of the nanoparticle transport problem. By simultaneously treating the energy transport in ways discussed in this review as related to momentum transport, the ultimate goal of understanding nanoscale heat transport in confined flows may be achieved.

*Corresponding author: rradhak@seas.upenn.edu.

## 1. Introduction

Nanoscale fluid dynamics (NFDs) is the study of the motion of nanoparticles that are suspended in an external liquid medium. The liquid medium itself may be Newtonian or non-Newtonian, static or flowing under the influence of an external pressure gradient, unbounded or confined in a tube-like vessel. In addition, there could be temperature gradients in the medium which may cause heat transport in addition to the mass transfer. The nanosize is typically in the range of 1–100 nanometer (nm).

Based on experimental observations, it is now well known that under identical external conditions, transport properties such as diffusivity, viscosity, thermal conductivity, and electrical conductivity of Nanofluids are significantly different from those of suspensions containing larger sized particles. However, how the NP dispersion in the host medium influences these properties are still being intensely debated (see Refs. [1–4]). Clearly, for a given sum total of particle volumes in a suspension, the cumulative interfacial surface area of the particles that is exposed to the fluid will be larger with smaller sized particles. Surface area dependent properties and behavior will be impacted by this feature, and this is one reason for the comparatively enhanced transport noted with nanofluids. Apart from this, there are other important reasons such as the ones related to the dynamics of the NP random motion in a static or a flowing suspension (Brownian interactions and diffusivities), and the nature of the proximity-dependent interaction of a NP with a confining boundary.

Research work worldwide is being undertaken to ascertain and provide the reasons for the observed behavior of Nanofluids and NFD. A significant motivating factor for this large interest is the immediate impact on the associated technologies. A nanofluid with enhanced thermal conductivity and hence a high heat transfer coefficient will serve to very efficiently cool a tiny computer chip, thus enabling very high processing power for the system as a whole. In a completely different context, drug (for example, an antibiotic) laden optimally functionalized, sized, and shaped NPs may successfully negotiate their way through a micron scale blood vessel and deliver the drug to the intended target such as an endothelial cell surface on inflamed tissue. The implications are profound. The targeted drug delivery in this example would very much depend on the diffusivity of the NPs in a non-Newtonian fluid (blood) flow containing red blood cells and other constituents. The principal aim of this article is to discuss the fluid dynamics aspects associated with NP suspensions whether static or flowing.

## 2. Foundations

### 2.1 Conservation equations

The study of NFD as described in this chapter is largely based on concepts from non-equilibrium statistical mechanics combined with those from continuum fluid mechanics and transport that govern NP behavior in an external viscous fluid medium. In a fluid, the molecules are in continual random thermal motion consistent with its temperature. The dynamics at this molecular level can be described based on transitions between microstates. A microstate defines the complete set of positions and momenta of all the particles/molecules of the system. For molecular systems, the microstate of the system with a given

set of positions and momenta at a given time $t$ only depends on the microstate at the immediately preceding time-step. This memory-less feature is referred to as a Markov process, and all Markov processes obey the master equation [5]. The probability to access a microstate defined by a given value of the microstate variables $\gamma$ is denoted by $P(\gamma, t)$, which for a general dynamical process at non-equilibrium, is time-dependent. Every Markov process is governed by a set of probability balance equations, collectively referred to as the master equation given by:

$$\frac{\partial P(\gamma,t)}{\partial t} = \int d\gamma' \{ w(\gamma|\gamma') P(\gamma',t) - w(\gamma'|\gamma) P(\gamma,t) \} . \quad (1)$$

Here, $\gamma$ and $\gamma'$ denote different microstates and $w(\gamma/\gamma')$ is the transition probability (which is a rate of transition in units of a frequency) from state $\gamma'$ to state $\gamma$. Macroscopic conservation equations can be derived from the master equation by taking the appropriate moment:

$$\frac{\partial}{\partial t}\left\langle \gamma \right\rangle = \int \gamma \frac{\partial P(\gamma,t)}{\partial t} d\gamma = \iint d\gamma d\gamma' (\gamma' - \gamma) w(\gamma'|\gamma) P(\gamma,t) . \quad (2)$$

Indeed, a reduced form of the master equation is the Boltzmann equation [6], where the microstates defined in terms of the positions and momenta of all particles (assumed to be hardspheres) are reduced to a one-particle (particle $j$) distribution by integrating over the remaining $n-1$ particles; here, the operator for the total derivative $d/dt$ is expressed as the operator for the partial derivative $\partial/\partial t$ plus the convection term $u \bullet \frac{\partial}{\partial r}$, where $u$ is the velocity. The moments of the Boltzmann equation were derived by Enskog for a general function $\psi_j$ [6]. Substituting $\psi_j$ as $m_j$, the mass of particle $j$ yields the continuity equation, as $m_j v_j$, the momentum of particle $j$ yields the momentum components of the Navier-Stokes equation, and as $\frac{1}{2} m_j v_j^2$, the kinetic energy of the particle, yields the energy equation, which together represent conservation equations that are the pillars of continuum hydrodynamics.

## 2.2 Thermal and Brownian effects

One of the main attributes of NFD that differentiates it from traditional hydrodynamics is that the fluid mechanics and thermal effects have to be treated with equal importance. It is worth noting that while the thermal effects and fluctuations are described within the scope of the master equation (Eq. 1), by taking the moment to derive the conservation law (Eq. 2), often the thermal effects are averaged out to produce only a mean field equation. Indeed, the continuity, momentum (Navier-Stokes), and energy equations cannot accommodate thermal fluctuations that are inherent in Brownian motion even though such effects are fully accommodated at the level of the parent master equation. Therefore, NFD must be approached differently than traditional hydrodynamics.

One approach is to start with the mean-field conservation equation such as the Boltzmann equation and add the thermal fluctuations as a random forcing term, which results in the Boltzmann-Langevin equation derived by Bixon and Zwanzig [7]. This approach amounts to

random fluctuating terms being added as random stress terms to the Navier-Stokes equations. The above procedure referred to as the fluctuating hydrodynamics (FHDs) approach was first proposed by Landau and Liftshitz [8]. In the FHD formulation, the fluid domain satisfies:

$$\nabla \cdot \mathbf{u} = 0 \tag{3}$$

$$\rho \frac{D\mathbf{u}}{Dt} = \nabla \cdot \sigma, \tag{4}$$

where, **u** and $\rho$ are the velocity and density of the fluid respectively, and $\boldsymbol{\sigma}$ is the stress tensor given by,

$$\sigma = -p\mathbf{J} + \mu\left[\nabla \mathbf{v} + (\nabla \mathbf{v})^T\right] + \mathbf{S}. \tag{5}$$

Here, $p$ is the pressure, **J** is the identity tensor, and $\mu$ is the dynamic viscosity. The random stress tensor **S** is assumed to be a Gaussian white noise that satisfies:

$$\left\langle S_{ij}(\mathbf{x}, t)\right\rangle = 0 \tag{6}$$

$$\left\langle S_{ik}(\mathbf{x}, t) S_{lm}(\mathbf{x}', t')\right\rangle = 2k_B T\mu\left(\delta_{il}\delta_{km} + \delta_{im}\delta_{kl}\right)\delta(\mathbf{x} - \mathbf{x}')\delta(t - t'), \tag{7}$$

where, $\langle \bullet \rangle$ denotes an ensemble average, $k_B$ is the Boltzmann constant, $T$ is the absolute temperature, and $\delta_{ij}$ is the Kronecker delta. The Dirac delta functions $\delta(\mathbf{x} - \mathbf{x}')$ and $\delta(t - t')$ denote that the components of the random stress tensor are spatially and temporally uncorrelated. The mean and variance of the random stress tensor of the fluid are chosen to be consistent with the fluctuation-dissipation theorem and it is symmetric [9]. By including this stochastic stress tensor due to the thermal fluctuations in the governing equations, the macroscopic hydrodynamic theory is generalized to include the relevant physics of the mesoscopic scales ranging from tens of nanometers to a few microns.

An alternative approach to NFD (and one that is different from FHD) is to start with a form of the master equation referred to as the Fokker-Planck equation. Formally, the Fokker-Planck equation is derived from the master equation by expanding $w(\gamma'|\gamma)P(\gamma, t)$ as a Taylor series in powers of $r = \gamma' - \gamma$. The infinite series is referred to as the Kramers-Moyal expansion, while the series truncated up to the second derivative term is known as the Fokker-Planck or the diffusion equation, which is given by Ref. [5]:

$$\frac{\partial P(\gamma, t)}{\partial t} = -\frac{\partial}{\partial \gamma}\left\{a_1(\gamma)P\right\} + \frac{\partial^2}{\partial \gamma^2}\left\{a_2(\gamma)P\right\}. \tag{8}$$

Here, $a_n(\gamma) = \int r^n w dr$. The solution to the Fokker-Planck equation yields the probability distribution of particles which contains the information on Brownian effects. At equilibrium (i.e., when all the time-dependence vanishes), the solution can be required to conform to the solutions from equilibrium statistical mechanics. This approach leads to a class of identities

for transport coefficients, including the famous Stokes-Einstein diffusivity for particles undergoing Brownian motion to be discussed later in this article. Furthermore, there is a one-to-one correspondence between the Fokker-Planck equation and a stochastic differential equation (SDE) that describes the trajectory of a Brownian particle. The generalized Fokker-Planck equation is written in terms of a generalized order parameter $S$, given by:

$$\frac{\partial P(S,t)}{\partial t} = \frac{D}{k_B T}\frac{\partial}{\partial S}\left\{P\frac{\partial F(S)}{\partial S}\right\} + D\frac{\partial^2 P}{\partial S^2}, \tag{9}$$

where, $F(S)$ is the free energy density (also referred to as the Landau free energy) along $S$ [10], $D$ is the diffusion coefficient along $S$ which is also related to the $a_n$'s of the original Fokker-Planck equation, i.e., $a_2 = 2D$. The quantity $k_B T$ which has the units of energy is called the Boltzmann factor and serves as a scale factor for normalizing energy values in NFD. Corresponding to every generalized Fokker-Planck equation (Eq. 9), there exists a SDE given by:

$$\frac{\partial S}{\partial t} = -\frac{D}{k_B T}\frac{\partial F(S)}{\partial S} + \sqrt{2D}\xi(t), \tag{10}$$

where, $\xi(t)$ represents a unit-normalized white noise process. The SDE encodes for the Brownian dynamics (BDs) of the particle in the limit of zero inertia. The corresponding equation when the inertia of the particle is added is often referred to as the Langevin equation. In summary, Brownian or thermal effects are described within the hydrodynamics framework either using the FHD approach or the BD/Langevin equation approach.

### 2.3 Multiphase NFD: stochastic dynamics of NP; preliminary concepts

Thus far, our discussion of NFD has been general and applicable mostly to single phase flows such as pure-fluids or dispersion of a miscible dye in a single phase. However, the case of a nanoparticle suspended in a fluid medium creating a moving interface as the particle experiences Brownian motion is of much interest. We will discuss the general framework for describing its dynamics as well as the equilibrium properties of such a system.

A NP experiencing random motion in a fluid is influenced by hydrodynamic interactions. The fluid around the particle is dragged in the direction of motion of the particle. On the other hand, the motion of the particle is resisted by viscous forces arising due to its motion relative to the surrounding fluid. In this context, it is helpful to recall the results for the motion of a sphere in steady Stokes flow ($Re \leq O(1)$, with $Re$ based on the radius of the particle). For a sphere, the Stokes law for drag force, $f_D = 6\pi\mu Ua$, where $f_D$ is the drag force on a sphere in steady Stokes flow, $a$ is the radius of sphere, $\mu$ is the dynamic viscosity of the fluid, and $U$ is the translational speed of the sphere in the direction of its motion, is frequently invoked. The quantity, $\zeta^{(t)} = 6\pi\mu a$, separately, is called the Stokes dissipative friction force coefficient for a spherical NP or simply the friction force coefficient. Similarly, a rotational friction coefficient, $\zeta^{(r)} = 8\pi\mu a^3$, defined for a rotating sphere (see, [11]) is used in the context of describing NP rotation. However, there is a basic difference between a particle in steady Stokes flow and a NP in Brownian motion. With a NP, the momentum of the fluid surrounding the particle at any instant is related to its history. This memory can be

understood in light of the linear response theory which is the foundation of non-equilibrium thermodynamics. A system at equilibrium evolving under a Hamiltonian $\mathscr{H}$ experiences a perturbation $\mathbf{\Delta}\mathscr{H} = fA$, where $f$ is the field variable (such as an external force), and $A$ is the extensive variable (such as the displacement) that is conjugate to the field. The perturbation throws the system into a non-equilibrium state, and when the field is switched off, the system relaxes back to equilibrium in accordance with the regression process as described by Onsager [12–14]:

$$\mathbf{\Delta}\bar{A}(t) = \left(f/k_B T\right)\left\langle \mathbf{\Delta}A(0)\mathbf{\Delta}A(t)\right\rangle, \tag{11}$$

where, $\mathbf{\Delta}A(t) = A(t) - \langle A\rangle$. The above identity holds under linear response, when $\mathbf{\Delta}\mathscr{H}$ is small, or equivalently, when $\mathbf{\Delta}A(t, \lambda f) = \lambda\mathbf{\Delta}A(t, f)$. The most general form to relate the response $A$ to the field $f$ under the linear response is given by:

$$\mathbf{\Delta}\bar{A}(t) = \int_{-\infty}^{\infty} \chi(t - t')f(t')dt' . \tag{12}$$

Here, we have further assumed that physical processes are stationary in the sense that they do not depend on the absolute time but only the time elapsed, i.e., $\chi(t, t') = \chi(t - t')$. One can use the linear-response relationship to derive an equation for the dynamics of NP interacting with a thermal reservoir of fluid (also called a thermal bath). The dynamics of the particle (in one-dimension along the $x$-coordinate for simplicity of illustration) is given by $m\frac{dU}{dt} = -\frac{dV(x)}{dx} + f$, where $V(x)$ is the potential energy function and $f$ is an external driving force including random Brownian forces from the solvent degrees of freedom. The thermal bath will experience forces $f_r$ in the absence of the particle, and when the particle is introduced, the perturbation will change the bath forces to $f$. This change $f - f_r$ can be described under linear response as:

$$\mathbf{\Delta}\bar{f}(t) = f - f_r = \int_{-\infty}^{\infty} dt' \chi_b(t - t')x(t') . \tag{13}$$

Using this relationship, and by performing integration by parts, the dynamics of the particle may be written as:

$$m\frac{dU}{dt} = -\frac{dV(x)}{dx} + f_r - \int_{-\infty}^{t} dt'\zeta_b(t - t')U(t') . \tag{14}$$

Here $f_r$ is the random force from the bath that is memoryless, U = dx/dt, and $\chi = -\mathrm{d}\zeta/\mathrm{dt}$. This form of the equation for the dynamics of the NP is referred to as the generalized Langevin equation, and it accounts for the memory/history forces. We note that while the parent equation (i.e., the master equation) is Markovian, the memory emerges as we coarse-grain the timescales to represent the fluid-particle interaction and is a consequence of the second law of thermodynamics. The strength of the random force that drives the fluctuations

in the velocity of a NP is fundamentally related to the coefficient representing the dissipation or friction present in the surrounding viscous fluid. This is the fluctuation-dissipation theorem [15]. The friction coefficient, $\zeta$, associated with NP motion is time-dependent (see Eq. 14) and is no longer given by the constant Stokes value. In any description of NP motion, therefore, the mean and the variance of the thermal fluctuations have to be chosen to be consistent with the fluctuation-dissipation theorem. In order to achieve thermal equilibrium, the correlations between the state variables should be such that there is an energy balance between the thermal forcing and the dissipation of the system as required by the fluctuation-dissipation theorem [15,16].

### 2.4 Equilibrium and transport properties

According to equilibrium statistical mechanics, in a uniform temperature fluid, the molecular velocities will be Maxwellian, and the energy components related to the various degrees of freedom will satisfy the equipartition principle. Indeed, the solutions to the Fokker-Planck equation written for the velocity variable at steady state yields the Maxwell-Boltzmann distribution consistent with the picture from equilibrium statistical mechanics. If a NP is introduced into the fluid medium, it will experience molecular collisions and the associated fluctuating impulses. As a net result, the fluctuating NP will randomly translate in the fluid while experiencing rotation. If the bulk fluid is driven by an external pressure gradient, the random translational and rotational motions will still be significant at very low Reynolds numbers, $Re$ (say, $Re$ based on the vessel diameter). In NFD, most of the quantities associated with the fluid and the NP are evaluated by ensemble averaging as noted and defined earlier. In a numerical simulation, this ensemble average is obtained by averaging over successive configurations that are generated in the process of simulation. Customarily implicit to this averaging is the Ergodic assumption that an ensemble average of a property of a system over many replicas is the same as an average taken over a long enough time of one particular replica of the system that is being numerically simulated. If the NP and the surrounding fluid are in thermal equilibrium, just as for the fluid molecules, the velocity components of the NP will also be Maxwellian and the NP energy components related to the various degrees of freedom will also satisfy the equipartition principle. Thus, the equilibrium probability density function (PDF) of each of the cartesian components of the velocity of the NP, $U_i$, will follow the Maxwell-Boltzmann (MB) distribution,

$$P(U_i) = \sqrt{\left(\frac{m}{2\pi k_B T}\right)} \exp\left\{-\frac{mU_i^2}{2k_B T}\right\}, \tag{15}$$

where, $m$ is the NP mass, and the equilibrium statistics of the three components $U_i$ along the three coordinate directions are independent of each other; note we denote the velocity of the fluid using $v$ and that of the NP using $U$. In thermal equilibrium, the mean (or the average) value of $U_i$ is,

$$\langle U_i \rangle = 0. \tag{16}$$

Moreover, the mean squared value is,

$$\left\langle U_i^2 \right\rangle = \frac{k_B T}{m}. \tag{17}$$

From the equipartition theorem, at thermal equilibrium, the translational and rotational temperatures of the NP are given by:

$$T^{(t)} = \frac{m\left\langle \mathbf{U}^2 \right\rangle}{3k_B}; \quad T^{(r)} = \frac{\mathbf{I}\left\langle \boldsymbol{\omega}^2 \right\rangle}{3k_B}, \tag{18}$$

where, **U** and $\boldsymbol{\omega}$ are the translational and angular velocities of the NP, and **I** is its moment of inertia.

Another important application of the Onsager regression relationship (Eq. 11) is the emergence of a class of relationships that relate transport properties to correlation functions that are known as the Green-Kubo relationships [14,17]. These relationships are also a consequence of the fluctuation-dissipation theorem.

The mathematical formulation of this fluctuation-dissipation theorem is an equation for the coefficient of a transport process in terms of the Fourier component of time dependent fluctuations of the dynamical variables at the microscopic scale. Thus,

$$\gamma = \frac{1}{3}\int_0^\infty dt \left\langle \mathrm{A}(0) \right\rangle \bullet \left\langle \mathrm{A}(t) \right\rangle. \tag{19}$$

Here, $\gamma$ is the transport coefficient of interest, $t$ is time, A is the current that drives it, and the integrand of Eq. (19) is the autocorrelation function (ACF) of quantity A. As dynamic properties, one can determine the transport coefficients such as diffusion ($D$), shear viscosity ($\eta_s$) and thermal conductivity ($k$) using the Green-Kubo formula.

Diffusion as a mass transport mechanism has been the subject of numerous theoretical, experimental, and computer simulation studies. The Green-Kubo formula for the self-diffusion coefficient is expressed in terms of the individual molecular velocity autocorrelation function (VACF):

$$D = \frac{1}{3N}\int_0^\infty dt \left\langle \mathbf{U}(0) \right\rangle \left\langle \mathbf{U}(t) \right\rangle. \tag{20}$$

Here, **U** is the center of mass velocity vector of NP and the integrand of Eq. (20) is called the VACF. The self-diffusion coefficient in Eq. (20) is obtained with high statistical accuracy by time averaging over all $N$ molecules.

The Green-Kubo relations for other Navier-Stokes transport coefficients including thermal conductivity and shear viscosity are derived in a similar manner. The thermal conductivity in the Green-Kubo method is predicted using the equilibrium fluctuations of the heat current

vector (**J**). For a cubically isotropic material, the diagonal elements of the thermal conductivity are given by:

$$k = \frac{1}{3k_B T^2 \Omega} \int_0^\infty dt \left\langle \mathbf{J}(0) \right\rangle \left\langle \mathbf{J}(t) \right\rangle. \tag{21}$$

Here, $\Omega$ and $T$ are the system volume and temperature, respectively, and $\langle \mathbf{J}(0) \rangle \langle \mathbf{J}(t) \rangle$ is the heat current autocorrelation function (HCACF). The heat current vector characterizes the change with time of the spatial average of the local energy and was derived by Hardy [18]:

$$\mathrm{J} = \frac{1}{\Omega} \sum_i \left\{ \frac{\mathbf{p}_i}{m_i} \left( \frac{p_i^2}{2m_i} + V_i \right) + \sum_i \sum_j \left( \frac{\partial V_{ij}}{\partial \mathbf{r}_i} \bullet \mathbf{U}_i \right) \mathbf{r}_{ij} \right\}, \tag{22}$$

where **p** is the momentum, **r** the position, $m$ the mass, $V$ the potential energy, and summation is over particles denoted by $i$.

The application of Green-Kubo relations allows one to extract the shear viscosity by integration of the stress (pressure) autocorrelation function (SACF) [19]:

$$\eta_{\mathbf{s}} = \frac{\Omega}{3k_B T} \int_0^\infty dt \left\langle \mathbf{S}_{xy}(t) \mathbf{S}_{xy}(0) \right\rangle, \tag{23}$$

where $\mathbf{S}_{xy}$ refers to the off-diagonal elements of the stress tensor defined by:

$$\mathbf{S}_{xy}(t) = \sum_i \left\{ m_i U_{ix} U_{iy} - \frac{1}{2} \sum_{j \neq i} \frac{x_{ij} y_{ij}}{\mathbf{r}_{ij}} \frac{\partial \mathbf{\Phi}(\mathbf{r}_{ij})}{\partial \mathbf{r}_{ij}} \right\}, \tag{24}$$

where, $i$ and $j$ denote different particles, $\mathbf{r}_{ij} = |\mathbf{r}_i - \mathbf{r}_j|$, $\mathbf{r}_i = (x_i, y_i)$ is the position of particle $i$, and $\mathbf{\Phi}(\mathbf{r}_{ij})$ is the interparticle potential energy. It must be noted that the positions and velocities of particles vary with time accounting for the time dependence of $\mathbf{S}_{xy}$.

The bulk viscosity (i.e., $\eta_v$) is similarly calculated by just replacing the integrand of above equation with $\langle \delta S(t) \delta S(0) \rangle$, where $\delta S(t) = S(t) - \langle S(t) \rangle$ with $S(t)$ as the instantaneous pressure of the system at time $t$ and $\langle S(t) \rangle$ as the average pressure [20].

## 3. Computational methods and implementation

### 3.1 The fluctuating hydrodynamics method

Simulating suspensions of submicron-sized particles or polymers while including short-range particle-particle interaction, thermal fluctuation and many-body hydrodynamic interactions (HIs) is a challenging task. Over the past decades, numerical simulations of the fluctuating hydrodynamics approach have been carried out employing the finite volume method [21,22], lattice Boltzmann method (LBM) [23–29] and stochastic immersed boundary method [30]. A coarse-graining methodology has been developed to bridge molecular dynamics and fluctuating hydrodynamic simulations [31,32]. Serrano and Español

[33] and Serrano et al. [34] have solved the fluctuating hydrodynamic Navier-Stokes equations without a particle using the finite volume Lagrangian discretization in a moving Voronoi grid. They have ensured that their discretized governing equations cast in the GENERIC (General Equation for Non-Equilibrium Reversible/Irreversible Coupling) formalism [35,36] satisfies the fluctuation-dissipation theorem. The GENERIC formalism proposed by Grmela and Öttinger [35] and Öttinger and Grmela [36] ensures the correct treatment of thermal fluctuations and fluctuating hydrodynamics. Following the idea of coupling fluctuating particles dynamics with nonfluctuating hydrodynamics, Mynam et al. [37] and Liu et al. [38] developed a coupled lattice Boltzmann/Lange-vin dynamics (LB-LDs) approach to simulate nanoscale particle and polymer (NPP) suspensions in the presence of both thermal fluctuation and many-body HI. The Brownian motion of the NPP is explicitly captured by a stochastic forcing term in the LD method. The LD method is two-way coupled to the non-fluctuating LB fluid through a discrete LB forcing source distribution to capture the long-range HI. A Eulerian-host algorithm was also developed to handle the short-range pairwise particle search and interaction, which ensures localization and hence linear scalability of the method while performing particle neighbor search. Patankar has simulated the thermal motion of two-dimensional particles in a stationary medium with the Finite Element Method (FEM) [26]. Sharma and Patankar [21] have employed a distributed-Lagrangian multiplier (DLM) based finite volume method to simulate the thermal motion of particles. The computational domain is periodic in all directions, and the thermal fluctuations are included in the fluid equations using random stress tensor. They have validated the numerical results by comparison with analytical expressions. Nie and Lin [29] have employed the fluctuating LBM to simulate Brownian motion of particles and have validated their numerically obtained velocity autocorrelation function (VACF) by comparison with theoretical predictions. It is shown that the temperature characterizing the translational motion of the particle in three coordinate directions agree with each other after a lapse of time, but the predicted particle temperature is 15% lower than the effective temperature of the fluid fluctuations. This observation is in accord with the earlier findings of Ladd [25], who first proposed the use of fluctuating LBM. Adhikari et al. [27] have established agreement between fluctuation and dissipation by introducing ghost noise to the fluctuating LBM in the formulation (see Dünweg and Ladd [28] for further discussions of [27]).

As depicted in Fig. 1, computational techniques that can be used to determine the flow and heat transfer characteristics in nanofluid flows maybe classified under three main categories, namely: continuum or grid-based models, particle-based mesoscopic models and particle-based microscopic models.

### 3.2 Continuum models based on finite elements

In this section, we discuss the direct numerical simulations (DNSs) based on the arbitrary Lagrangian-Eulerian (ALE) finite element method [39–42] to accurately resolve the fluid-particle interfacial motions. An ALE technique can be used to handle the movement of the particle in the fluid domain, see Ref. [40]. Both translational and rotational motions of a nanoparticle in a (i) stationary fluid medium, and (ii) Poiseuille flow have been investigated. An unstructured finite element mesh, generated by the Delaunay-Voronoi method [43], has

enabled a significantly higher number of mesh points in the regions of interest (i.e., close to the particle and wall surfaces compared to the regions farther away). This feature also keeps the overall mesh-size computationally reasonable even with a nanoparticle moving in a very large domain [39,40,44–46]. Thermal fluctuations are included in the equations of linearized hydrodynamics by adding stochastic components to the stress tensor as white noise in space and time as prescribed by the FHD method [11,47]. As noted in Español et al. [47], "even though the original equations of fluctuating hydrodynamics are written in terms of stochastic partial differential equations, at a very fundamental level the inclusion of thermal fluctuations always requires the notion of a 'mesoscopic cell' in order to define the fluctuating quantities". In Español et al. [47], it is shown that fluctuating hydrodynamic equations discretized in terms of finite element shape functions based on the Delaunay triangulation satisfy the fluctuation-dissipation theorem. The numerical schemes for the implementation of thermal fluctuations in the Landau-Lifshitz Navier-Stokes equations are expected to perform very delicate tasks [48,49], and obtaining accurate numerical results is a challenging endeavor.

### 3.3 The lattice Boltzmann method

While the vast application of LBM in simulating heat and mass transfer in fluids, particularly in complex geometries and with multicomponents, have been demonstrated by previous researchers [24,25,50–53], the LBM has only been used recently to investigate the transport of heat in nanofluids [54–63]. The primary goal of this approach is to incorporate the microscopic physical interactions of the fluid particles in the numerical simulation and reveal the mesoscale mechanism of hydrodynamics. The LBM uses the density distribution functions $f(\mathbf{x}, \xi, t)$ to represent a collection of particles with the microscopic velocity $\xi$ at the position $\mathbf{x}$ and time $t$, and model the propagation and collision of particle distribution taking the Boltzmann equations for flow and temperature fields into consideration. The LBM solves the discretized Boltzmann equation in velocity space through the propagation of the particle distribution functions $f(\mathbf{x}, t)$ along the discrete lattice velocities $\mathbf{e}_i$ and the collision operation of the local distributions to be relaxed to the equilibrium distribution $f_i^0$. The collision term is usually simplified to the single-relaxation-time Bhatnagar-Gross-Krook collision operator [64], while the more generalized multi-relaxation-time collision operator [65] can be also adopted to gain numerical stability. The evolution equation for a set of particle distribution function with a single relaxation time is defined as:

$$f_i(\mathbf{x} - \mathbf{\Delta x}, t + \mathbf{\Delta} t) = f_i(\mathbf{x}, t) - \frac{\mathbf{\Delta} t}{\tau}\left[f_i(\mathbf{x}, t) - f_i^0(\mathbf{x}, t)\right] + \mathbf{F}_s, \tag{25}$$

where $\mathbf{\Delta} t$ is the time step, $\mathbf{\Delta x} = \mathbf{\Delta} t\mathbf{e}_i$ is the unit lattice distance, and $\tau$ is the single relaxation time scale associated with the rate of relaxation to the local equilibrium, and $\mathbf{F}_s$ is a forcing source term introduced to account for the discrete external force effect. The macroscopic variables such as density and velocity are then obtained by taking moments of the distribution function, i.e., $\sum_i f_i^{eq}$ and $\rho\mathbf{u} = \sum_i \mathbf{e}_i f_i^{eq}$. As explained earlier, through averaging the mass and momentum variables in the discrete Boltzmann equation, the continuity and Navier-Stokes equations may be recovered. Simulation of nanofluid flow behavior using the LBM requires the analysis of the dynamic properties at the mesoscale due to several forces

acting on the nanoparticles. Xuan and coworkers were among the first who predicted the flow characteristics of nanofluids using LBM [54–56]. The distribution of the suspended nanoparticles is determined by a series of applied external forces and potentials, and conclude that the dominant factor for the aggregation or random displacement of nanoparticles is the strength of the Brownian force. They have also demonstrated that the nanoparticle distribution will be influenced by rising temperature and the bulk flow of the fluid. Summaries of research studies that have been conducted on the use of LBM to investigate the convective heat transfer as well as thermal and hydrodynamic behavior of nanofluids are provided in Refs. [59,60].

### 3.4 Particle-based mesoscopic models

As stated earlier, a simple continuum description based on the Navier-Stokes equation is not sufficient to study nanofluid flows, since microscopic-level details including thermal fluctuations play an essential role in demonstrating the dynamic behavior. One example of such a system is the presence of flexible polymers in a solution where thermal fluctuations, i.e., configurational entropy, play a key role in the coil state and the stretching elasticity of the polymer [66]. On the other hand, there exist too many microscopic degrees of freedom in atomic simulations which require very small time-steps to resolve the high-frequency modes. As a result, it is virtually impossible to study the long-time behavior such as self-assembly and other mesoscale phenomena using purely continuum descriptions. Development of mesoscale simulation methods overcomes these difficulties, and the most common coarse-grained models used to simulate the nanofluid flows are Brownian dynamics (BDs) and multi-particle collision dynamics (MPCDs) methods. The general approach used in all these methods is to average out relatively insignificant microscopic details in order to obtain reasonable computational efficiency while preserving the essential microscopic-level details.

### 3.5 Brownian dynamics simulations

The physical system of nanofluids contains relatively small solvent molecules and relatively larger nanoparticles which move much more slowly due to their larger size. A large range of time scales, from short time steps for the fast motion to very long runs for the evolution of the slower mode, needs to be accommodated by any simulation method as applied to nanofluids, making the process time-consuming. However, in the BD simulation technique, explicit solvent molecules are replaced by a stochastic force and the hydrodynamic forces mediated by them are accounted for through a hydrodynamic interaction kernel. Newton's equations of motion are thus replaced by the Langevin equation in the absence of inertia:

$$r_i = r_i^0 + \sum_j \frac{D_{ij}^0 F_j^0}{k_B T} \Delta t + R_i(\Delta t), \tag{26}$$

where the superscript 0 denotes the value of the variable at the beginning of the time step, $r_i$ is the position of the $i$th nanoparticle, $D_{ij}$ is the diffusion tensor, and $F_j$ refers to the force acting to the $j$th nanoparticle. The displacement $R_i$ is the unconstrained Brownian displacement with a white noise having an average value of zero and a covariance of

$2D_{ij}^{0}\delta(t)$. The Rotne-Prager-Yamakawa hydrodynamic mobility tensor [67,68] is the suggested diffusion tensor to approximate the hydrodynamic interactions mediated by the fluid. The trajectories and interactions between the coarse-grained molecules are calculated using the stochastic differential equation (Eq. 26) which is integrated forward in time, allowing for the study of the temporal evolution and the dynamics of complex fluids, such as polymers [69–71] and colloids.

### 3.6 Multi-particle collision dynamics

Multi-particle collision dynamics (MPCDs) which was introduced by Malevanets and Kapral [72,73] is a novel algorithm that can model both hydrodynamic interactions and Brownian motion with relatively low computational costs [66,74]. The algorithm consists of discrete streaming and collision steps at fixed discrete time intervals that have been shown to yield the correct long-time hydrodynamics [66]. The effects of Brownian motion and hydrodynamic interactions are incorporated into the simulation through the collision step, and the solvent is characterized by a large number $N$ of point-like particles with a given mass $m$ that move in space with a continuous distribution of velocities [75]. The hydrodynamic interactions may be easily switched off while retaining the thermal fluctuations and friction coefficients in the algorithm to reveal the importance of hydrodynamic interactions [76,77]. The positions of the solvent particles $\mathbf{r}_i(t)$ are then updated in the streaming steps, and their velocities $\mathbf{v}_i(t)$ are obtained through multi-particle collisions in the collision steps:

$$\mathbf{r}_i(t+\Delta t) = \mathbf{r}_i(t) + \Delta t \mathbf{v}_i(t) \tag{27}$$

$$\mathbf{v}_i(t+\Delta t) = \mathbf{u}(t) + \mathbf{R} \bullet \delta \mathbf{v}_i(t)\,. \tag{28}$$

The stochastic rotational dynamics (SRDs) is one of the most widely used MPCD algorithm in which the collision step consists of a random rotation $\mathbf{R}$ of the relative velocities of the particles, i.e., $\delta\mathbf{v}_i(t) = \mathbf{v}_i - \mathbf{u}$, in a collision cell, where $\mathbf{u}$ is the mean velocity of all particles in a cell. The MPCD algorithm has been widely used by researchers to simulate various systems [66] including flexible and rod-like polymers [78,79], star polymers [75,77,80], vesicles [81,82], flow in microchannels [83], as well as suspensions of various shapes of particles [84]. In the most widely used version of MPCD, SRD is coupled with the molecular dynamics simulation to simulate complicated flow problems [66,75,77–83]. Gompper et al. [66] provided a review of several widely used MPC algorithms and recent applications of MPC algorithm to study colloid and polymer dynamics as well as the behavior of vesicles and cells in hydrodynamic flow environments.

### 3.7 Microscopic models: molecular dynamics simulations

Molecular dynamics simulation is one of the most commonly used technique to model systems of biomolecules and biomaterials because it can track individual atoms and therefore, answer questions pertaining to specific material properties [85,86]. The starting point for a MD simulation is defining the initial coordinates and initial velocities of the

atoms characterizing the model system, e.g., the desired biomolecule plus the biologically relevant environment; i.e., water molecules or other solvent and/or membranes. The coordinates of the desired biomolecule can usually be found as structural data (X-ray or NMR) deposited into the protein data bank (PDB) [87]; otherwise, it is possible to derive initial geometry and coordinate data from model building techniques, including homology methods [88]. This step also typically includes the placement and positioning of the environment of the molecules (solvation, ionic strength, etc.). The initial velocities are typically derived from the Maxwell-Boltzmann distributions at the desired temperature of the simulation. The potentials of interactions of each of the atoms are calculated using a force field, which parameterizes the non-bonded and bonded interaction terms of each atom depending on its constituent atom connectivity: bond terms, angle terms, dihedral terms, improper dihedral terms, non-bonded Lennard-Jones terms, and electrostatic terms. The potential interactions are summed across all the atoms contained in the system, to compute an overall potential energy function for the system [89–93], as in:

$$\begin{aligned} V(\mathbf{R}) = & \sum_{bonds} K_b(b-b_0)^2 + \sum_{angles} K_\theta(\theta-\theta_0)^2 + \sum_{dihedral} K_\chi(1+\cos(\eta\chi-\delta)) \\ & + \sum_{impropers} K_\phi(\phi-\phi_0)^2 + \sum_{nonbonded}\left(\varepsilon_{ij}\left[\left(\frac{R_{min,ij}}{r_{ij}}\right)^{12} + \left(\frac{R_{min,ij}}{r_{ij}}\right)^{6}\right]\right) \\ & + \frac{q_i q_j}{\varepsilon r_{ij}}, \end{aligned} \tag{29}$$

Taking the derivative of the potential energy function yields the force, and from Newton's second law, this is equal to mass times acceleration. Although, the process seems simple, the derivative function results in a set of 3N-coupled second order ordinary differential equations that must be solved numerically. The solution procedure consists of a numerical recipe to advance the positions and the velocities by one timestep. This process is repeated over and over again to generate MD trajectories of constant energy. Constant temperature dynamics are derived by coupling the system to a thermostat using well established formulations such as the Langevin dynamics or the Nose-Hoover methodologies [94]. Application of MD simulations to biomolecules is facilitated by several popular choices of force fields such as CHARMM27 [95], AMBER [96], and GROMOS [97], as well as dynamic simulations packages and visualization/analysis tools such as NAMD [98] and VMD [99].

## 4. Illustrative examples of nanofluid studies and select applications

In regard to the great interest in recent times to pursue nanofluid research, as obtained from the Scopus database for the past few years, the number of publications in the nanofluids have, indeed, increased dramatically as seen in Fig. 2.

Considerable efforts on a worldwide basis are being undertaken to understand how and why a suspension of nanoscale particles with an average size of 100 nm into conventional heat transfer fluids, can have a substantial impact on the efficiency of the heat transfer process and hence on the associated technologies ranging from engineering [100–102], medical

applications [103,104], and many other applications [105]. As an engineering application, successful incorporation of nanofluids can support the current trend toward component miniaturization in electronics and microelectromechanical systems by enabling the design of smaller and lighter heat exchanger systems. As a biomedical application, non-deformable and deformable NPs in body fluids can be used as drug delivery vehicles providing new early/correct treatment techniques [106–109].

Maxwell appears to be among the first to propose the idea of dispersing solids in fluids and through his theoretical work demonstrates the conductivity effectiveness of heterogeneous solid suspensions [110]. Other researchers [111–113] have employed similar ideas for suspensions of μm and mm sized particles in a fluid. However, such large particles settle rapidly and cause clogging, erosion, and require a large pressure drop for transport [114]. Nanofluids have shown a promise to overcome such difficulties due to the small particle sizes which will not block the flow passages making them suitable for use in transport equipment. The most commonly investigated types of nanoparticles are made of metals, metal oxides and carbon nanotubes while the most common base fluids are water and ethylene glycol [114]. Thermal conductivities of different organic materials, heat transfer fluids, metals, and metal oxides are provided in Fig. 3 [115]. For illustration, we note that the thermal conductivity of Copper at room temperature is 700 and 1500 times higher than that of water and ethylene glycol, respectively. It is therefore expected that the thermal conductivity of a nanofluid is enhanced due to the dispersing of metallic nanoparticles in the fluid.

### 4.1 Thermal conductivity in nanofluids

The unique feature of a nanofluid exhibiting increased thermal conductivity requires thorough investigations of the mechanisms behind the associated enhanced energy transport. In this context, significant experimental and theoretical researches have been conducted in quantifying the physical-thermal properties such as viscosity and thermal conductivity which have essential roles in improving the heat transfer efficiency and such other aspects.

Classical theories such as those of Maxwell [110] and Hamilton and Crosser [116] fail to account for the high thermal conductivity enhancement noted in nanofluids. This led to the suggestion that the thermal conductivity enhancement may be dependent on the particle volume fraction and the shape [117–120]. The current literature shows that the enhancement in the thermal conductivity of a nanofluid is not entirely due to the aforementioned parameters but also to such other parameters as temperature [121–132], particle size [119,120,124,127,129,133–141], pH [142], and the type of base fluid [143]. A large number of researchers attribute the enhancement in thermal conductivity to a number of mechanisms that include the Brownian motion of nanoparticles [144–149], layering of liquid molecules at the liquid-solid interface [144,150–154], Brownian motion of nanoparticles induced micro convection in the base fluid [147,155–164], and nanoparticle clustering [144,145,165–169]. Other mechanisms proposed by the researchers include the ballistic nature of heat transport in nano-structures [144] and thermal interaction between nanoparticle and base fluid molecules [157].

Although experiments have revealed that nanofluids have enhanced heat transfer characteristics [111,113,117,118,121–123,126,133,146,159,165,168,170–179], the reported data on the effects of specific parameters such as particle size, shape, aggregation, volume fraction, system temperature, and the choice of dispersant to stabilize the suspension demonstrate a lot of scatter on the extent of heat transfer enhancement with no clear consensus arising from these many studies. The primary reason for the scattered and conflicting data on thermal conductivity appears to be the poor characterization of the nanofluids in many of these studies. These include the method of preparation, difficulties in producing a mono-dispersed suspension of nanoparticles, noting the extent of experimental conditions, precision in the measurements of particle size and distribution, as well as prevailing nanoparticle clustering. Nanofluids are usually prepared by a one-step process where the synthesis and dispersion of nanoparticles are done at the same time or by two-step process where nanoparticles are first synthesized in dry powder form and then mixed with the base fluid. Different methods of preparation of nanofluids especially the two-step process, which is not stable but is most often preferred by the researchers due to its low setup cost, may cause a discrepancy in the stability of the suspension. The exact particle size and distribution and aggregation in the suspension are often disregarded in the real test sample, and many experiments are performed and reported based on the average size of the particles provided by the manufacturer. Although some of the experiments have provided invaluable data, it is now abundantly clear that carefully developed and detailed models to explain the various mechanisms at play are badly needed.

Statistical mechanics provides an effective way to establish the relationship between solid and liquid states occurring at the nanoscale, and the macroscale transport properties. Molecular dynamics (MDs) simulations can predict the static and dynamic properties of solids and liquids and have been employed by several researchers to complement the gap between the experimental and theoretical understanding of thermal transport mechanisms at the nanoscale. With molecular dynamics simulations, one may compute the transport coefficients using the Green-Kubo relationship based on computing the appropriate time correlation functions [180–182].

Keblinski et al. [144] have performed MD simulations to calculate the thermal conductivity of a simple model of the liquid and solid by employing the Green-Kubo relationship. They consider a single NP, 2 nm in diameter, and 10% volume fraction surrounded by fluid molecules in a cubic box, 3.5 nm in length. They have demonstrated that the HCACF in the fluid and particle decay monotonically and in an oscillatory manner, respectively, and observe that the effect of collisions between NPs due to Brownian motion is not significant since the ratio of thermal diffusion to Brownian motion is much larger. They have stated that the Brownian motion might promote cluster formation and this may serve to improve the thermal conductivity of nanofluids.

Sarkar et al. [183] carried out MD simulations and utilized the Green-Kubo relationships for a system of 2 nm copper (Cu) NP in argon (Ar) fluid to calculate the thermal conductivity of the nanofluid and have also investigated the influence of system size on the transport properties. They state that the results are in good agreement with the experimental values for pure argon when the number of atoms considered is larger than 500, and for nanofluid when

the number is larger than 1,372. In the experimental observation of [184], two regimes of conductivity enhancement have been noted as a function of volume fractions. At small volume fractions ($\phi$), i.e., $\phi = 8\%$, the thermal conductivity of the nanofluid increased by 52% which is significantly higher than that predicted by the Maxwell model (26%) and the noted increase was attributed to Brownian effects, while a saturation behavior was observed at larger $\phi$. Bhattacharya et al. [185] have carried out Brownian dynamics simulations coupled with a trajectory analysis using the Green-Kubo relationship and found good agreement with the experimental predictions for the effective thermal conductivity of nanofluids. However, their results are based on correlated parameters to match with experimental data, and as a result, their predictions cannot be generalized to other systems involving nanofluids.

Eapen et al. [186] also utilized MD simulations [20] for platinum (Pt) NPs of sub-nanometer size surrounded by liquid Xe in a cubic domain. Through the use of Green-Kubo relationship of the heat current, they report a maximum of 35% increase in the thermal conductivity of the nanofluid for $\phi = 0.8\%$. They decompose the heat flux vector into kinetic, potential and collision constituents; as observed in Ref. [187], the kinetic and potential energy components contribute to energy transport due the convective effects, while the collisional component contributes to energy transport due to the inter-atomic collisions of molecules in the system. According to their findings, while the collisional component has the highest contribution to the thermal conductivity of the nanofluid, the enhanced thermal conductivity mainly arises from the potential energy contribution which is attributable to the strong short-ranged attraction between NPs and the liquid. A dynamic layer of interfacial fluid molecules is formed around the NPs that exchange the potential energy between the fluid and NPs, and as a result, enhance the thermal transport in nanofluids.

Similar to the approach used by Ref. [183], Teng et al. [187] investigated the influence of the particle size at $\phi = 0.688\%$ and reported an increase of up to 300-fold in the thermal conductivity of the nanofluid. Through the heat current decomposition into convection and collision (or diffusion) modes, they observed a higher contribution from the convection mode than the collision mode and this is in agreement with the findings of [183,186].

Sankar et al. [188] studied nanofluid systems consisting Ar and Cu NP with various sizes and volume fractions. They found that the effective thermal conductivity of Cu-Ar nanofluids to be enhanced by about 70%, which is much greater than that predicted by the Hamilton-Crosser model, for volume fractions in the range of ($\phi < 0.4\% - \phi = 8\%$). They find that the motion of the liquid atoms in the nanofluid increases considerably compared to that in the pure base fluid. The Brownian motion of the nanoparticles was, in comparison, too slow to transport the heat. Localized fluid movement around the NP is induced by the faster-moving liquid atoms. They conclude that these are the main competing mechanisms for enhanced thermal conductivity of nanofluids. Their simulations have only considered dispersed NPs and neglect the effects of aggregation. In the calculations of Sachdeva et al. [189] utilizing the Green-Kubo relationship for Cu-water nanofluid, an advanced flexible-3-center (F3C) model for water and the finitely extensible nonlinear elastic (FENE) potential for Cu are employed. The results show an enhancement of 80% for $\phi = 5\%$ for a 1 nm NP. This enhancement is attributed to the formation of hydration layers around the Cu NPs. This

observation is consistent with experimental investigations suggesting the formation of a hydration nanolayer.

Jain et al. [190] utilized the Brownian dynamics simulations coupled with the Green-Kubo relationship to calculate the effective thermal conductivity of nanofluids by considering the effect of various parameters, including $\phi$ ranging from 0.5 to 3%, particle sizes ranging from 15 to 150 nm, and temperatures ranging from 290K to 320K. A parallel model was used for the calculation of the effective thermal conductivity by invoking the assumption that thermal conduction caused by the motion of nanoparticles and the base fluid molecules occur in parallel. This assumption leads to $k_{eff} = \phi k_p + (1 - \phi) k_{bf}$, where $k_p$ is the thermal conductivity due to the Brownian motion of the nanoparticles as calculated by using the Green-Kubo relation and $k_{bf}$ is the thermal conductivity of the base fluid. They conclude that their model could predict the effective thermal conductivity of nanofluids properly and the Brownian motion of the particles is the key mechanism for the enhancement in the thermal conductivity of nanofluids.

Kang et al. [191] have studied the effect of nanoparticle aggregation on the transport properties, including thermal conductivity and viscosity of nanofluids via MD simulations, where the transport properties of the nanofluid are calculated using the Green-Kubo relationship. The results show that the nanoparticle aggregation induces a significant enhancement of thermal conductivity in the nanofluid, while the increase in viscosity is moderate. The results also indicate that different configurations of the nanoparticle cluster result in different enhancements of thermal conductivity and increase in viscosity of the nanofluid. Through the use of MD simulations coupled with the Green-Kubo relationships, Lee et al. [192] have investigated the effects of temperature and size of nanoparticles on the thermal properties of Ar-Cu nanofluid. They report an enhancement of 50% in the thermal conductivity of Ar-Cu nanofluids with Cu NPs having a size of 2 nm and a volume fraction of 8%. However, by increasing the temperature, no significant effect on the thermal conductivity of the nanofluid was noted. In their computational analysis, they find that an increase in the size of the NP is associated with a reduction of viscosity and thermal conductivity of the nanofluid.

Muraleedharan et al. [193] have conducted MD simulations in combination with the Green-Kubo relation for alumina (Al)-water nanofluids and have calculated the effective thermal conductivity for a range of volume fractions (1–10%) and particle sizes (1–3 nm). For a particle size of 1 nm and volume fraction of 9%, an enhancement of 235% has been noted which is much higher than the Maxwell model predictions. However, their analysis with the presence of multiple particles shows no anomalous enhancements in the thermal conductivity of nanofluid. The enhancement was explained to be primarily due to the vibrations of the alumina crystals that can act as low-frequency perturbations, traveling a long distance in the surrounding fluid. These vibrations reinforce the system as a result of the periodic boundary, causing a circular resonance of thermal perturbations between the Al and its own image and lead to spurious correlations in the HCACF, which increase the values of the calculated thermal conductivities abnormally. When more Al NPs are added those fluctuations get dissipated before reentering the periodic images. This study shows the importance of system size scaling in MD simulations.

In summary, it is clear that the MD simulations approach shows promise in exploring and verifying various heat transport mechanisms in nanofluids.

**4.1.1 Effect of particle volume fraction—**Both experimental, as well as computational studies have shown a nearly linear increase in the thermal conductivity of nanofluids as a function of particle volume fraction [118,122,126,171,183,186,187], and just a small volume fraction of particles leads to a significant enhancement in the thermal conductivity of the nanofluids. However, depending on the choice of the particle type and the base fluid, the size of the particle, and the temperature of the system, the slope of this linear increase in the thermal conductivity enhancement can be different as reported in Refs. [118,137,186,194–198].

Most of the MD-based predictions show that with increasing the volume fraction of NPs, the rate of thermal conductivity enhancement decreases [199]. For instance, In their MD studies, Sarkar et al. [183] increased the volume fraction of Cu NPs from 0.5 to 8% and observed thermal conductivity enhancement of Ar-Cu nanofluids from 14% up to 52%, with steeper increase at lower volume fraction and a saturation behavior at higher volume fractions. Similar behavior was also reported by Eapen et al. [186] for Xenon (Xe)-Pt nanofluids using the MD simulation.

**4.1.2 Effect of particle size—**Existing studies provide significantly inconsistent results and report on difficulties in estimating the extent of enhancement in thermal transport as a function of particle size distribution in nanofluids. Despite the vast number of experimental and computational studies that are available, it is not possible to draw conclusions in regard to the effect of particle size since researchers observed both increasing [136,137,139–141,200] and decreasing [119,120,124,127,129,133–135,138] thermal conductivities of nanofluid with increasing NP size. In earlier studies, heat transfer enhancement in nanofluids was mainly attributed to the exposed surface area of NPs [111]. As a result, larger sized particles with higher surface area were expected to produce higher thermal conductivity enhancement compared to those with lower exposed surface area. However, this enhancement due to the particle size has been intensely debated. For suspension of oxide NPs at 0.5% volume fraction, Chopker [119] reported a decrease in thermal conductivity enhancement of $Al_{70}Cu_{30}$-ethylene glycol nanofluids from 38% to 3% as the size of NP increased from 9 to 83 nm. This trend was further confirmed in their later study [120] for the same parameter range with $Al_2Cu$. On the other hand, in another experimental study [129], the thermal conductivity enhancement was reported to decrease significantly for $Al_2O_3$-water nanofluids with a particle volume fraction of 0.5% when the size of the particle was increased from 72 to 137 nm.

The MD simulations conducted by Lu and Fan [201] for $Al_2O_3$ in water and ethylene glycol-based nanofluids show a decrease in the thermal conductivity enhancement as the size of the NP increases to 30 nm and noted a saturation for the size of NPs larger than 30 nm. The decrease noted agree with the trend described in Ref. [129]. Cui et al. [196] performed MD simulations for a nanofluid system consisting of liquid Ar and Cu NPs and noted a decrease of enhanced thermal conductivity with increasing NP size. Contrary results to the above findings are reported in the measurements by Beck [137]. The thermal conductivity

enhancement measured experimentally by Timofeeva [139] for suspension of 4.1% α-SiC in water demonstrates an increase from 7% to 12.5% as the particle size increases from 16 nm to 90 nm. In their MD simulations, Teng et al. [187] also conclude that there is an increase of thermal conductivity of the Ar-Cu nanofluids with increasing size of NPs. Thus, there is much controversy in this literature.

While the MD simulations do not show consensus in the calculated effects of the thermal conductivity with particle size, the experimental study performed by Xie [173] for a suspension of $Al_2O_3$ NPs surrounded by oil and ethylene glycol based fluids showed a non-monotonic trend, i.e., a decrease, followed by an increase in the thermal conductivity enhancement with increasing particle size.

**4.1.3 Effect of system temperature—**An important factor related to the enhancement of thermal conductivity of nanofluids is the system temperature. The temperature dependence of thermal conductivity of nanofluids have made them attractive heat transfer fluids for diverse applications such as in the heat exchanger, high-temperature laser, nuclear power plants, as well as space exploration applications. Some of the published studies report on an increase in the thermal conductivity of nanofluids based on increasing the temperature of system, especially at higher particle concentrations [121–132,183]. The idea of increasing thermal conductivity of nanofluids with increasing the temperature was explored by Das et al. [121], for a suspension of 1% of $Al_2O_3$ in water. The thermal conductivity of nanofluid increased from 2% to 10.8% as the temperature increased from 21°C to 51°C. Additionally, when the particle volume fraction was increased to 4%, the thermal conductivity was enhanced from 9.4% to 24.4% in the same temperature range. Such temperature dependence of thermal conductivity enhancement was also observed by Li and Paterson [125] where an enhancement of about 3 times was reported for water in the temperature range of 27.5°C–34.7°C and particle volume fractions of 2%–10%. Experimental study of Lee et al. [129] demonstrates the significant effects of the particle size and the volume fraction of particle suspension, on the temperature dependence of the thermal conductivity enhancement of $Al_2O_3$-water nanofluids at 50% particle volume fraction with average diameters of 72, 115, and 137 nm, and the temperature in range of 21°C–51°C.

In regard to simulations, Sarkar et al. [183] showed an enhancement of thermal conductivity due to the increase in temperature for Ar-Cu nanofluids for $\phi$ in the range of 0.2, 1 and 2%. For a 0.2% of Cu nanoparticle suspension, they obtained an increase of 11% and 31% for thermal conductivity of nanofluids in a temperature range of 85°C and 103°C. For the same temperature range, they observed an enhancement of 37% and 68% for the suspension of 2% volume fraction. Their findings on the effects of temperature on the thermal conductivity enhancement are in agreement with the results reported by Sankar et al. [188].

However, even with temperature effects, there is much controversy [202–211]. While the measured thermal conductivity of water based $Al_2O_3$ and CuO nanofluids, for an increase of temperature from 22°C to 47°C, shows a steep increase [121], a moderate increase is reported by Beck et al. [205] over a range of 17°C–147°C. Timofeeva et al. [206] investigated the effect of the temperature increase on the thermal conductivity enhancement of $Al_2O_3$ in water and ethylene glycol-based nanofluids with particle volume fraction of 5%.

While they demonstrated an increase in the thermal conductivity with an increase in the temperature from 10°C to 65°C, the temperature dependence of the base fluid was noted to be correlated with the temperature dependence of the nanofluid; this suggests a temperature independent thermal conductivity enhancement for nanofluids. Beck et al. [209] considered a wider range of temperature effects from 22°C to 137°C for suspension of $Al_2O_3$ in water, ethylene glycol as well as mixtures of water and ethylene glycol-based nanofluids and observed that the temperature dependence of thermal conductivity tracked that of the base fluid. Mohebbi [211] measured the thermal conductivity enhancement of nanofluids through the use of MD simulations and noted smaller thermal conductivity enhancement at a higher temperature, i.e. 15% at 140°C, compared to a lower temperature, i.e., 50% at 107°C.

## 4.2 Viscosity of nanofluids

There are fewer studies on the shear viscosity of nanofluids, especially involving MD simulations. Thermal conductivity enhancement in nanofluids is always noted to be accompanied by higher viscosity [170,212–221]. A major concern with higher viscosity systems in engineering applications is the requirement of higher power, resulting in high operating costs to pump the nanofluids through the system, reducing the overall efficacy of the nanofluids. There is a need to simultaneously investigate the increase in the thermal conductivity and viscosity of nanofluids to identify the optimal combination of thermal conductivity and viscosity in the design of nanofluids. This aspect remains open for further study. It is now well-recognized in the convection heat transfer studies of nanofluids that the heat transfer coefficients for energy systems depend on both thermal conductivity and viscosity.

### 4.2.1 Effect of particle volume fraction—

Similar to the prediction of the thermal conductivity, the classical theory of viscosity [222,223] is well described for a suspension of microparticles than for nanoparticles. Here, viscosity is only dependent on the particle volume fraction. Many experiments have been conducted to measure the viscosity enhancement of nanofluids as summarized in Fig. 4 [224]. A clear trend that may be noted in the figure is the increase in the viscosity of nanofluids with increasing particle volume fraction. However, the debate here is on the magnitude of the viscosity enhancement, which varies with the volume fraction of the suspension. Das et al. [225] show an increase in the viscosity enhancement of $Al_2O_3$-water nanofluid as a function of increasing volume fraction of NPs. The measured viscosity enhancement reported by Nguyen et al. [215] for $Al_2O_3$-water nanofluids with particle volume fractions of 1%, 4%, 9%, and 12% and size of 47 nm shows viscosity enhancements of 12%, 60%, 200%, and 430% respectively. They have also carried out similar experiments with smaller size NPs and observe a similar trend, but one that involves a smaller viscosity enhancement.

One of the important features of nanofluids where viscosity plays a dominant role is in the presence of flow. Putra et al. [226] measured the viscosity of CuO-water and $Al_2O_3$-water nanofluids as concerned with the shear rate and observed a Newtonian behavior of these nanofluids in the range of 1–4%.

Computational studies of the role of particle volume fraction with different nanofluid types as related to shear viscosity enhancement report similar results [201,227–230]. The MD simulation study conducted by Lu and Fan [201] illustrates viscosity enhancement of the $Al_2O_3$-water and $Al_2O_3$-ethylene glycol upon addition of a larger number of nanoparticles to the base fluid. Lou and Yang [229] obtained similar results for the enhancement of shear viscosity of $Al_2O_3$-water as a function of particle volume fraction. By increasing the volume fraction of $Al_2O_3$ from 1.24% to 3.72% the shear viscosity enhanced from 1.21 mPa s to 3.68 mPa s at 26.85°C.

**4.2.2 Effect of particle size—**There is controversy among the results published in the literature as related to the viscosity dependence of nanofluids on the particle size. Viscosity has been shown to not only decrease [139,143,217,227,231,232] or increase [134,215,216] with increasing the particle size, but also shown to be independent of the particle size [233]. Pastoriza-Gallego [232] used 11 nm and 33 nm CuO nanoparticles suspended in water and for particle volume fraction of 1–10% over a temperature range of 10°C-50°C and reported that the smaller particle size yielded a higher increase in the viscosity enhancement. Timofeeva et al. [139] also observed the same trend of higher viscosity for smaller particles in their nanofluid suspension consisting of 4.1% volume fraction of SiC NPs in water at a controlled pH of 9.4 and four particle sizes of 16, 29, 66 and 90 nm.

The maximum and minimum viscosity enhancements reported were 85% for a particle size of 16 nm and 30% for a particle size of 90 nm, respectively. Such behavior on the effect of the particle size on enhanced viscosity is also supported by MD simulations [201,227–229,234]. Lu and Fan [201] studied the effect of NP size on the viscosity of nanofluids using computations, and similar to the predictions on thermal conductivity, reported a decrease in the shear viscosity with an increase of the particle size.

However, He et al. [134] used $TiO_2$ nanofluids and reported a viscosity increase at a volume fraction of 0.6% as the particle size increased from 95 to 210 nm. Nguyen et al. [215] conducted experiments with 36 nm and 47 nm $Al_2O_3$ NPs suspended in water and for volume fractions smaller than 4% and reported viscosity enhancements for both particle size. For higher particle volume fractions, they report larger enhancements in the viscosity of Al-water nanofluids for 47 nm particle size than those for 36 nm particle size. As noted in Ref. [139], the effect of the particle size on the viscosity of nanofluids may be identified in experiment, through controls over the actual particle size and the pH of suspension. Such controls have been absent in earlier studies. Prasher et al. [233] demonstrated that the viscosity enhancement in nanofluids is independent of particle size and this is consistent with the classical theories describing viscosity.

**4.2.3 Effect of the system temperature—**The temperature of the system is another effective parameter which is not taken into account in classical theories of viscosity prediction but can influence the thermal conductivity and therefore the shear viscosity of nanofluids. Most experimental studies have reported a non-linear decrease in viscosity and viscosity enhancement of nanofluids with increasing temperature [128,131,139,143,210,215,216,229,235–237] making nanofluids to be promising candidates for higher temperature applications. Some researchers, however, have reported a

contradictory result where viscosity enhancement is shown to be independent of temperature [213,214,233]. Murshed et al. [236] conducted experiments for water-based $SiO_2$ and $TiO_2$ nanofluids at 0.05% particle volume fraction when the system temperature was increased from 21°C to 57°C. Results show a decrease of 42% and 37% in viscosity of nanofluids with $SiO_2$ and $TiO_2$, respectively. Namburu et al. [235] studied a suspension of CuO nanoparticles in the mixtures of water and ethylene glycol and reported a decrease of viscosity as the nanofluid temperature was raised from 35°C to 50°C. As the particle volume fraction was increased from 1 to 6.12%, they observed a higher change in the viscosity enhancement over the temperature range. Nguyen et al. [216] also measured the viscosity of $Al_2O_3$-water nanofluids over a temperature range of 21°C–75°C. Around ambient temperature, i.e., 22°C–40°C, a higher change in the viscosity enhancement was observed, which shows stronger temperature dependence at higher particle volume fraction.

Lou and Yang [229] have carried out molecular dynamics simulation with the Green-Kubo analysis and report a decrease in the viscosity of $Al_2O_3$-water nanofluids as the temperature of the system is raised. Their calculation over the same temperature rise also shows that the shear viscosity of the nanofluids at a higher volume fraction of particle decreases. This is attributed to the higher energy of the system, causing the role of the temperature to be substantial. Similar behavior has also been reported by Loya et al. [237] who have used MD simulations for the CuO-water nanofluids.

Experimental measurements of viscosity by Chen et al. [214] for $TiO_2$-ethylene glycol nanofluids with the particle volume fraction of 0.5–8% over a temperature range of 20°C–60°C have shown a strong dependence on the temperature. The trend of the temperature dependence on the viscosity of nanofluids follows the trend for the base fluid, suggesting negligible contributions due to Brownian diffusion for nanofluids compared to those due to convection under high shear flow.

### 4.3 Effects of nanoparticle aggregation on transport properties of nanofluids

Although a nanofluid has well-dispersed nanoparticles in the base fluid, experiments have demonstrated that an aggregated state exists in the nanofluid [118,176,178,232]. The suspended NPs experience random Brownian motion in the base fluid as well as van der Waals interactions which may lead to the development of aggregation and clustering of dispersed nanoparticles. This may result in a state of minimized surface energy. The fact that the NPs are mostly found in the form of aggregate in the fluids makes the liquid inside and adjacent to these aggregates less mobile and as a result, makes the nanofluid more viscous. Then the applied shear breaks the aggregates into smaller or primary structures. Most of the experimental and computational studies report on the influence of NP aggregation as related to the thermal conductivity of nanofluids while fewer research articles have been published on the effect of aggregation on viscosity and diffusion coefficient of nanofluids [58,165,213,219,238–243]. More research is needed to consider such an effect on the viscosity and diffusion coefficient of nanofluid via molecular level techniques.

The aggregation of nanoparticles has been identified by several experimental and theoretical researchers as the most potential mechanism on the enhancement of thermal conductivity of

nanofluids [144,145,148,151–154,159,165–169,244]. Some investigations, however, have shown an opposite trend on the role of aggregation in enhanced thermal transport [245,246].

Keblinski et al. [144] were among the earliest groups to propose that the clustered NPs make linear chains or percolation-like conduction paths in the base fluid which generates a network of lower thermal resistance to enhance the thermal conductivity of nanofluids. This mechanism has further been explained through the development of an aggregation-based model for rapid conduction of nanofluids [145,165–169,244,247] with the three-level homogenization model as the most recognized model [165,168]. The assumption made in this model is that a fractal aggregate is enclosed within a sphere consisting of few linear chains that span the entire cluster, namely the backbone chains, and side chains which do not span the whole aggregate, namely the dead-end particles, as shown in Fig. 5. The backbone chains crucially contribute to the thermal conductivity due to the high aspect ratio allowing for fast heat flow over larger distance and reduced thermal resistance.

Prediction of heat conduction for such fractal aggregates through the use of three-level homogenization models is in agreement with that of Monte Carlo simulation [165,168]. It is observed from experimental data that there is a strong correlation between NP aggregation and thermal conductivity [206,248–253]. Gao et al. [252] conducted a structural analysis in liquid and solid states for $Al_2O_3$ nanoparticles suspended in animal oil and hexadecane base fluids. While the Brownian motion was frozen, the thermal conductivity enhancement for the hexadecane based nanofluids in the solid state was reported higher than the liquid state. On the contrary, the thermal conductivity enhancement for the animal oil-based nanofluids in the solid state was observed to be slightly lower than at the liquid state. While transmission electron microscope photographs in $Al_2O_3$ nanofluids showed the formation of linear chains of nanoparticles in the hexadecane base fluid which are pushed into the grain boundaries, such linear chains of nanoparticles are not observed when the base fluid is the animal oil. Therefore, they conclude that rather than the Brownian effects, the linear chain of nanoparticle aggregation is the essential mechanism for enhancement of thermal conductivity of nanofluids. Similarly, higher thermal conductivity was reported for a gelled sample, formed with interconnected nanoparticles, than the fluidic sample where the NPs are fully moving in the suspension [251,253].

MD simulation studies have also supported the role of nanoparticle aggregation in thermal conductivity enhancement of nanofluids with a higher thermal conductivity than well-dispersed nanofluids. The configuration of nanoparticle aggregation has been identified as the key that governs the level of thermal conductivity enhancement in nanofluids [191,198,254]. Lee et al. [198] used MD simulation with the Green-Kubo method to model Ar-Cu nanofluid systems in both aggregated and non-aggregated states. Their results show that as the volume fraction of nanoparticles increases the thermal conductivity is enhanced at both states. Additionally, they conclude that there is higher thermal conductivity enhancement for aggregated nanoparticles at higher volume fractions of over 3.89%. The enhanced thermal conductivity of nanofluids in the aggregated state and at low particle volume fraction is attributed to the higher number of collisions between nanoparticles, and as the volume fraction of the Cu NPs increases, the convective effect, more specifically the potential energy of both Ar and Cu, of the heat current also plays a role in enhancing the

thermal conductivity of nanofluids. For nanofluids in the non-aggregated state, the thermal conductivity enhancement is dominated by the increase in the potential energy of the base fluid.

While the studies mentioned above revealed the important role of NP aggregation on thermal conductivity enhancement, the underlying mechanisms have not been studied or characterized in these studies.

Another factor in the context of NP aggregation is the time dependence of the thermal conductivity [206,245,246,255,256]. Angayarkanni and Philip [256] have measured the thermal conductivity of oxide water-based nanofluids by applying the sonication treatment and have noted an increase of thermal conductivity enhancement over some duration after the sonication process, followed by a decrease. They conclude that the nanoparticles are most likely in a well-dispersed state right after the process and as time passes, the NPs get closer leading to high thermal conductivity enhancement as a result of agglomeration. The nanoparticle aggregation becomes significant at later times and eventually the aggregate settles down as a result of gravity, leading to a decrease in the thermal conductivity. A different trend has been noted by other researchers [245,246] for CuO and Fe nanofluids right after the sonication process, where the size of aggregated particles increases as a function of time, resulting in a continuous decrease of thermal conductivity enhancement with the elapsed time. It is therefore concluded that the key parameter to improve the thermal conductivity in the aggregated state may be the suspension stability of the well-dispersed nanoparticles.

### 4.4 Equilibrium and transport properties from fluctuating hydrodynamics numerical studies

While smaller NPs (1–10 nm) in small systems (limited to a few nanometers), often called Quantum dots, may be modeled using MD, systems approaching 100 nm to microns, such as 100 nm NP confined in a micron-sized fluid domain are not accessible via MD. At a continuum-level, a NP suspended in a fluid undergoes random motion due to the thermal fluctuations in the fluid. The fluid may be static or flowing under an external pressure gradient. In determining the translational and rotational motions of the NP in an incompressible Newtonian fluid (static or flowing) the performance of the fluctuating hydrodynamics method (FHD) has been examined. As a general rule, for stochastic numerical simulations, a large number of realizations are required to acquire satisfactory statistics of the dynamical properties. This ensemble averaging is usually computationally challenging and intensive.

The results reported in Ref. [257] are obtained from five different realizations of a FHD simulation, with each realization consisting of $N = 20{,}000$ time steps. The error bars have been plotted from standard deviations of the temperatures obtained with the different realizations, based on which the statistical error is established to be less than 5%. The evolution of translational and rotational dynamics of a spherical particle ($a = 250$ nm) in the inertial regime, when immersed in a Newtonian fluid (with properties of water) and confined at the center of a cylindrical vessel ($D = 20$ μm), has been simulated using the FHD approach at a temperature of $T_0 = 310K$. The probability distributions of the Cartesian

components of the translational and rotational velocities show the adherence to the corresponding Maxwell Boltzmann distributions. The short-time ($t \sim \tau_V = a^2/\nu$, where $\nu = \mu/\rho$ and ρ is the fluid density) evolution of the linear velocity autocorrelation function (VACF) and angular velocity autocorrelation function (AVACF) in the inertial regime show the correct asymptotic transition from the exponential behavior ($\xi^{(tr)} = 6\pi\mu a$ and $\xi^{(rot)} = 8\pi\mu a^3$) for $t \to 0$ to algebraic behavior for $t > \tau_V$. We note that the results described above pertain only to spherical NP and the corresponding treatment for ellipsoidal NPs are described in Ref. [258].

### 4.4.1 NP diffusivity

**Diffusivity in Unbounded Medium:** The study by Uma for spherical NP [257] reported both the short and long time translational and rotational mean square displacements (MSDs) of a neutrally buoyant NP ($a$ = 250 nm) initially placed at the center of a large cylindrical vessel of diameter and length, $D$ = 10 μm and $L$ = 10 μm, respectively. In the regime where the particle's motion is dominated by its own inertia (ballistic), $0.346\tau_V \le t \le 0.63\tau_V$ (translation), and $0.174\tau_V \le t \le 0.316\tau_V$ (rotation), the translational and rotational motions of the particle follow $(3k_BT/M)t^2$ and $(3k_BT/\mathbf{I})t^2$, respectively. In the diffusive regime, $t \gg \tau_b$, and when $t \ge 7\tau_V$ (translation) and $t \ge 1.2\tau_V$ (rotation), the translational and rotational MSDs increase linearly in time to follow $6D_\infty^{(t)}t$ and $6D_\infty^{(r)}t$, respectively, where $D_\infty^{(t)} = k_BT/\zeta^{(t)}$, and $D_\infty^{(r)} = k_BT/\zeta^{(r)}\left(\zeta^{(r)} = 8\pi\mu a^3\right)$ are the translational and rotational self-diffusion coefficients. The MSDs in an intermediate regime between the ballistic and the diffusive are related to hydrodynamic memory effects. The translational and rotational MSDs of the particle follow Stokes-Einstein [259,260] and Stokes-Einstein-Debye [261] relations, respectively.

**4.4.2 Wall confinement effects—**In many technological applications, boundary effects and confining potentials are important, which make the evaluation of particle motion and associated transport much more complicated. The timescales of these motions overlap with the inertial timescale of the fluid, and as such, the temporal correlations in the inertial regime are strongly influenced by the confining boundaries and potentials. How the presence of a bounding planar wall alters the algebraic scaling of the VACF in the inertial regime has been analyzed by Gotoh and Kaneda [262], Pagonabarraga et al. [263,264], Felderhof [265], and Franosch and Jeney [266]. Collectively, these studies have investigated the dynamics of the motion of a spherical particle near the wall by confining the particle to different distances $h$ from the wall. In the absence of an external potential, the parallel motion in the bulk-regime ($h/a \to \infty$) showing the $t^{-1.5}$ scaling of the VACF transitions to a $t^{-2.5}$ scaling with positive amplitude in the near-wall regime ($h/a > 1$), while for the perpendicular motion, a $t^{-3.5}$ scaling for the intermediate times is followed by a long-time tail that exhibits a $t^{-2.5}$ scaling with negative amplitude. In the presence of a confining potential, the VACF is characterized by a $t^{-3.5}$ scaling in the bulk regime and a $t^{-4.5}$ scaling in the near-wall regime $\left(\frac{h}{a} > 1\right)$. For a particle in the lubrication regime (where $(h - a)/a \to 0$), a detailed and consistent study of the hydrodynamic interactions and important aspects of the cylindrical wall effects in the lubrication and other hydrodynamic regimes are available in Ref. [267]. Also, for the majority of scaling relationships for VACF under various spatial and adhesion

regimes that have been obtained through the asymptotic analysis of linear hydrodynamics, their validity through direct numerical simulations have been established in Ref. [267].

The results for the long-time behavior of the velocity (or the VACF) in the inertial regime for a particle at different locations relative to the boundary is analyzed together with the effect of the wall curvature are displayed in Fig. 6 for the translational velocity components. The limit $D/d \to \infty$ denotes the limit of the infinite planar wall. For the parameter range examined in the study, an interesting effect observed in this study on cylindrical wall effects is that, apart from the short-time exponential decay and the intermediate-time algebraic decay, at much longer times, $t > C_1^{tr}\tau_D$ or $C_1^{rot}\tau_D$, with $\tau_D = D^2/\nu$, a second exponential decay ($\exp\left(-C_2^{tr}t/\tau_D\right)$ or $\exp\left(-C_2^{rot}t/\tau_D\right)$ with prefactors $C_2^{tr}$ and $C_2^{rot}$) occurs. In the insets of Fig. 6A for different $D/d$, the time scales at which the second exponential decay appears, where the particle velocity deviates from the algebraic scaling at least by 10%, are compared. This characteristic time is found to be only a function of $D/d$ or $\tau_D/\tau_\nu$. Detailed results for a particle located in the near-wall regime, $(h-a)/a = 1$ have been presented in Ref. [267]. The parallel and perpendicular components are illustrated in Fig. 6C and D for translational velocities.

The results for the translational motion show that for $D/\mathrm{d} < 20$, the velocity decays exponentially without a clear intermediate algebraic scaling. For larger diameters, after the initial Stokes-exponential decay, algebraic correlations are observed, where the parallel motion displays a $t^{-2.5}$ scaling, and the perpendicular motion first displays a $t^{-3.5}$ scaling behavior at intermediate times ($t \sim h^2/\nu$) followed by a $t^{-2.5}$ scaling with a negative sign (anticorrelation) due to the wall reflection of the diffused vortex. Eventually, the algebraic decay transitions to a final exponential decay due to the wall confinement. Fig. 6D also illustrates that the presence of a curved wall causes an anticorrelation to occur at later times compared to those for a particle near a planar wall [265]. Similar trends are observed for the angular velocity relaxation where it first shows an initial exponential decay characterized by the instantaneous Stokes drag followed by an algebraic decay ($t^{-2.5}$ scaling for rotation about the parallel axis and $t^{-3.5}$ for perpendicular axis [263]) and a long-time second exponential decay. In Fig. 6E and F, the time evolution of the velocity for a particle in the lubrication layer, or $(h-a)/a < 1$ is depicted. The general characteristics of the velocity versus time are similar to those for the near-wall case. However, the enhanced Stokes drag for the lubrication layer leads to a more distinct separation between the two exponential decays such that the intermediate algebraic decay is manifest even for smaller vessel diameters. It is noted that the anticorrelation in the smaller vessel occurs at later times, indicating that the vessel curvature constrains the evolution of the particle motion. Eventually, the algebraic decay changes to a final exponential correlation due to the presence of strong confinement of the vessel wall. The angular velocity relaxation about the parallel axis exhibits the same general trend as in the near-wall case where the anticorrelation is noted to occur at later time scales for smaller tube diameters. In the lubrication regime, this effect is significant for rotation about the perpendicular axis such that anticorrelation is observed. The diffusion coefficient of the NP at different distances from the confining wall can be obtained from the VACF by solving the corresponding integral in the Green-Kubo relationship, as demonstrated in Ref. [267].

### 4.5 Construction of thermostats

The FHD essentially consists of adding stochastic stresses (random stress) to the stress tensor in the momentum equation of the fluid [11]. The stochastic stress tensor depends on the temperature and the transport coefficients of the fluid medium [9,33]. FHD numerical simulations have been carried out employing the finite volume method [21,22,33,34], lattice Boltzmann method (LBM) [23–29], finite element method [47,257,268] and stochastic immersed boundary method [30]. Direct numerical simulations (DNSs) of fluctuating hydrodynamics (FHDs) approach has been carried out by employing the finite volume method [21,48,49,269], lattice Boltzmann method [23–29], smoothed-particle method [270,271], and stochastic Eulerian-Lagrangian method [30,272]. A comparison of these methods are described in Uma et al. [257]. In the following, we review the extensions to the work of Uma et al. [257] by employing arbitrary Lagrangian-Eulerian (ALE) finite element method (FEM) to account for the fluid-particle interaction. A key feature and strength of the ALE method is that due to the adaptive mesh approach, it can resolve multiple hydrodynamic regimes such as bulk, near-wall, and lubrication amid arbitrarily shaped boundaries. In the GLE, the effects of thermal fluctuations are incorporated as random forces and torques in the particle equation of motion [271,273–278]. The properties of these forces depend on the grand resistance tensor. The tensor in turn depends on the fluid properties, particle shape, and its instantaneous location such as its proximity to a wall or a boundary. In the generalized Langevin equation approach, a robust thermostat can be implemented by suitably tuning the noise spectrum of the random forces and torques by adding memory, but the coupling of the thermostat to the fluid equations of motion alters the true hydrodynamic behavior as quantified by the nature of the velocity autocorrelation function (VACF) and the value of the diffusion coefficient computed using mean squared displacement (MSD) versus time [278]. Both the Markovian (white noise) and non-Markovian (Ornstein-Uhlenbeck (O-U) noise and Mittag-Leffler (ML) noise) processes may be considered. For the non-Markovian approach, an appropriate choice of colored noise is required to satisfy the power law decay in the velocity autocorrelation function at long times. The non-Markovian ML noise simultaneously satisfies the equipartition theorem and the hydrodynamic correlations for a range of memory correlation times. The O-U process, however, may not provide the appropriate hydrodynamic correlations.

For NP motion in an incompressible fluid, the FHD resolves the hydrodynamics correctly but does not impose the correct equipartition of energy based on the nanoparticle mass because of the added mass of the displaced fluid. In contrast, the Langevin approach with appropriate memory can show the correct equipartition of energy, but not the correct short- and long-time hydrodynamic correlations. In a third approach referred to as the hybrid approach [279], it is shown for the first time, that it is possible to simultaneously satisfy the equipartition theorem and the (short- and long-time) hydrodynamic correlations. In effect, this results in a thermostat that also simultaneously preserves the true hydrodynamic correlations. Thus, the hybrid approach enables a thermostat for the NP which maintains a set temperature and the correct thermal distributions (i.e., preserve the canonical ensemble), while simultaneously preserving the hydrodynamic effects (i.e., velocity auto-correlation and diffusion coefficient).

All the three methods described above are computationally expensive (large computational overhead), with the GLE perhaps the least expensive. A fourth procedure called the Deterministic method enables a computationally inexpensive calculation to study the long-time behavior of the VACF and the AVACF of a NP in a quiescent medium. The rationale for this method is derived both from the fluctuation-dissipation relation which states that the temporal correlation in the thermal stresses is equivalent to the correlation in the hydrodynamic memory of a stationary fluid [280] and the Onsager regression hypothesis which states that the regression of microscopic thermal fluctuations at equilibrium follows the macroscopic law of relaxation of small non-equilibrium disturbances [12,13]. Related to this, earlier studies [267,281–283] have shown that the averaged time correlation in the velocity of a Brownian particle in a stationary medium, is equivalent to that for a driven particle computed in the absence of thermal fluctuations. It must be noted that the trajectories identified by Deterministic simulations are not reflective of that for a fluctuating particle.

### 4.6 Memory function inspired coarse-graining: treatment with the generalized Langevin equation

The equation of stochastic motion for each component of the velocity of a nanoparticle immersed in a fluid in an unbounded domain (in the limit of the linearized Navier-Stokes equation) takes the form of a GLE and is given by:

$$M\frac{dU}{dt} = -6\pi\mu a U(x,t) + 3a^2\sqrt{\pi\rho\mu}\int_{-\infty}^{t}|t-t'|^{-\frac{3}{2}}U(x,t')\mathrm{d}t' - kx(t) + R(t)\,. \tag{30}$$

Here, $\zeta^{(t)}(t) = 12\pi\mu a\delta(t) - 3a^2\sqrt{\pi\rho\mu}t^{-\frac{3}{2}}$, and $R(t) = R_w(t) + R_c(t)$, with a white noise correlation $\langle R_w(t)R_w(t')\rangle = 12\pi\mu a k_B T\delta(t-t')$, a colored noise correlation $\left\langle R_c(t)R_c(t')\right\rangle = -3a^2\sqrt{\pi\rho\mu}k_B T|t-t'|^{-\frac{3}{2}}$, and $\langle R_w(t)R_c(t')\rangle = \langle R_w(t)\rangle\langle R_c(t')\rangle = 0$. Eq. (30) representing a particle in an unbounded fluid domain can be extended to incorporate the effect of the boundaries on hydrodynamic interactions. In a recent study, Yu et al. [283] formulated a composite GLE that explicitly encodes the transition from a bulk domain to a near-wall domain as the particle is approaching a confining boundary. This is accomplished by using a pertinent bridging function that transitions the GLE from that for the bulk regime at early times (when the momentum diffusion from the particle is yet to reach the boundary, i.e., $t \lesssim h^2/\nu$) to that for near-wall regimes for later times (when the reflected momentum wave from the boundary begins to impact the temporal velocity correlations of particle motion, i.e., $t \gtrsim h^2/\nu$). For perpendicular motion, the composite GLE for that case is given by:

$$M\frac{dU_{\perp}}{dt} = -6\pi\mu a\beta U_{\perp}(x,t) - A_1(t)\int_{-\infty}^{t}|t-t'|^{-\frac{3}{2}}U_{\perp}(x,t')\mathrm{d}t' - A_2(t)\int_{-\infty}^{t}|t-t'|^{-\frac{5}{2}}U_{\perp}(x,t')\mathrm{d}t' - kx(t) + R(t), \quad (31)$$

where, $\beta = \left(1-\frac{9a}{8h}\right)^{-1}$, $M = (3m/2)\left(1-\frac{a^3}{8h^3}\right)^{-1}$, $A_1(t) = -3a^2\sqrt{\pi\rho\mu}\left(e^{-\frac{t}{\tau_w}}\right)$ and $A_2(t) = \frac{9}{8}am\sqrt{\frac{\rho}{\pi\mu}}\beta^2\left(1-e^{-\frac{t}{\tau_w}}\right)$ complements $A_1(t)$; here, $\tau_w = h^2/v$.

The random forces and force correlations consistent with the fluctuation dissipation theorem are given by:

$$R(t) = R_w(t) + e^{-\frac{t}{\tau_w}}R_{c1}(t) + \left(1-e^{-\frac{t}{\tau_w}}\right)R_{c2}(t) \text{ with } \left\langle R_w(t)R_w(t')\right\rangle = 12\pi\mu a\beta k_B T\delta(t-t'),$$

$$\left\langle R_{c1}(t)R_{c1}(t')\right\rangle = -3a^2\sqrt{\pi\rho\mu}k_B T|t-t'|^{-\frac{3}{2}},$$

$$\left\langle R_{c2}(t)R_{c2}(t')\right\rangle = \frac{9}{8}am\sqrt{\frac{\rho}{\pi\mu}}\beta^2 k_B T|t-t'|^{-\frac{5}{2}}, \text{ and}$$

$$\left\langle R_w(t)R_{c1}(t')\right\rangle = \left\langle R_w(t)R_{c2}(t')\right\rangle = \left\langle R_{c1}(t)R_{c2}(t')\right\rangle = 0.$$

Discussions related to these descriptions are offered in the next section.

**4.6.1 Deterministic method for VACF and AVACF calculations—**For stochastic simulations, a large number of realizations are required to reach satisfactory statistics of the dynamical properties. Since $\zeta^{(t)}(t)$ is hydrodynamic in origin, the scaled relaxation of $U(t)$ can also be obtained in the absence of the random force $R(t)$. This is the Deterministic method. The Deterministic method is based on the Onsager regression hypothesis, which states that the regression of microscopic thermal fluctuations at equilibrium follows the

macroscopic law of relaxation of small non-equilibrium disturbances [12,13].

Mathematically, this yields $\left\langle \Delta U(t) \right\rangle / \left\langle \Delta U(0) \right\rangle = \frac{\langle \Delta U(t) \Delta U(0) \rangle}{\left\langle \Delta U(0)^2 \right\rangle}$, where $\Delta U(t) = U(t) - \langle U(t) \rangle$.

The above relationship provides a convenient frame work for employing the deterministic method for evaluating VACFs and AVACFs. The deterministic simulations consider the situation in which the particle is driven initially by a weak impulse giving $U(0)$ in the absence of the $R(t)$. The correlation between a macroscopically-driven $U(0)$ and the subsequent $U(t)$ would be equivalent to the calculated VACF (also denoted as $C_v(t)$) obtained from the stochastic simulations, according to Onsager's regression hypothesis [284].

In Fig. 7A, for a non-neutrally-buoyant Brownian particle at various distances from the wall, the deterministic numerical solutions to the composite GLE have been compared with the analytical solutions of the linearized Navier-Stokes equation for the same particle-wall system in a quiescent fluid. This result shows excellent agreement between theory and simulations. In Fig. 7B, the deterministic, (i.e., without thermal noise), and the stochastic, (i.e., with thermal noise), results for the composite GLE are compared to those from the FHD method for a particle in the lubrication regime, and bound via a harmonic potential, again showing excellent agreement between the coarse-grained GLE approach [283] and the full-scale FHD/DNS simulations [267].

In Vitoshkin et al. [267], the dynamics and correlations in the presence of flow, wall-confinement, and adhesion interactions have been resolved by carrying out the FHD method in three different hydrodynamic regimes, namely bulk ($(h - a)/a \gg 1$), near-wall ($(h - a)/a \sim 1$), and lubrication ($(h - a)/a \ll 1$)regimes. The formulation and results of that study provide a systematic approach for studying the temporal hydrodynamic correlations in the presence of a curved vessel wall, particle size, particle-fluid density variations, adhesive interactions (confining potential), and low Reynolds number flows, especially focusing on the lubrication regime. The significance of the DNS approach using FHD in terms of capturing the VACF of nanoparticle motion under a variety of confinement and flow conditions can be recognized in relation to the GLE formalism for nanoparticle motion. Indeed, the composite GLE framework [283] correctly captures the different hydrodynamic correlations at different time scales, when boundaries, confining potentials, and flow-fields are introduced. Therefore, the VACF determined by DNS provides direct input to the GLE by defining the memory function. As demonstrated there, the GLE then represents a reduced dimensional and computationally efficient framework for encoding nanoparticle dynamics. Parallel approaches to bridge the molecular and hydrodynamic scales in pure fluids by combining molecular dynamics simulations and linearized fluctuating hydrodynamics equations have been described by Chu et al. [31,285–287].

#### 4.6.2 Generalized Langevin equations for bridging colloidal and molecular scale dissipation in the context of mass transfer—

In nanoscale mass transport that occurs in many biological systems employing nanoparticles, the adhesive dynamics of nanoparticles to receptors are governed by the binding interactions, which are more often than not, mediated by receptor-ligand complexes. The example of a harmonic spring in Fig. 7B represents such an interaction at a coarse-grained level. The confining potential can have

a range of values for the reactive compliance (or alternatively the stiffness) depending on the receptor-ligand pair, the use of spacers or tethers, the properties of the nanoparticle or the adhesive surface (e.g., flexible vs. rigid); within the harmonic approximation, in which the adhesive potential is approximated as $V(x) = \frac{1}{2}kx^2$, the values for $k$ typically fall in the range of $10^{-6} - 10$ N/m. Such potentials influence nanoparticle dynamics in an obvious way through influencing the energy landscape of adhesion, i.e., through $V(x)$. However, in the inertial timescale of $t \sim a^2/\nu$, the internal dynamics of receptor-ligand complexes can also influence nanoparticle adhesion, independent of the energy landscape, $V(x)$. Single-molecule laser spectroscopy studies [288] have shown that fluctuations within a single protein exhibits wide relaxation spectrum characterizing a long time memory, implying that the protein dynamics should also be described suitably by a GLE. If we consider the dimensions of the receptor-ligand complex (in the scale of $\sim 10^1$ nm), which are much smaller than the nanoparticle ($a \sim 10^2$ nm), the particle dynamics itself occurs in the lubrication regime, (i.e., with $(h - a)/a \ll 1$). Therefore, in order to precisely encode the position-dependent, enhanced hydrodynamic drag when the particle binds to the surface in such a regime, and simultaneously account for the dynamical relaxation of the ligand-receptor pair, we formulate and simultaneously solve two coupled GLEs:

$$M\frac{d^2\overline{x_p}(t)}{dt^2} = -\int_{-\infty}^{t}\zeta_p^{(t)}(t-t')\frac{d\overline{x_p}}{dt'}dt' + k(x(t) - \overline{x_p}(t)) + R_p(t) \tag{32}$$

$$0 = -\int_{-\infty}^{t}\zeta_r^{(t)}(t-t')\frac{dx}{dt'}dt' - (k + k_s)x(t) + k\overline{x_p}(t) + R_r(t)\,. \tag{33}$$

Eq. (32) corresponds to the nanoparticle equation of motion subject to a strong lubrication force and adhesion, while Eq. (33) describes the receptor dynamics. $\overline{x_p} = x_p - a - l - x_r^0$ is the rescaled nanoparticle center-of-mass position, $l$ the ligand length, and $x_r^0$ the equilibrium position of the receptor tip, $x = x_r - x_r^0$ is the instantaneous receptor tip position relative to its equilibrium value. The hydrodynamic memory function in Eq. (32), $\zeta_p^{(t)} = 2\zeta_{p,0}^{(t)}\delta(t-t')$ with $\zeta_{p,0}^{(t)} = 6\pi\mu a\{a/(h(t) - a)\}$, denotes the enhanced resistance of the nanoparticle in the lubrication layer. $\zeta_r^{(t)}(t-t') = \zeta_r^0(\lambda_r)|t-t'|^{\lambda_r}$ in Eq. (33) is the memory function for receptor internal dynamics with $\zeta_r^0$ being the fiction coefficient and $\lambda_r$ being the power-law index. Following the fluctuation-dissipation theorem [15], the random forces of the particle($R_p$) and receptor($R_r$) are related to the frictional terms via $\langle R_p(t)R_p(t')\rangle = 2k_BT\zeta_{p,0}^{(t)}\delta(t-t')$ and $\langle R_r(t)R_r(t')\rangle = k_BT\zeta_r^{(t)}(t-t')$.

Yu et al. reported results from the stochastic simulations of Eqs. (32) and (33) at $T = 310$ K for a nanoparticle ($a = 250$ nm) adhered to a planar wall, (with equilibrium separation $x_r^0 = 19$ nm, $l = 15$ nm, and $k = 1$ N/m), see Ref. [283]. The conformational force constant $k_s$

= 1.88 N/m, the friction coefficient $\zeta_r^0 = 1.32\,\mathrm{Ns}^{0.5}\mathrm{m}^{-1}$, and the power-law index $\lambda_r = 0.5$ for the receptor protein are taken from the measurements of Ref. [289]. The authors presented the normalized velocity autocorrelation functions of the nanoparticle $C_v(t) = \langle U(t)U(0)\rangle$, and the normalized position autocorrelation functions of the nanoparticle ($C_x(t) = \langle x_p(t)x_p(0)\rangle$) and of the receptor tip ($C_x(t) = \langle x(t)x(0)\rangle$) as a function of the scaled time, $t/\tau_v$. The nature of the velocity autocorrelation function for a bound nanoparticle was found to be completely distinct from that for an unbound nanoparticle either in the bulk fluid or close to the vessel wall. For a free nanoparticle in bulk medium, the analytical solution of the Stokes equation predicted an exponentially-decaying $C_v(t)$, and the DNS of the Navier-Stokes equation [267] yields a $C_v(t)$ that exhibits a $t^{-3/2}$ long-time tail. When the particle moves to the proximity of the wall but not bound to the wall, the lubrication force enhances the hydrodynamic resistance felt by the particle and leads to a faster decay of $C_v(t)$, where the steady-state lubrication theory predicts an exponential decay with an augmented drag coefficient, and the long-time tail of the DNS solution is altered by the wall-induced vortex reflection. Once the particle is bound to the wall due to ligand-receptor interactions, the strong adhesion leads to oscillations in $C_v(t)$ that prevail in the hydrodynamic correlations. In the results for $C_x(t)$, the long-time decay for the bound nanoparticle was found to be consistent with that observed in $C_v(t)$. In terms of the receptor dynamics, the much faster-decaying $C_x(t)$ for the bound receptor tip compared with the slowly-decaying correlation for a free receptor indicated that the dynamical relaxation of the protein is strongly coupled with the instantaneous motion of the nanoparticle. The probability distributions of the nanoparticle center of mass position and the receptor tip position were presented. The presence of ligand-receptor relaxation makes the nanoparticle distribution close to the Boltzmann distribution for a harmonically-bound particle. However, the nanoparticle binding makes conformational distribution of the receptor highly constrained, as evidenced by the much narrower receptor tip distribution compared to the unbound receptor. These observations suggested that the fluctuations of the antibody-antigen complex indeed play a significant role in the nanoparticle binding and relaxation dynamics.

### 4.7 Effect of multiple particles and hydrodynamic interactions

Particulate suspensions in cylindrical pipe flows have evinced great interest due to their relevance in a wide range of applications such as in oil, food, construction, pharmaceutical industry. While full numerical treatment of multiparticle FHD simulations in flow is computationally intensive, the microstructure of flow-driven suspension of hardspheres in cylindrical confinement can be studied using dynamical density functional theory and Monte Carlo methods. Yu et al. [290] have studied the microstructure of a flow-driven hardsphere suspension inside a cylinder using dynamical density functional theory and Monte Carlo simulations. In order to be representative of various physical conditions that may prevail in experiments, they have investigated the problem using both the grand canonical ($\mu VT$) ensemble and the canonical ($NVT$) ensemble. In both ensembles, the hydrodynamic effect on the suspension mediated by the presence of the confining wall is implemented in a mean-field fashion by incorporating the thermodynamic work done by the inertial lift force on the particle, given the average flow field. The predicted particle distribution in the $\mu VT$ ensemble displays strong structural ordering at increasing flow rates due to the

correspondingly higher particle concentrations inside the cylinder. In the *NVT* ensemble, for dilute suspensions, they reported a peak in the distribution of density at a location similar to that of the Segré-Silberberg annulus, while for dense suspensions the competing effects of the inertial lift and the hardsphere interaction lead to the formation of several annuli.

The multiparticle suspension work has been later extended to study the rheology of colloidal suspensions in confined flow including the treatment of hydrodynamic interactions in particle-based simulations inspired by dynamical density functional theory. Jabeen et al. [291] investigated the microstructure and rheology of a hardsphere suspension in a Newtonian fluid confined in a cylindrical channel and undergoing pressure-driven flow using Monte Carlo simulations. They developed a hydrodynamic framework inspired by dynamical density functional theory approaches in which the contributions due to various flow-induced hydrodynamic interactions (HIs) are included in the form of thermodynamic work done by these HI-derived forces in displacing the hardspheres. Using this framework, one can self-consistently determine the effect of the local microstructure on the average flow-field and vice versa and co-evolve the inhomogeneous density distribution and the flattening velocity profile with an increase in density of suspended particles. Specifically, the study explored the effect on the local microstructure due to the inclusion of forces arising from confinement-induced inertial effects, forces due to solvent-mediated interparticle interactions and the dependence of the diffusivity on the local density. The authors examined the dependence of the apparent viscosity of the suspension on the volume fraction of hardspheres in the cylinder, the flow rate and the diameter of the cylinder, and investigate their effects on the local microstructure.

Larger particulates in suspension such as RBCs can modulate carrier interactions with the underlying surfaces. Using the dynamical density functional theory (DDFT) approaches introduced by Yu et al. and Jabeen et al. [290,291] one can include the effect of inertial margination due to flow on the spheres.

The expression for the mean-field DDFT equation in the presence of convective flow and external potentials is defined as:

$$\frac{\partial \rho^{\mathrm{RBC}}(\mathbf{r},t)}{\partial t} + \nabla \bullet \rho^{\mathrm{RBC}}(\mathbf{r},t)\left\langle \mathbf{v}_1 \right\rangle_1 = \nabla \bullet \frac{\left\langle D_s \right\rangle_1}{k_{\mathrm{B}}T} \bullet \rho^{\mathrm{RBC}}(\mathbf{r},t)\nabla \frac{\delta F\left[\rho^{\mathrm{RBC}}(\mathbf{r},t)\right]}{\delta \rho^{\mathrm{RBC}}(\mathbf{r},t)}, \quad (34)$$

where, $\langle\rangle_1$ denotes a conditional average with the position of one particle held fixed, $\mathbf{v}_1$ is the velocity of the chosen particle, $D_s$ is the self-diffusivity tensor for a particle and $F$ is the Helmholtz free energy defined as a function of the one-body particle density, i.e., $F[\rho^{\mathrm{RBC}}(\mathbf{r}, t)] = F^{\mathrm{id}}[\rho^{\mathrm{RBC}}(\mathbf{r}, t)] + F^{\mathrm{ex}}[\rho^{\mathrm{RBC}}(\mathbf{r}, t)] + \int_v U_{\mathrm{ext}}(\mathbf{r}, t)\rho^{\mathrm{RBC}}(\mathbf{r}, t)]$. Here, $F^{\mathrm{id}}$ is the ideal gas free energy, i.e., $F^{\mathrm{id}} = k_{\mathrm{B}}T\int_v \rho^{\mathrm{RBC}}(\mathbf{r}, t)[\ln(\rho^{\mathrm{RBC}}(\mathbf{r}, t)\mathbf{\Lambda}^3)-1]d\mathbf{r}$ with $\mathbf{\Lambda}$ being the thermal de Broglie wavelength of the particle, $U_{ext}$ is the external potential energy, and $F^{\mathrm{ex}}$ denotes the excess Helmholtz free energy.

Considering the steady-state behavior of the system, the DDFT equation for $\rho^{\mathrm{RBC}}(\mathbf{r})$ under fixed particle number condition is expressed as:

$$\rho^{\mathrm{RBC}}(r) = \rho_{\mathrm{b}} \exp\left\{ -\frac{1}{k_{\mathrm{B}}T} \frac{\delta F^{\mathrm{ex}}\left[\rho^{\mathrm{RBC}}(r)\right]}{\delta \rho^{\mathrm{RBC}}(r)} + \frac{1}{k_{\mathrm{B}}T} \frac{\delta F^{\mathrm{ex}}(\rho_{\mathrm{b}})}{\delta \rho_{\mathrm{b}}} - \frac{U_{\mathrm{ext}}(r)}{k_{\mathrm{B}}T} + \int_0^r \frac{f_{\mathrm{lift}}(r')}{k_{\mathrm{B}}T} \mathrm{d}r' \right\}, \tag{35}$$

where, $\rho_{\mathrm{b}}$ is the particle number density in the bulk and $f_{\mathrm{lift}}$ is the lift force acting on a chosen particle. The margination potential felt by each NP at every position $r'$ is defined as:

$$\mathbf{\Phi}^{\mathrm{RBC}}(r') = \int_V \rho^{\mathrm{RBC}}(r) \left\langle \phi(r', r) \right\rangle \mathrm{d}r, \tag{36}$$

where $\rho^{\mathrm{RBC}}$ is the density of RBCs at some distance $r$ and $\phi$ represents the interaction of a given spherical particle with RBCs using the following Weeks-Chandler-Andersen (WCA) type potential:

$$\phi(r, r') = 4\varepsilon \left[ \left( \frac{\sigma}{r - r'} \right)^{12} - \left( \frac{\sigma}{r - r'} \right)^{6} + \frac{1}{4} \right]. \tag{37}$$

Here, $\varepsilon = 0.7 k_{\mathrm{B}} T$ and $\sigma = \frac{a+b}{2}$ with $a$ and $b$ being the radius of NP and RBC respectively, denote the energy and length units, respectively. The margination potential defined in Eq. (36) comes from hydrodynamic origin at the steady-state as clearly demonstrated in Ref. [290] in the DDFT approach. The force due to margination, i.e., $F^{\mathrm{marg}} = -\nabla \mathbf{\Phi}^{\mathrm{RBC}}$ is stochastically exerted by passing RBCs, which migrate to the axis of flow and varies with distance from the wall. It is possible to include the margination force on the NP, based on the NP effective radius, as an external non-Brownian force term.

Finally, the lift force felt by a given spherical NP with radius of $r_s$ in the region of the parabolic flow of length $L$ is determined by Yu et al. [290]:

$$\frac{F_{\mathrm{lift}}(\gamma)}{k_{\mathrm{B}}T} = RePe \beta_{\perp} \frac{5}{288} \left( \frac{r_s}{L^2} \right) \left( 1 - \frac{\gamma}{L} \right) \left( 22 - 73 \frac{\gamma}{L} \right). \tag{38}$$

Here, $RePe$ is product of the Reynolds number and Peclet number, and $\beta_{\perp}$ denotes the wall-induced resistivity factor, defined as $\beta_{\perp} = 1 - \frac{9}{8}\left(\frac{r_s}{\gamma}\right) + \frac{1}{2}\left(\frac{r_s}{\gamma}\right)^3 - \frac{2}{8}\left(\frac{r_s}{\gamma}\right)^5$ [292].

### 4.8 Nanoparticle transport and heat transfer in nanomedicine applications

Targeted NPs loaded with drugs that are directed to precise locations in the body (referred to as targeted drug delivery) can improve the treatment and detection of many diseases [293–298]. Targeting of NPs functionalized with antibodies to vascular endothelial surface molecules such as the intracellular adhesion molecule-1 or ICAM1 depends on several physiological factors such as antibody density, receptor expression, cellular mechanical factors, hydrodynamic conditions such as hematocrit (HCT) density, blood flow rates, and

vessel diameters [299,300]. In addition, several design factors such as size, shape, flexibility/stiffness, and NP architecture, collectively influence targeting efficacy (i.e., tissue selectivity as well as avidity), see Refs. [300,301] and references therein. However, the individual contributions of this multitude of factors are often not discernible leading to largely an empirical and exhaustive search for optimal design. In particular, there is a need for precise control of the specificity and selectivity of binding of the NPs to the target (inflamed or diseased) tissue of interest under varying pathophysiological and hydrodynamic conditions in the vasculature.

In previous studies, it has been shown that modeling can serve as a predictive tool in designing the functionalization characteristics of rigid NPs [302–311]. In this case, the enthalpy of multivalent binding is compensated by the translational entropy loss of bound receptors on the cell surface to a large extent, as well as the entropy loss of NP translation and rotation. These studies demonstrate that modeling can play a crucial role by providing rational design principles for rigid NP based on the underlying thermodynamic and hydrodynamic considerations.

Experimental and modeling studies (using Brownian dynamics) of flexible NPs have revealed that the flexibility can introduce different hydrodynamic effects that can be exploited in targeted drug delivery [69,70,312,313]. How precisely the internal hydrodynamics of NP relaxation is coupled to the external hemodynamics, hydrodynamic lift, effect of confinement on carrier mobility to determine NP deformability, multivalent adhesion to cells, and drug release kinetics, is not obvious, and little quantitative mechanistic analyses have been reported to date.

The rules governing multivalent binding behavior for flexible NPs will be quite different from those for rigid NPs noted above on both hydrodynamic as well as adhesion aspects. Specifically, on the hydrodynamic front, the shear, confinement, and interaction with HCT will collectively define the shape of the flexible NP, which through shape-dependent hydrodynamic interactions will impact NP spatial distribution and margination. On the adhesive front, upon multivalent binding, the entropy loss per receptor-ligand bond model is lower for the flexible NP compared to its rigid counterpart, thereby driving larger multivalency [71]. However, an additional contribution to entropy loss resulting from a change in accessible conformations of NP upon binding applies for the flexible NP, which is absent for the rigid NP [71]. The cumulative effects of these entropic contributions will compensate with the enthalpy of multivalent binding leading to new rules for NP binding [71]. Such findings will have a direct impact on the design of flexible NP for a given application demanding a desired selectivity and specificity of binding to the target tissue, which necessitates a departure in our intuition and rational thinking when switching from rigid to flexible functionalized NP. These competing effects can be tuned by controlling the degree of flexibility by tuning the NP stiffness.

Recently, Farokhirad et al. [70,71] reported computational investigations of deformable polymeric nanoparticles (NPs) under colloidal suspension flow and adhesive environment. In these studies, the authors employed a coarse-grained model for the polymeric NP and performed Brownian dynamics (BDs) simulations with hydrodynamic interactions and in the

presence of wall-confinement, particulate margination using DDFT, and wall-adhesion for obtaining NP microstructure, shape, and anisotropic and inhomogeneous transport properties for different NP stiffness. These microscopic properties are utilized in solving the Fokker-Planck equation to obtain the spatial distribution of NP subject to shear, margination due to colloidal microparticles, and confinement due to a vessel wall. Comparing the computational results for the amount of NP margination to the near-wall adhesion regime with those of available binding experiments in cell culture under shear, the study found quantitative agreement on shear-enhanced binding, the effect of particulate volume fraction, and the effect of NP stiffness. The reported combined computational approach and results are expected to enable fine-tuning of design and optimization of flexible NP in targeted drug delivery applications.

Another benefit of using NPs to deliver therapeutics to tumors selectively is their potential to release a large amount of heat in a specific area. In this regard, one treatment type currently under much research because of its potential in applying a dose sufficient to ablate cancerous cells selectively without damaging the surrounding tissue is the use of heat delivered wirelessly by a magnetic ($Fe_3O_4$) nanoparticle (MNP) [314–317]. On the nanoscale, iron oxide particles exhibit superparamagnetic behavior making them as the potential candidate to heat more efficiently than larger magnetic nanoparticles [318]. Certain NPs can be heated by alternating magnetic fields and can be directed by constant magnetic fields [319]. The magnetic fields pass unaffected through healthy tissue and thus can be more localized to specific areas. While this magnetic hypertherapy has shown a great promise, the critical challenge toward heating inside the body is the concern over dispersing of MNPs throughout the tumor but not in the surrounding tissue [320,321]. To achieve a controlled heat release from MNPs, one can distribute the nanoparticles throughout a thermosensitive polymer composite matrix with critical temperature above body temperature. Such composites can create a coating that prohibits the dispersion problems faced in cancer therapy, and at the same time the heat source is more localized to the target tissue through controlling and predicting the heat rates. Then using an external source, a specific area can be heated by raising the temperature from body temperature (about 37°C) to between 41°C and 46°C, which eventually causes the polymers to break down and the drug to be released. However, the elevated temperatures are usually combined with other forms of treatment such as chemotherapy and radiation therapy as the temperature increases are alone not enough to kill all of the tumor cells [322] and as a result, sensitize the tumor [323]. Usually, one or more of the following methods are involved in determining the heat transfer for such thermal ablation of tumors: direct in vivo temperature measurement [324,325], numerical modeling [326–332] and in vitro modeling using tissue phantoms [333–336]. A popular approach is to pursue analytical and numerical solutions modeling the heat transport through blood-perfused tissue [326–328] based on the Pennes equation [326], but it is well acknowledged that the Pennes equation has serious limitations and may only be used for approximate estimates.

## 5. Conclusions

Multiscale hydrodynamic models of NP transport that incorporate multiple scales (e.g., the macroscopic regime, the mesoscopic and the molecular regime), and which couple directly

with each other to define the coupled transport properties of the fluid and the NP provides the algorithmic methodology for a rapid and accurate prescription for optimal nanoparticle design. Due to competing hydrodynamic and molecular forces at disparate lengthscales, traditional multiscale frameworks are not easily amenable for addressing the associated challenges. In this review, we have primarily considered and focused on foundations, numerical implementation, as well as dynamics of nanoparticles in fluids, transport properties, hydrodynamic interactions in the presence of flow fields and hydrodynamic confinement. Fluctuating hydrodynamics, generalized Langevin equations, microscopic including molecular dynamics methods, as studied in existing literature, have all been discussed. Select computations and results for transport properties and flow characteristics in various regimes have been included. In particular, the determination of the autocorrelation functions accurately for long times (compared to the inertial relaxation time) using the deterministic approach provides a direct route for computing transport properties using the appropriate Green-Kubo formula [337]. Several works in the literature have reported calculations of transport properties for models of simple and complex fluids [338,339]. Encouraged by these studies which focused on the molecular level, we propose that the Green-Kubo methodologies can be used to study the properties of suspensions of nanoparticles and nanocomposites at the mesoscopic scale, when combined with computational methods that resolve hydrodynamic interactions and thermal effects simultaneously, including the examples described in this article.

## Acknowledgements

We thank Natesan Ramakrishnan, Uma Balakrishnan, Helena Vitoshkin, Hsiu-Yu Yu, Zahera Jabeen, Yaohong Wang, Karthik Mukundakrishnan, Tirumani Swaminathan, Arijit Sarkar, and Jin Liu for insightful discussions. This work was supported in part by the National Institutes of Health grants 1U54CA193417 and U01CA227550. We acknowledge shared computational resources provided by XSEDE (Grant No. MCB060006). One of the authors (P.S.A) gratefully acknowledges the support given to him at UCLA/MAE where he is a visiting professor.

## Nomenclature

| | |
|---|---|
| $\beta_{\perp}$ | Wall-induced resistivity factor |
| $\delta_{ij}$ | Kronecker delta |
| $\eta_s$ | Shear viscosity |
| **I** | Moment of inertia |
| **J** | Identity tensor |
| **S** | Random stress tensor |
| **u**, $U$ | Velocity |
| $\mu$ | Dynamic Viscosity |
| $\nu$ | Kinematic Viscosity |
| $\rho$ | Density |
| $\sigma$ | Stress tensor |

| | |
|---|---|
| $\tilde{\xi}(t)$ | Unit-Normalized White noise process |
| $\zeta^{(t)}, \zeta^{(r)}$ | Translational and rotational friction coefficient |
| **D** | Diffusion coefficient |
| **F** | Force |
| **k** | Thermal conductivity |
| $k_B$ | Boltzmann constant |
| **m** | Mass |
| **p** | Pressure |
| $P(y, t)$ | Probability |
| **T** | Absolute temperature |
| **t** | Time |
| **V** | Potential energy |
| $x, y, r$ | Position |
| **ALE** | Arbitrary Lagrangian-Eulerian |
| **BD** | Brownian Dynamics |
| **DDFT** | Dynamical density functional theory |
| **DLM** | Distributed-Lagrangian multiplier |
| **DNS** | Direct numerical simulations |
| **FEM** | Finite element method |
| **FENE** | Finitely extensible nonlinear elastic |
| **FHD** | Fluctuating hydrodynamics |
| **GENERIC** | General Equation for Non-Equilibrium Reversible/ Irreversible Coupling |
| **GLE** | Generalized Langevin equations |
| **HCACF** | Heat Current autocorrelation function |
| **HCT** | Hematocrit |
| **HI** | Hydrodynamic interactions |
| **ICAM1** | Intracellular adhesion molecule-1 |
| **LBM** | Lattice Boltzmann method |

| | |
|---|---|
| **LD** | Langevin Dynamics |
| **MD** | Molecular Dynamics |
| **MNP** | Magnetic nanoparticle |
| **MPCD** | Multi-particle collision dynamics |
| **MSD** | Mean Squared Displacement |
| **NFD** | Nanoscale fluid dynamics |
| **NP** | Nanoparticle |
| **NPP** | Nanoscale particle and polymer |
| **PDB** | Protein Data Bank |
| **PDF** | Probability density function |
| **Pe** | Peclet number |
| **RBC** | Red blood cell |
| **Re** | Reynolds number |
| **SACF** | Stress autocorrelation function |
| **SDE** | Stochastic differential equation |
| **SRD** | Stochastic rotational dynamics |
| **VACF** | Velocity autocorrelation function |
| **WCA** | Weeks-Chandler-Andersen |

## References

[1]. Prasher R, Bhattacharya P, Patrick P, Brownian-motion-based convective-conductive model for the effective thermal conductivity of nanofluids, J. Heat Transf 128 (6) (2006a) 588–595, 10.1115/1.2188509.

[2]. Keblinski P, Prasher R, Jacob E, Thermal conductance of nanofluids: is the controversy over? J. Nanoparticle Res 10 (7) (10 2008) 1089–1097, 10.1007/s11051-007-9352-1. ISSN 1572–896X. URL, https://doi.org/10.1007/s11051-007-9352-1.

[3]. Buongiorno J, et al., A benchmark study on the thermal conductivity of nanofluids, J. Appl. Phys 106 (9) (2009), 094312, 10.1063/1.3245330. URL, https://doi.org/10.1063/1.3245330.

[4]. Michaelides E.E. (Stathis), Fundamentals of Nanoparticle Flow and Heat Transfer, Springer International Publishing, Cham, Switzerland, 2014, ISBN 978-3-319-05621-0, pp. 1–45, 10.1007/978-3-319-05621-01. URL, https://doi.org/10.1007/978-3-319-05621-0_1.

[5]. Van Kampen NG, Stochastic Processes in Physics and Chemistry, third ed. edition, Elsevier, Amsterdam, 2007, 10.1016/B978-0-444-52965-7.50023-4. URL, https://www.sciencedirect.com/science/article/pii/B9780444529657500234.

[6]. Chapman S, Burnett D, Cowling TG, The Mathematical Theory of Non-uniform Gases, Cambridge University Press, 1970.

[7]. Bixon M, Zwanzig R, Boltzmann-Langevin equation and hydrodynamic fluctuations, Phys. Rev 187 (1) (11 1969) 267–272.

[8]. Landau LD, Lifshitz EM, in: Landau LD, Lifshitz EM (Eds.), Fluid Mechanics, Second Edition, 2 editionCourse of Theoretical Physics, vol. 6, Butterworth-Heinemann, 1987.

[9]. Hauge EH, Martin-Löf A, Fluctuating hydrodynamics and Brownian motion, J. Stat. Phys 7 (3) (1973) 259–281, 10.1007/BF01030307.

[10]. Chaikin PM, Lubensky TC, Principles of Condensed Matter Physics, Cambridge University Press, Cambridge, England, 2000.

[11]. Landau LD, Lifshitz EM, Fluid Mechanics, Pergamon Press, London, 1959.

[12]. Onsager L, Reciprocal relations in irreversible processes, I. Phys. Rev 37 (1931a) 405–426.

[13]. Onsager L, Reciprocal relations in irreversible processes. II, Phys. Rev 38 (12 1931) 2265–2279.

[14]. Chandler D, Introduction to Modern Statistical Mechanics, Oxford University Press, New York, 1987a.

[15]. Kubo R, The fluctuation-dissipation theorem, Rep. Prog. Phys 29 (1) (1966a) 255–284, 10.1088/0034-4885/29/1/306.

[16]. Kubo R, Toda M, Hashitsume N, Statistical Physics II Nonequilibrium Statistical Mechanics, 2 edition, vol. II, Springer-Verlag, Berlin, 1991.

[17]. Balakrishnan V, Elements of Nonequilibrium Statistical Mechanics, Ane Books, 3 2008.

[18]. Hardy RJ, Energy-flux operator for a lattice, Phys. Rev 132 (1963) 168, 10.1103/PhysRev.132.168.

[19]. Allen MP, Atomic and molecular representations of molecular hydrodynamic variables, Mol. Phys 52 (1984) 705, 10.1080/00268978400101491.

[20]. Allen MP, Tildesley DJ, Computer Simulation of Liquids, second ed., Oxford University Press, New York, 1989.

[21]. Sharma N, Patankar NA, Direct numerical simulation of the Brownian motion of particles by using fluctuating hydrodynamic equations, J. Comput. Phys 201 (2) (2004) 466–486, 10.1016/j.jcp.2004.06.002.

[22]. Donev A, Vanden-Eijnden E, Garcia AL, Bell JB, On the accuracy of explicit finite-volume schemes for fluctuating hydrodynamics, Commun. Appl. Math. Comput. Sci 5 (2) (2010a) 149–197.

[23]. Ladd AJC, Short-time motion of colloidal particles: numerical simulation via a fluctuating Lattice-Boltzmann equation, Phys. Rev. Lett 70 (9) (3 1993) 1339–1342, 10.1103/PhysRevLett.70.1339. [PubMed: 10054351]

[24]. Ladd AJC, Numerical simulations of particulate suspensions via a discretized Boltzmann equation. part 1. theoretical foundation, J. Fluid Mech 271 (1994a) 285–309, 10.1017/S0022112094001771.

[25]. Ladd AJC, Numerical simulations of particulate suspensions via a discretized Boltzmann equation. part 2. numerical results, J. Fluid Mech 271 (1994b) 311–339, 10.1017/S0022112094001783.

[26]. Patankar NA, Direct numerical simulation of moving charged, flexible bodies with thermal fluctuations, in: Technical Proceedings of the 2002 International Conference on Computational Nanoscience and Nanotechnology, vol. 2, Nano Science and Technology Institute, 2002, pp. 93–96.

[27]. Adhikari R, Stratford K, Cates ME, Wagner AJ, Fluctuating lattice–Boltzmann, EPL (Europhysics Letters) 71 (3) (2005) 473–479.

[28]. Dünweg B, Ladd AJC, Lattice–Boltzmann simulations of soft matter systems, Adv. Polym. Sci 221 (2008) 89–166, 10.1007/978-3-540-87706-62.

[29]. Nie D, Lin J, A fluctuating lattice-Boltzmann model for direct numerical simulation of particle Brownian motion, Particuology 7 (6) (2009) 501–506, 10.1016/j.partic.2009.06.012. ISSN 1674–2001.

[30]. Atzberger PJ, Kramer PR, Peskin CS, A stochastic immersed boundary method for fluid-structure dynamics at microscopic length scales, J. Comput. Phys 224 (2) (2007) 1255–1292, 10.1016/j.jcp.2006.11.015. ISSN 0021–9991.

[31]. Voulgarakis NK, Chu J-W, Bridging fluctuating hydrodynamics and molecular dynamics simulations of fluids, J. Chem. Phys 130 (13) (2009) 134111, 10.1063/1.3106717. URL, https://doi.org/10.1063/1.3106717 [PubMed: 19355721]

[32]. Voulgarakis NK, Satish S, Chu JW, Modeling the nanoscale viscoelasticity of fluids by bridging non-markovian fluctuating hydrodynamics and molecular dynamics simulations, J. Chem. Phys 131 (23) (2009a) 234115, 10.1063/1.3273210. [PubMed: 20025322]

[33]. Serrano M, Español P, Thermodynamically consistent mesoscopic fluid particle model, Phys. Rev. E 64 (4) (2001), 046115, 10.1103/PhysRevE.64.046115.

[34]. Serrano M, Gianni DF, Español P, Flekkøy EG, Coveney PV, Mesoscopic dynamics of voronoi fluid particles, J. Phys. A Math. Gen 35 (7) (2002) 1605, 10.1088/0305-4470/35/7/310.

[35]. Grmela M, Öttinger HC, Dynamics and thermodynamics of complex fluids. i. development of a general formalism, Phys. Rev. E 56 (6) (1997) 6620–6632, 10.1103/PhysRevE.56.6620.

[36]. Öttinger HC, Grmela M, Dynamics and thermodynamics of complex fluids. ii. illustrations of a general formalism, Phys. Rev. E 56 (6) (1997) 6633–6655, 10.1103/PhysRevE.56.6633.

[37]. Mynam M, Sunthar P, Ansumali S, Efficient lattice Boltzmann algorithm for brownian suspensions, Philos. Trans. Royal Soc. A 369 (2011) 2237–2245, 10.1098/rsta.2011.0047.

[38]. Liu Z, Zhu Y, Rao RR, Clausen JR, Aidun CK, Efficient Lattice Boltzmann Algorithm for Brownian Suspensions, 2011 arXiv preprint arXiv:180102299.

[39]. Hu HH, Direct simulation of flows of solid-liquid mixtures, Int. J. Multiph. Flow 22 (2) (1996) 335–352, 10.1016/0301-9322(95)00068-2. ISSN 0301-9322.

[40]. Hu HH, Patankar NA, Zhu MY, Direct numerical simulations of fluid-solid systems using the arbitrary langrangian-Eulerian technique, J. Comput. Phys 169 (2) (2001) 427–462, 10.1006/jcph.2000.6592. ISSN 0021–9991.

[41]. Zhang L, Gerstenberger A, Wang X, Liu WK, Immersed finite element method, Comput. Methods Appl. Mech. Eng 193 (21–22) (2004) 2051–2067, 10.1016/j.cma.2003.12.044. ISSN 0045–7825.

[42]. Wang XS, Zhang LT, Liu WK, On computational issues of immersed finite element methods, J. Comput. Phys 228 (7) (2009) 2535–2551, 10.1016/j.jcp.2008.12.012. ISSN 0021–9991.

[43]. George PL, Automatic Mesh Generation: Application to Finite Element Methods, Wiley, New York, 1991.

[44]. Swaminathan TN, Mukundakrishnan K, Hu HH, Sedimentation of an ellipsoid inside an infinitely long tube at low and intermediate Reynolds numbers, J. Fluid Mech 551 (2006a) 357–385, 10.1017/S0022112005008402.

[45]. Swaminathan TN, Hu HH, Patel AA, Numerical analysis of the hemodynamics and embolus capture of a greenfield vena cava filter, J. Biomech. Eng 128 (3) (2006b) 360–370, 10.1115/1.2187034. [PubMed: 16706585]

[46]. Mukundakrishnan K, Hu HH, Ayyaswamy PS, The dynamics of two spherical particles in a confined rotating flow: pedalling motion, J. Fluid Mech 599 (2008) 169–204, 10.1017/S0022112007000092.

[47]. Español P, J.G. Anero1, I. Zúñiga, Microscopic derivation of discrete hydrodynamics, J. Chem. Phys 131 (2009) 244117, 10.1063/1.3274222. [PubMed: 20059064]

[48]. Bell JB, Garcia AL, Williams SA, Numerical methods for the stochastic Landau-Lifshitz Navier-Stokes equations, Phys. Rev. E 76 (1) (7 2007), 016708, 10.1103/PhysRevE.76.016708.

[49]. Williams SA, Bell JB, Garcia AL, Algorithm refinement for fluctuating hydrodynamics, Multiscale Model. Simul 6 (2008) 1256–1280, 10.1137/070696180.

[50]. Farokhirad S, Morris JF, Lee T, Coalescence-induced jumping of droplet: inertia and viscosity effects, Phys. Fluids 27 (2015) 102102, 10.1063/1.4932085.

[51]. Farokhirad S, Lee T, Computational study of microparticle effect on self-propelled jumping of droplets from superhydrophobic substrates, Int. J. Multiph. Flow 95 (2017) 220, 10.1016/j.ijmultiphaseflow.2017.05.008.

[52]. Farokhirad S, Shad MM, Lee T, Coalescence-induced jumping of immersed and suspended droplets on microstructured substrates, Eur. J. Comput. Mech 26 (2017a) 1–19, 10.1080/17797179.2017.1306830.

[53]. Shad MM, Lee T, Phase-field lattice Boltzmann modeling of boiling using a sharp-interface energy solver, Phys. Rev. E 96 (2017), 013306, 10.1103/PhysRevE.96.013306. [PubMed: 29347090]

[54]. Xuan Y, Li Q, Yao Z, Application of lattice Boltzmann scheme to nanofluids, Sci. China Ser. E Technol. Sci 47 (2004) 129–140, 10.1360/03ye0163.

[55]. Xuan Y, Yao Z, Lattice Boltzmann model for nanofluids, Heat Mass Transf 41 (2005) 199–205, 10.1007/s00231-004-0539-z.

[56]. Xuan Y, Yu K, Li Q, Investigation on flow and heat transfer of nanofluids by the thermal lattice Boltzmann model, Prog. Comput. Fluid Dyn 5 (2005) 13–19, 10.1504/PCFD.2005.005813.

[57]. Zhou L, Xuan Y, Li Q, Multiscale simulation of nanofluid multiphase flows, J. Comput. Phys 26 (2009) 849–856, 10.1142/S1756973709000074.

[58]. Zhou L, Xuan Y, Li Q, Multiscale simulation of flow and heat transfer of nanofluid with lattice Boltzmann method, Int. J. Multiph. Flow 36 (2010) 364–374, 10.1016/j.ijmultiphaseflow.2010.01.005.

[59]. Sidik NAC, Razali SA, Lattice Boltzmann method for convective heat transfer of nanofluids - a review, Renew. Sustain. Energy Rev 38 (2014) 864–875, 10.1016/j.rser.2014.07.001.

[60]. Sidik NAC, Mamat R, Recent progress on lattice Boltzmann simulation of nanofluids: a review, Int. Commun. Heat Mass Transf 66 (2015) 11–22, 10.1016/j.icheatmasstransfer.2015.05.010.

[61]. Kalteh M, Hasani H, Lattice Boltzmann simulation of nanofluid free convection heat transfer in an l-shaped enclosure, Superlattice Microstruct 66 (2014) 112–128, 10.1016/j.spmi.2013.12.004.

[62]. Mliki B, Abbasi MA, Omri A, Belkacem Z, Lattice Boltzmann analysis of mhd natural convection of cuo-water nanofluid in inclined c-shaped enclosures under the effect of nanoparticles brownian motion, Powder Technol 308 (2017) 70–83, 10.1016/j.powtec.2016.11.054.

[63]. Zhou W, Yan Y, Xie Y, Liu B, Three-dimensional lattice Boltzmann simulation for mixed convection of nanofluids in the presence of magnetic field, Int. Commun. Heat Mass Transf 80 (2017) 1–9, 10.1016/j.icheatmasstransfer.2016.11.012.

[64]. Bhatnagar PL, Gross EP, Krook M, A model for collision processes in gases. i. small amplitude processes in charged and neutral one-component systems, Phys. Rev 94 (1954) 511–525, 10.1103/PhysRev.94.511.

[65]. d'Humires D, Ginzburg I, Krafczyk M, Lallemand P, Luo LS, Multiple-relaxation-time lattice Boltzmann models in three dimensions, Phil. Trans. R. Soc. Lond. A 360 (2002) 437–451, 10.1098/rsta.2001.0955.

[66]. Gompper G, Ihle T, Kroll DM, Winkler RG, Multi-particle collision dynamics a particle-based mesoscale simulation approach to the hydrodynamics of complex fluids, Adv. Polym. Sci 221 (2009) 1–87, 10.1007/978-3-540-87706-6_1.

[67]. Rotne J, Prager S, Variational treatment of hydrodynamic interaction in polymers, J. Chem. Phys 50 (1969) 4831–4837, 10.1063/1.1670977.

[68]. Yamakawa H, Transport properties of polymer chains in dilute solution: hydrodynamic interaction, J. Chem. Phys 53 (1970) 436–443, 10.1063/1.1673799.

[69]. Sarkar A, Eckmann DM, Ayyaswamy PS, Radhakrishnan R, Hydrodynamic interactions of deformable polymeric nanocarriers and the effect of crosslinking, Soft Matter 11 (2015) 5955–5969, 10.1039/C5SM00669D. URL, https://doi.org/10.1039/C5SM00669D. [PubMed: 26126781]

[70]. Farokhirad S, Ramakrishnan N, Eckmann DM, Ayyaswamy PS, Radhakrishnan R, Nanofluid dynamics of flexible polymeric nanoparticles under wall confinement, J. Heat Transf 141 (5) (2019a), 052401 URL, 10.1115/1.4043014.

[71]. Farokhirad S, Ranganathan A, Myerson J, Muzykantov V, Ayyaswamy PS, Eckmann DM, Radhakrishnan R, Stiffness can mediate balance between hydrodynamic forces and avidity to impact the targeting of flexible polymeric nanoparticles in flow, Nanoscale 11 (2019b) 6916–6928. URL, 10.1039/C8NR09594A. [PubMed: 30912772]

[72]. Malevanets A, Kapral R, Mesoscopic model for solvent dynamics, J. Chem. Phys 110 (1999) 8605, 10.1063/1.478857.

[73]. Malevanets A, Kapral R, Solute molecular dynamics in a mesoscale solvent, J. Chem. Phys 112 (2000) 7260, 10.1063/1.481289.

[74]. Kapral R, Multiparticle collision dynamics: simulation of complex systems on mesoscales, Adv. Chem. Phys 140 (2008) 89–146, 10.1002/9780470371572.ch2.

[75]. Yamamoto T, Masaokal N, Numerical simulation of star polymers under shear flow using a coupling method of multi-particle collision dynamics and molecular dynamics, Rheol. Acta 54 (2015) 139–147, 10.1007/s00397-014-0817-8.

[76]. Kikuchi N, Gent A, Yeomans JM, Polymer collapse in the presence of hydrodynamic interactions, Eur. Phys. J 9 (2002) 63–66, 10.1140/epje/i2002-10056-6.

[77]. Ripoll M, Winkler RG, Gompper G, Hydrodynamic screening of star polymers in shear flow, Eur. Phys. J 23 (2007) 349–354, 10.1140/epje/i2006-10220-0.

[78]. Winkler RG, Mussawisade K, Ripoll M, Gompper G, Rodlike colloids and polymers in shear flow: a multi-particle-collision dynamics study, J. Phys. Condens. Matter 16 (2004) S3941–S3954, 10.1088/0953-8984/16/38/012.

[79]. Mussawisade K, Ripoll M, Winkler RG, Gompper G, Dynamics of polymers in a particle-based mesoscopic solvent, J. Chem. Phys 123 (2005), 10.1063/1.2041527, 1449051–11.

[80]. Ripoll M, Winkler RG, Gompper G, Star polymers in shear flow, Phys. Rev. Lett 96 (2006), 10.1103/PhysRevLett.96.188302, 1883021–4.

[81]. Noguchi H, Gompper G, Dynamics of fluid vesicles in shear flow effect of membrane viscosity and thermal fluctuations, Phys. Rev. E 72 (2005a), 011901, 10.1103/PhysRevE.72.011901.

[82]. Noguchi H, Gompper G, Shape transitions of fluid vesicles and red blood cells in capillary flows, Proc. Natl. Acad. Sci 102 (2005b) 14159–14164, 10.1073/pnas.0504243102. [PubMed: 16186506]

[83]. Cannavacciuolo L, Winkler RG, Gompper G, Mesoscale simulations of polymer dynamics in microchannel flows, Europhys. Lett 83 (2008) 34007, 10.1209/0295-5075/83/34007.

[84]. Heine DR, Petersen MK, Grest GS, Effect of particle shape and charge on bulk rheology of nanoparticle suspensions, J. Chem. Phys 132 (2010) 184509, 10.1063/1.3419071.

[85]. Karplus M, Brunger AT, Elber R, Kuriyan J, Molecular dynamics: applications to proteins, Cold Spring Harbor Symp. Quant. Biol 52 (1987) 6679–6685, 10.1101/SQB.1987.052.01.044.

[86]. Karplus M, Kuriyan J, Molecular dynamics and protein function, Proc. Natl. Acad. Sci. U.S.A 102 (19) (2005) 381–390, 10.1073/pnas.0408930102.

[87]. Berman HM, Westbrook J, Feng Z, Gilliland G, Bhat TN, Weissig H, Shindyalov IN, Bourne PE, The protein data bank, Nucleic Acids Res 28 (2000) 235–242, 10.1093/nar/28.1.235. [PubMed: 10592235]

[88]. Farokhirad S, Bradley RP, Sarkar A, Shih A, Telesco S, Liu Y, Venkatramani R, Eckmann DM, Ayyaswamy PS, Radhakrishnan R, Comprehensive Biomaterials II Computational Methods Related to Molecular Structure and Reaction Chemistry of Biomaterials, vol. 3, Elsevier, Amsterdam, Netherlands, 2017b, pp. 245–267.

[89]. MacKerell AD, et al., All-atom empirical potential for molecular modeling and dynamics studies of proteins, J. Phys. Chem. B 102 (18) (1998) 3586–3616, 10.1021/jp973084f. [PubMed: 24889800]

[90]. Foloppe N, Mackerell AD, All-atom empirical force field for nucleic acids i, parameter optimization based on small molecule and condensed phase macromolecular target data, J. Comput. Chem 21 (2000) 86–104, 10.1002/(SICI)1096-987X(20000130)21:2<86::AID-JCC2>3.0.CO;2-G.

[91]. MacKerell AD, Banavali NK, All-atom empirical force field for nucleic acids ii, application to molecular dynamics simulations of DNA and RNA in solution, J. Comput. Chem 21 (2000) 105–120, 10.1002/(SICI)1096-987X(20000130)21:2&<105::AID-JCC3&>3.0.CO;2-PCitedby:374.

[92]. Cheatham TE, Cieplak P, Kollman PA, A modified version of the cornell. force field with improved sugar pucker phases and helical repeat, J. Biomol. Struct. Dyn 16 (1999) 845–862, 10.1080/07391102.1999.10508297. [PubMed: 10217454]

[93]. Wang W, Donini O, Reyes CM, Kollman PA, Biomolecular simulations: recent developments in force fields, simulations of enzyme catalysis, protein-protein, and protein-nucleic acid

noncovalent interactions, Annu. Rev. Biophys. Biomol. Struct 30 (2001) 211–243, 10.1146/annurev.biophys.30.1.211. [PubMed: 11340059]

[94]. Glenn JM, Douglas JT, Michael LK, Constant pressure molecular dynamics algorithms, J. Chem. Phys 101 (5) (1994) 4177–4189, 10.1063/1.467468.

[95]. Brooks BR, Bruccoleri RE, Olafson BD, States DJ, Swaminathan S, Karplus M, Constant pressure molecular dynamics algorithms, J. Chem. Phys 4 (2) (1983) 187–217, 10.1002/jcc.540040211.

[96]. Weiner PW, Kollman PA, Camber: assisted model building with energy refinement, J. Comput. Chem 2 (1981) 287–303, 10.1002/jcc.540020311.

[97]. Scott WRP, Hunenberger PH, Tironi IG, Mark AE, Billeter SR, Fennen J, Torda AE, Huber T, Kruger P, van Gunsteren WF, The gromos biomolecular simulation program package, J. Comput. Chem 103 (1999) 3596–3607, 10.1021/jp984217f.

[98]. Phillips JC, Braun R, Wang W, Gumbart J, Tajkhorshid E, Villa EC, Skeel RD, Kale L, Schulten K, Scalable molecular dynamics with NAMD, J. Comput. Chem 26 (2005) 1781–1802, 10.1002/jcc.20289. [PubMed: 16222654]

[99]. Humphrey W, Dalke A, Schulten K, Vmd - visual molecular dynamics, J. Mol. Graph 14 (1996) 33–38, 10.1016/0263-7855(96)00018-5. [PubMed: 8744570]

[100]. Coco-Enrquez L, Munoz-Anton J, Martinez-Val JM, New text comparison between co2 and other supercritical working fluids (ethane, xe, ch4 and n2) in line-focusing solar power plants coupled to supercritical brayton power cycles, Int. J. Hydrogen Energy 42 (2017) 17611–17631, 10.1016/j.ijhydene.2017.02.071.

[101]. Memon AG, Memon RA, Aermodynamic analysis of a trigeneration system proposed for residential application, Energy Convers. Manag 145 (2017) 182–203, 10.1155/2013/604852.

[102]. Sharma T, Reddy ALM, Chandra TS, Ramaprabhu S, Development of carbon nanotubes and nanofluids based microbial fuel cell, Int. J. Hydrogen Energy 33 (2008) 6749–6754, 10.1016/j.ijhydene.2008.05.112.

[103]. Lapotko D, Plasmonic nanoparticle-generated photothermal bubbles and their biomedical applications l, Nanomedicine 4 (2016) 813–845, 10.2217/nnm.09.59.

[104]. Ramakrishnan N, Tourdot RW, Eckmann DM, Ayyaswamy PS, Muzykantov V, Radhakrishanan R, Biophysically inspired model for functionalized nanocarrier adhesion to cell surface: roles of protein expression and mechanical factors, J. Royal Society Open Science 3 (2016a) 160260.

[105]. Taylor R, Coulombe S, Otanicar T, Phelan P, Gunawan A, Lv W, Rosengarten G, Prasher R, Tyagi H, Small particles, big impacts: a review of the diverse applications of nanofluids, J. Appl. Phys 113 (2013), 011301, 10.1063/1.4754271.

[106]. Peer D, Karp JM, Hong S, Farokhzad OC, Margalit R, Langer R, Nanocarriers as an emerging platform for cancer therapy, Nat. Nanotechnol 2 (2007a) 751–760, 10.1038/nnano.2007.387. [PubMed: 18654426]

[107]. Mitragotri S, Burke BA, Langer R, Overcoming the challenges in administering biopharmaceuticals: formulation and delivery strategies, Nat. Rev. Drug Discov 13 (2014a) 655–672, 10.1038/nrd4363. [PubMed: 25103255]

[108]. Shi J, Kantoff PW, Wooster R, Farokhzad OC, Cancer nanomedicine: progress, challenges and opportunities, Nat. Rev. Cancer 17 (2016) 20–37, 10.1038/nrc.2016.108. [PubMed: 27834398]

[109]. Cooley M, Sarode A, Hoore A, Fedosov DA, Mitragotri S, Gupta AS, Influence of particle size and shape on their margination and wall-adhesion: implications in drug delivery vehicle design across nano-to-micro scale, Nanoscale 10 (2018) 15350. [PubMed: 30080212]

[110]. Maxwell JC, A Treatise on Electricity and Magnetism, second ed. edition, Clarendon Press, Oxford, UK, 1881.

[111]. Choi US, Tran TN, Recent Developments in Non-newtonian Flows and Industrial Applications: Experimental Studies of the Effects of Non-newtonian Surfactant Solutions on the Performance of a Shell-and-Tube Heat Exchanger, vol. 124, American Society of Mechanical Engineers, New York, NY, 1991, pp. 47–52.

[112]. Choi SUS, Cho YI, Kasza KE, Degradation effects of dilute polymer solutions on turbulent friction and heat transfer behavior, J. Non-Newtonian Fluid Mech 41 (1992) 289–307, 10.1016/0377-0257(92)87003-T.

[113]. Xuan Y, Li Q, Heat transfer enhancement of nanofluids, Int. J. Heat Fluid Flow 21 (2000) 58–64, 10.1016/S0142-727X(99)00067-3.

[114]. Das SK, Choi SU, Yu W, Pradeep T, Nanofluids: Science and Technology, John Wiley and Sons, New Jersey, 2008, 10.1002/9780470180693.

[115]. Wen D, Lin G, Vafaei S, Zhang K, Review of nanofluids for heat transfer applications, Particuology 7 (2009) 141–150, 10.1016/j.partic.2009.01.007.

[116]. Hamilton RL, Crosseri OK, Thermal conductivity of heterogeneous two-component systems, Ind. Eng. Chem. Fundam 1 (1962) 187–191, 10.1021/i160003a005.

[117]. Choi SUS, Zhang ZG, Yu WI, Lockwood FE, Grulke EA, Anomalous thermal conductivity enhancement in nanotube suspensions, Appl. Phys. Lett 79 (2001) 2252–2254, 10.1063/1.1408272.

[118]. Eastman JA, Choi SUS, Li S, Yu W, Thompson LJ, Anomalously increased effective thermal conductivities of ethylene glycol-based nanofluids containing copper nanoparticles, Appl. Phys. Lett 78 (2001) 718–720, 10.1063/1.1341218.

[119]. Chopkar M, Das PK, Manna I, Synthesis and characterization of nanofluid for advanced heat transfer applications, Scr. Mater 55 (2006) 549–552, 10.1016/j.scriptamat.2006.05.030.

[120]. Chopkar M, Kumar S, Bhandari D, Das PK, Manna I, Development and characterization of Al2Cu and Ag2Al nanoparticle dispersed water and ethylene/glycol based nanofluid, Mater. Sci. Eng., B 139 (2007) 141–148, 10.1016/j.mseb.2007.01.048.

[121]. Das SK, Putra N, Thiesen P, Roetzel W, Temperature dependence of thermal conductivity enhancement for nanofluids, Mater. Sci. Eng., B 125 (2003a) 567–574, 10.1115/1.1571080.

[122]. Patel HE, Das SK, Sundarajan T, Nair AS, George B, Pradeep T, Thermal conductivities of naked and monolayer protected metal nanoparticle based nanofluids: manifestation of anomalous enhancement and chemical effects, Appl. Phys. Lett 83 (2003) 2931, 10.1063/1.1602578.

[123]. Wen D, Ding Y, Experimental investigation into convective heat transfer of nanofluids at the entrance region under laminar flow conditions, Int. J. Heat Mass Transf 47 (2004) 5181–5188, 10.1016/j.ijheatmasstransfer.2004.07.012.

[124]. Chon CH, Kihm KD, Lee SP, Choi SUS, Empirical correlation finding the role of temperature and particle size for nanofluid (Al2O3) thermal conductivity enhancement, Appl. Phys. Lett 87 (15) (2005) 153107, 10.1063/1.2093936.

[125]. Li CH, Peterson G, Experimental investigation of temperature and volume fraction variations on the effective thermal conductivity of nanoparticle suspensions (nanofluids), J. Appl. Phys 99 (2006), 084314, 10.1063/1.2191571.

[126]. Murshed SMS, Leong KC, Yang C, Investigations of thermal conductivity and viscosity of nanofluids, Int. J. Therm. Sci 47 (2008) 560–568, 10.1016/j.ijthermalsci.2007.05.004.

[127]. Minsta HA, Roy G, Nguyen CT, Doucet D, New temperature dependent thermal conductivity data for water-based nanofluids, Int. J. Therm. Sci 48 (2009) 363–373, 10.1016/j.ijthermalsci.2008.03.009.

[128]. Kole M, Dey T, Enhanced thermophysical properties of copper nanoparticles dispersed in gear oil. applied thermal engineering, Appl. Therm. Eng 56 (2013) 45–53, 10.1016/j.applthermaleng.2013.03.022.

[129]. Lee JH, Lee SH, Jang SP, Do temperature and nanoparticle size affect the thermal conductivity of alumina nanofluids? Appl. Phys. Lett 104 (2014) 10.1063/1.4872164, 161908–53.

[130]. Mehrali M, Sadeghinezhad E, Latibari ST, Mehrali M, Togun H, Zubir M, Metselaar HSC, Preparation, characterization, viscosity, and thermal conductivity of nitrogen-doped graphene aqueous nanofluids, J. Mater. Sci 49 (2014) 7156–7171, 10.1007/s10853-014-8424-8.

[131]. Sundar LS, Ramana EV, Singh MK, Sousa AC, Thermal conductivity and viscosity of stabilized ethylene glycol and water mixture Al2O3 nanofluids for heat transfer applications: an experimental study, Int. Commun. Heat Mass Transf 56 (2014) 86–95, 10.1016/j.icheatmasstransfer.2014.06.009.

[132]. Esfe MH, Saedodin S, Akbari M, Karimipour A, Afrand M, Wongwises S, Dahari M, Experimental investigation and development of new correlations for thermal conductivity of Cuo/EG-water nanofluid, Int. Commun. Heat Mass Transf 65 (2015) 47–51, 10.1016/j.icheatmasstransfer.2015.04.006.

[133]. Lee S, Choi SUS, Li S, Eastman JA, Measuring thermal conductivity of fluids containing oxide nanoparticles, J. Heat Transf 121 (1999) 8–89, 10.1115/1.2825978.

[134]. He Y, Jin Y, Chen H, Ding Y, Cang D, Lu H, Heat transfer and flow behaviour of aqueous suspensions of TiO2 nanoparticles (nanofluids) flowing upward through a vertical pipe, Int. J. Heat Mass Transf 50 (11) (2007) 7–8, 10.1016/j.ijheatmasstransfer.2006.10.024.

[135]. Kim SH, Choi SR, Kim D, Thermal conductivity of metal-oxide nanofluids: particle size dependence and effect of laser irradiation, Journal of Heat and Mass Transfer 129 (3) (2006) 298–307, 10.1115/1.2427071.

[136]. Chen G, Yu W, Singh D, Cookson D, Routbort J, Application of saxs to the study of particle-size-dependent thermal conductivity in silica nanofluids, J. Nanoparticle Res 10 (7) (2008) 1109–1114, 10.1007/s11051-007-9347-y.

[137]. Beck MP, Yuan Y, Warrier P, Teja AS, The effect of particle size on the thermal conductivity of alumina nanofluids, J. Nanoparticle Res 11 (5) (2009) 1129–1136, 10.1007/s11051-008-9500-2.

[138]. Teng TP, Hung YH, Teng TC, Mo HE, Hsu HG, The effect of alumina/water nanofluid particle size on thermal conductivity, Appl. Therm. Eng 30 (2010) 2213–2218, 10.1016/j.applthermaleng.2010.05.036.

[139]. Timofeeva EV, Smith DS, Yu W, France DM, Singh D, Routbort JL, Particle size and interfacial effects on thermo-physical and heat transfer characteristics of water-based alpha-SiC nanofluids. nanotechnology, Nanotechnology 21 (21) (2010) 215703, 10.1088/0957-4484/21/21/215703. [PubMed: 20431197]

[140]. Warrier P, Teja A, Effect of particle size on the thermal conductivity of nanofluids containing metallic nanoparticles, Nanoscale Research Letters 6 (1) (2011) 1–6, 10.1186/1556-276X-6-247.

[141]. Angayarkanni S, Sunny V, Philip J, Effect of nanoparticle size, morphology and concentration on specific heat capacity and thermal conductivity of nanofluids, Journal of Nanofluids 4 (3) (2015) 302–309, 10.1166/jon.2015.1167.

[142]. Lee D, Kim JW, Kim BG, A new parameter to control heat transport in nanofluids: surface charge state of the particle in suspension, J. Phys. Chem. B 110 (2006) 4323–4328, 10.1021/jp057225m. [PubMed: 16509730]

[143]. Timofeeva EV, Yu W, France DM, Singh D, Routbort JL, Base fluid and temperature effects on the heat transfer characteristics of sic in ethylene glycol/H2O and H2O nanofluids, J. Appl. Phys 109 (2011), 014914, 10.1063/1.3524274.

[144]. Keblinski P, Phillpot SR, Choi SU, Eastman JA, Mechanisms of heat flow in suspensions of nanosized particles (nanofluids), Int. J. Heat Mass Transf 45 (2002) 855–863, 10.1016/S0017-9310(01)00175-2.

[145]. Xuan Y, Li Q, Hu W, Aggregation structure and thermal conductivity of nanofluids, AIChE J 94 (2003) 038–1043, 10.1002/aic.690490420.

[146]. Kumar DH, Patel HE, Kumar VR, Sundararajan T, Pradeep T, Das SK, Model for heat conduction in nanofluids, Phys. Rev. Lett 93 (2004) 144301, 10.1103/PhysRevLett.93.144301. [PubMed: 15524799]

[147]. Jang SP, Choi SUS, Role of brownian motion in the enhanced thermal conductivity of nanofluids, Appl. Phys. Lett 93 (2004) 144301, 10.1063/1.1756684.

[148]. Evans W, Fish J, Keblinski P, Role of brownian motion hydrodynamics on nanofluid thermal conductivity, Appl. Phys. Lett 88 (2006), 093116, 10.1063/1.2179118.

[149]. Murshed SMS, Leong KC, Yang C, A combined model for the effective thermal conductivity of nanofluids, Appl. Therm. Eng 29 (2009) 2477–2483, 10.1016/j.applthermaleng.2008.12.018.

[150]. Yu W, Choi SU, The role of interfacial layers in the enhanced thermal conductivity of nanofluids: a renovated maxwell model, J. Nanoparticle Res 5 (2003) 167–177, 10.1023/A:1024438603801.

[151]. Xue L, Keblinski P, Phillpot SR, Choi SUS, Eastman JA, Two regimes of thermal resistance at a liquid-solid interface, J. Chem. Phys 118 (2003) 337–339, 10.1063/1.1525806.

[152]. Xue L, Keblinski P, Phillpot SR, Choi SUS, Eastman JA, Effect of liquid layering at the liquid-solid interface on thermal transport, Int. J. Heat Mass Transf 47 (2004) 4277–4284, 10.1016/j.ijheatmasstransfer.2004.05.016.

[153]. Xie H, Fujii M, Zhang X, Effect of interfacial nanolayer on the effective thermal conductivity of nanoparticle-fluid mixture, Int. J. Heat Mass Transf 48 (2005) 2926–2932, 10.1016/j.ijheatmasstransfer.2004.10.040.

[154]. Xue Q, Xu WM, A model of thermal conductivity of nanofluids with interfacial shells, Mater. Chem. Phys 90 (2005) 298–301, 10.1016/j.matchemphys.2004.05.029.

[155]. Choi SUS, Zhang ZG, Keblinski P, Nanofluids in Encyclopedia of Nanoscience and Nanotechnology, vol. 6, American Scientific Publishers, CA, 2004, pp. 757–773.

[156]. Koo J, Kleinstreuer C, A new thermal conductivity model for nanofluids, J. Nanoparticle Res 6 (2004) 577–588, 10.1007/s11051-004-3170-5.

[157]. Ren Y, Xie H, Cai A, Effective thermal conductivity of nanofluids containing spherical nanoparticles, J. Phys. D Appl. Phys 38 (2005) 3958, 10.1088/0022-3727/38/21/019.

[158]. Prasher R, Bhattacharya P, Phelan PE, Thermal conductivity of nanoscale colloidal solutions (nanofluids), Phys. Rev. Lett 94 (2005), 025901, 10.1103/PhysRevLett.94.025901. [PubMed: 15698196]

[159]. Prasher R, Bhattacharya P, Phelan PE, Effect of aggregation kinetics on the thermal conductivity of nanoscale colloidal solutions (nanofluid), J Nano Let 6 (2006b) 1529–1534, 10.1021/nl060992s.

[160]. Krishnamurthy S, Bhattacharya P, Phelan PE, Prasher R, Enhanced mass transport in nanofluids, Nano Lett 6 (2006) 419–423, 10.1021/nl0522532. [PubMed: 16522034]

[161]. Patel HE, Anoop K, Sundararajan T, Das SK, A micro-convection model for thermal conductivity of nanofluids, Pramana 65 (2006) 863–869, 10.1615/IHTC13.p8.240.

[162]. Xuan Y, Li Q, Zhang X, Fujii M, Stochastic thermal transport of nanoparticle suspensions, J. Appl. Phys 100 (2006), 043507, 10.1063/1.2245203.

[163]. Patel HE, Sundararajan T, Das SK, A cell model approach for thermal conductivity of nanofluids, J. Nanoparticle Res 10 (2008) 87–97, 10.1007/s11051-007-9236-4.

[164]. Shima P, Philip J, Raj B, A role of microconvection induced by brownian motion of nanoparticles in the enhanced thermal conductivity of stable nanofluids, J. Nanoparticle Res 94 (2009) 223101, 10.1063/1.3147855.

[165]. Prasher R, Evans W, Meakin P, Fish J, Phelan PE, Keblinski P, Effect of aggregation on thermal conduction in colloidal nanofluids, Appl. Phys. Lett 89 (2006c) 14311, 10.1063/1.2360229.

[166]. Prasher R, Phelan PE, Bhattacharya P, Effect of aggregation kinetics on the thermal conductivity of nanoscale colloidal solutions (nanofluid), Nano Lett 6 (2006d) 1529–1534, 10.1021/nl060992s. [PubMed: 16834444]

[167]. Feng Y, Yu B, Xu P, Zhou M, The effective thermal conductivity of nanofluids based on the nanolayer and the aggregation of nanoparticles, J. Phys. D Appl. Phys 40 (2007) 3164, 10.1088/0022-3727/40/10/020.

[168]. Evans W, Prasher W, Fish J, Meakin P, Phelan P, Keblinski P, Effect of aggregation and interfacial thermal resistance on thermal conductivity of nanocomposites and colloidal nanofluids, Int. J. Heat Mass Transf 51 (2008) 1431–1438, 10.1016/j.ijheatmasstransfer.2007.10.017.

[169]. Pang C, Jung JY, Kang YT, Effect of aggregation and interfacial thermal resistance on thermal conductivity of nanocomposites and colloidal nanofluids, Int. J. Heat Mass Transf 72 (2014) 392–399, 10.1016/j.ijheatmasstransfer.2013.12.055.

[170]. Masuda H, Ebata A, Teramae K, Hishinuma N, Alteration of thermal conductivity and viscosity of liquid by dispersing ultra-fine particles. dispersion of Al2O3, SiO2 and TiO2 ultra-fine particles, Netsu Bussei 7 (1993) 227–233, 10.2963/jjtp.7.227.

[171]. Wang X, Xu XF, Choi SUS, Thermal conductivity of nanoparticle-fluid mixture, Thermophysics Heat Transfer 13 (1999) 474–480, 10.2514/2.6486.

[172]. Eastman JA, Choi SUS, Li S, Soyez G, Thompson LJ, Melfi RJD, Novel thermal properties of nanostructured materials, Mater. Sci. Forum 312–314 (1999) 629–634, 10.4028/www.scientific.net/MSF.312-314.629.

[173]. Xie HQ, Wang JC, Xi TG, Liu Y, Ai F, Wu QR, Thermal conductivity enhancement of suspensions containing nanosized alumina particles, J. Appl. Phys 91 (2002) 4568, 10.1063/1.1454184.

[174]. Heris SZ, Etemad SG, Esfahany AN, Experimental investigation of oxide nanofluids laminar flow convective heat transfer, Int. Commun. Heat Mass 33 (2006) 529–535, 10.1016/j.icheatmasstransfer.2006.01.005.

[175]. Hong TK, Yang HS, Choi CJ, Study of the enhanced thermal conductivity of fe nanofluids, J. Appl. Phys 97 (2005), 064311, 10.1063/1.1861145.

[176]. Murshed SM, Leong KC, Yang C, Enhanced thermal conductivity of TiO2-water based nanofluids, Int. J. Therm. Sci 44 (2005) 367–373, 10.1016/j.ijthermalsci.2004.12.005.

[177]. Leong KC, Yang C, Murshed SMS, A model for the thermal conductivity of nanofluids - the effect of interfacial layer, J. Nanoparticle Res 8 (2006) 245, 10.1007/s11051-008-9535-4.

[178]. Xhu H, Zhang C, Liu S, Tang Y, Yin Y, Effects of nanoparticle clustering and alignment on thermal conductivities of Fe3O4 aqueous nanofluids, Appl. Phys. Lett 89 (2006), 023123, 10.1063/1.2221905.

[179]. Zhang HY, Wu QC, Lin J, Chen J, Xu ZW, Thermal conductivity of polyethylene glycol nanofluids containing carbon coated metal nanoparticles, J. Appl. Phys 108 (2010) 124304, 10.1063/1.3486488.

[180]. Kubo R, Statistical-mechanical theory of irreversible processes: I. general theory and simple applications to magnetic and conduction problems, J. Phys. Soc. Jpn 12 (1957) 570–586, 10.1143/JPSJ.12.570.

[181]. Hoover WG, Computational Statistical Mechanics, Elsevier Science, New York, 1990.

[182]. Rapaport DC, The Art of Molecular Dynamics Simulation, second ed., Cambridge University Press, New York, 2004.

[183]. Sarkar S, Selvam RP, Molecular dynamics simulation of effective thermal conductivity and study of enhanced thermal transport mechanism in nanofluids, J. Appl. Phys 102 (2007), 074302, 10.1063/1.2785009.

[184]. Murshed SM, Leong KC, Yang C, Enhanced thermal conductivity of TiO2-water based nanofluids, Int. J. Therm. Sci 44 (2006) 367–373, 10.1007/s11051-008-9535-4.

[185]. Bhattacharya P, Saha S, Yadav A, Phelan P, Prasher R, Brownian dynamics simulation to determine the effective thermal conductivity of nanofluids, J. Appl. Phys 95 (2004) 6492–6494, 10.1063/1.1736319.

[186]. Eapen J, Li J, Yip S, Mechanism of thermal transport in dilute nanocolloids, Phys. Rev. Lett 98 (2007a), 028302, 10.1103/PhysRevLett.98.028302. [PubMed: 17358654]

[187]. Teng KL, Hsiao PY, Hung SW, Chieng CC, Liu MS, Lu MC, Enhanced thermal conductivity of nanofluids diagnosis by molecular dynamics simulations, J. Nanosci. Nanotechnol 8 (2008) 3710. [PubMed: 19051928]

[188]. Sankar N, Mathew N, Sobhan C, Molecular dynamics modeling of thermal conductivity enhancement in metal nanoparticle suspensions, Int. Commun. Heat Mass Transf 35 (2008) 867–872, 10.1016/j.icheatmasstransfer.2008.03.006.

[189]. Sachdeva P, Kumar R, Effect of hydration layer and surface wettability in enhancing thermal conductivity of nanofluids, Appl. Phys. Lett 95 (2009) 223105, 10.1063/1.3270003.

[190]. Jain S, Patel HE, Das SK, Brownian dynamics simulation for the prediction of effective thermal conductivity of nanofluid, J. Nanoparticle Res 11 (2009) 767–773, 10.1007/s11051-008-9454-4.

[191]. Kang H, Zhang Y, Yang M, Li L, Molecular dynamics simulation on effect of nanoparticle aggregation on transport properties of a nanofluid, J. Nanotechnol. Eng. Med 3 (2012), 021001, 10.1115/1.4007044.

[192]. Lee S, Saidur R, Sabri M, Min T, Effects of the particle size and temperature on the efficiency of nanofluids using molecular dynamic simulation, Numer. Heat Transf., Part A: Applications 69 (2016) 996–1013, 10.1080/10407782.2015.1109369.

[193]. Muraleedharan MG, Sundaram DS, Herry A, Yang V, Thermal conductivity calculation of nano-suspensions using green-kubo relations with reduced artificial correlations, J. Phys. Condens. Matter 29 (2017) 155302, 10.1088/1361-648X/aa5f08. [PubMed: 28170348]

[194]. Xie H, Lee H, Youn W, Choi M, Nanofluids containing multiwalled carbon nanotubes and their enhanced thermal conductivities, J. Appl. Phys 94 (2003) 4967–4971, 10.1063/1.1613374.

[195]. Babaei H, Keblinski P, Khodadadi JM, A proof for insignificant effect of brownian motion-induced microconvection on thermal conductivity of nanofluids by utilizing molecular dynamics simulations, J. Appl. Phys 113 (2013) 1–5, 10.1063/1.1613374.

[196]. Cui W, Zhaojie S, Jianguo Y, Shaohua W, Minli B, Influence of nanoparticle properties on the thermal conductivity of nanofluids by molecular dynamics simulation, The Royal Society of Chemistry 4 (2014) 55580–55589, 10.1039/C4RA07736A.

[197]. Lee JW, Meade AJ, Barrera EV Jr., Templeton JA, Thermal transport mechanisms in carbon nanotube-nanofluids identified from molecular dynamics simulations, J. Heat Transf 137 (2015a) 1–8, 10.1115/1.4029913.

[198]. Lee SL, Rahman S, Sabri MFM, Min TK, Molecular dynamic simulation on the thermal conductivity of nanofluids in aggregated and non- aggregated states, Numer. Heat Transf 68 (2015b) 432–453, 10.1080/10407782.2014.986366.

[199]. Jia T, Zhang Y, Ma HB, Chen JK, Investigation of the characteristics of heat current in a nanofluid based on molecular dynamics simulation, Appl. Phys. A 108 (2012) 537–544, 10.1007/s00339-012-7019-y.

[200]. Yu W, France DM, Routbort JL, Choi SUS, Review and comparison of nanofluid thermal conductivity and heat transfer enhancements, Heat Transf. Eng 29 (5) (2008) 43–46, 10.1080/01457630701850851.

[201]. Lu WQ, Fan QM, Study for the particle's scale effect on some thermophysical properties of nanofluids by a simplified molecular dynamics method, Eng. Anal. Bound. Elem 32 (2008) 282–289, 10.1016/j.enganabound.2007.10.006.

[202]. Venerus DC, Kabadi MS, Lee S, Perez-Luna V, Study of thermal transport in nanoparticle suspensions using forced Rayleigh scattering, J. Appl. Phys 100 (2006), 062501, 10.1063/1.2360378.

[203]. Zhang X, Gu H, Fujii M, Experimental study on the effective thermal conductivity and thermal diffusivity of nanofluid, Int. J. Thermophys 27 (2006a) 569–580, 10.1007/s10765-006-0054-1.

[204]. Zhang X, Gu H, Fujii M, Effective thermal conductivity and thermal diffusivity of nanofluids containing spherical and cylindrical nanoparticles, Exp. Therm. Fluid Sci 31 (2006b) 593–599, 10.1016/j.expthermflusci.2006.06.009.

[205]. Beck MP, Sun T, Teja AS, The thermal conductivity of alumina nanoparticles dispersed in ethylene glycol, Fluid Phase Equilib 260 (2007) 275–278, 10.1016/j.fluid.2007.07.034.

[206]. Timofeeva EV, Gavrilov AN, McCloskey JM, Tolmachev YV, Sprunt S, Lopatina LM, Selinger JV, Thermal conductivity and particle agglomeration in alumina nanofluids: experiment and theory, Physical Review E 76 (2007), 061203, 10.1103/PhysRevE.76.061203.

[207]. Penas JRV, Zarate JMO, Khayet M, Measurement of the thermal conductivity of nanofluids by the multicurrent hot-wire method, J. Appl. Phys 104 (2008), 044314, 10.1063/1.2970086.

[208]. Singh D, Timofeeva E, Yu W, Routbort J, France D, Smith D, Lopez-Cepero JM, An investigation of silicon carbide-water nanofluid for heat transfer applications, J. Appl. Phys 105 (2009), 064306, 10.1063/1.3082094.

[209]. Beck MP, Yuan Y, Warrier P, Teja AS, The thermal conductivity of alumina nanofluids in water, ethylene glycol, and ethylene glycol+ water mixtures, J. Nanoparticle Res 12 (2010) 1469–1477, 10.1007/s11051-009-9716-9.

[210]. Pastoriza-Gallego MJ, Lugo L, Legido JL, Pineiro MM, Thermal conductivity and viscosity measurements of ethylene glycol-based Al2O3 nanofluids, Nanoscale Research Letters 6 (2011a) 1–11, 10.1186/1556-276X-6-221.

[211]. Mohebbi A, prediction, Of specific heat and thermal conductivity of nanofluids by a combined equilibrium and non-equilibrium molecular dynamics simulation, J. Mol. Liq 175 (2012) 51–58, 10.1016/j.molliq.2012.08.010.

[212]. Pak BC, Cho YI, Hydrodynamic and heat transfer study of dispersed fluids with submicron metallic oxide particles, Exp. Heat Transf 11 (1998) 151–170, 10.1080/08916159808946559.

[213]. Chen H, Ding Y, He Y, Tan C, Rheological behaviour of ethylene glycol based titania nanofluids, Chem. Phys. Lett 444 (2007a) 333–337, 10.1016/j.cplett.2007.07.046.

[214]. Chen H, Ding Y, He Y, Tan C, Rheological behaviour of nanofluids, New J. Phys 9 (2007b) 367, 10.1088/1367-2630/9/10/367.

[215]. Nguyen CT, Desgranges F, Roy G, Galanis N, Mare T, Boucher S, Mintsa HA, Temperature and particle-size dependent viscosity data for water-based nanofluids-hysteresis phenomenon, Int. J. Heat Fluid Flow 28 (2007) 1492–1596, 10.1016/j.ijheatfluidflow.2007.02.004.

[216]. Nguyen CT, Desgranges F, Galanis N, Roy G, Mare T, Boucher S, Mintsa HA, Viscosity data for Al2O3/water nanofluid hysteresis: is heat transfer enhancement using nanofluids reliable? Int. J. Therm. Sci 47 (2008) 103–111, 10.1016/j.mseb.2007.01.048.

[217]. Anoop K, Sundararajan T, Das SK, Effect of particle size on the convective heat transfer in nanofluid in the developing region, Int. J. Heat Mass Transf 52 (2009) 2189–2195, 10.1016/j.ijheatmasstransfer.2007.11.063.

[218]. Chen H, Ding Y, Lapkin A, Fan X, Rheological behaviour of ethylene glycol-titanate nanotube nanofluids, J. Nanoparticle Res 11 (2009a) 1513–1520, 10.1007/s11051-009-9599-9.

[219]. Chen H, Witharana S, Jin Y, Kim C, Ding Y, Predicting thermal conductivity of liquid suspensions of nanoparticles (nanofluids) based on rheology, Particuology 7 (2009b) 151–157, 10.1016/j.partic.2009.01.005.

[220]. Chandrasekar M, Suresh S, Chandra BA, Experimental investigations and theoretical determination of thermal conductivity and viscosity of Al2O3/water nanofluid, Exp. Therm. Fluid Sci 34 (2010) 210–216, 10.1016/j.expthermflusci.2009.10.022.

[221]. Kole M, Dey T, Viscosity of alumina nanoparticles dispersed in car engine coolant, Exp. Therm. Fluid Sci 34 (2010) 677–683, 10.1016/j.expthermflusci.2009.12.009.

[222]. Einstein A, Investigation of the Brownian Theory of Movement, Dover Publication, New York, 1956.

[223]. Batchelor G, The effect of brownian motion on the bulk stress in a suspension of spherical particles, J. Fluid Mech 83 (1977) 97–117, 10.1017/S0022112077001062.

[224]. Mahbubul I, Saidur R, Amalina M, Latest developments on the viscosity of nanofluids, Int. J. Heat Mass Transf 55 (2012) 874–885, 10.1016/j.ijheatmasstransfer.2011.10.021.

[225]. Das SK, Putra N, Roetzel W, Pool boiling characteristics of nanofluids, Int. J. Heat Mass Transf 46 (2003b) 851–862, 10.1016/S0017-9310(02)00348-4.

[226]. Putra N, Roetzel W, Das SK, Natural convection of nanofluids, Heat Mass Transf 39 (2003) 775–784, 10.1007/s00231-002-0382-z.

[227]. Rudyak VY, Krasnolutskii SL, Dependence of the viscosity of nanofluids on nanoparticle size and material, Phys. Lett. A 378 (2014) 1845–1849, 10.1016/j.physleta.2014.04.060.

[228]. Rudyak VY, Krasnolutskii SL, Simulation of the nanofluid viscosity coefficient by the molecular dynamics method, Tech. Phys 60 (2015) 798–804, 10.1134/S1063784215060237.

[229]. Lou Z, Yang M, Molecular dynamics simulations on the shear viscosity of Al2O3 nanofluids, Comput. Fluids 117 (2015) 17–23, 10.1016/j.compfluid.2015.05.006.

[230]. Bushehri MK, Mohebbi A, Rafsanjani HH, Prediction of thermal conductivity and viscosity of nanofluids by molecular dynamics simulation, J. Eng. Thermophys 25 (2016) 389–400, 10.1134/S1810232816030085.

[231]. Chevalier J, Tillement O, Ayela F, Rheological properties of nanofluids flowing through microchannels, Appl. Phys. Lett 91 (2007) 233103, 10.1063/1.2821117.

[232]. Pastoriza-Gallego MJ, Casanova C, Legido JL, Pineiro MM, Cuo in water nanofluid: influence of particle size and polydispersity on volumetric behaviour and viscosity, Fluid Phase Equilib 300 (2011b) 188–196, 10.1016/j.fluid.2010.10.015.

[233]. Prasher R, Song D, Wang J, Phelan P, Measurements of nanofluid viscosity and its implications for thermal applications, Appl. Phys. Lett 89 (2006e) 133108, 10.1063/1.2356113.

[234]. Rudyak VY, Belkin A, Egorov V, On the effective viscosity of nanosuspensions, Tech. Phys 54 (2009) 1102–1109, 10.1134/S1063784209080039.

[235]. Namburu PK, Kulkarni DP, Misra D, Das DK, Viscosity of copper oxide nanoparticles dispersed in ethylene glycol and water mixture, Exp. Therm. Fluid Sci 32 (2007) 397–402, 10.1016/j.expthermflusci.2007.05.001.

[236]. Murshed SMS, Santos FJV, de Castro CAN, Rheology of nanofluids containing TiO2 and SiO2 nanoparticles, in: Proc. 8th World Conference on Experimental Heat Transfer, Fluid Mechanics, and Thermodynamics, 2013.

[237]. Loya A, Ren G, Molecular dynamics simulation study of rheological properties of CuO-water nanofluid, J. Mater. Sci 50 (2015) 4075–4082, 10.1007/s10853-015-8963-7.

[238]. Rubio FJ, Ayucar-Rubi MF, Velazquez-Navarro JF, Galindo-Rosales FJ, Intrinsic viscosity of SiO2, Al2O3 and TiO2 aqueous suspensions, J. Colloid Interface Sci 298 (2006) 967–972, 10.1016/j.jcis.2006.01.009. [PubMed: 16457835]

[239]. Chen H, Ding Y, Heat transfer and rheological behaviour of nanofluids; a review, in: Advances in Transport Phenomena, Springer, Berlin, Heidelberg, 2009, pp. 4135–4177, 10.1007/978-3-642-02690-43.

[240]. Pastoriza-Gallego MJ, Casanova C, Paramo R, Barbes B, Legido JL, Pineiro MM, A study on stability and thermophysical properties (density and viscosity) of Al2O3 in water nanofluid, J. Appl. Phys 106 (2009) 64301, 10.1063/1.3187732.

[241]. Zhou SQ, Ni R, Funfschilling D, Viscosity affected by nanoparticle aggregation in Al2O3-water nanofluids, J. Appl. Phys 6 (2011) 248, 10.1186/1556-276X-6-248.

[242]. Srivastava S, Viscosity affected by nanoparticle aggregation in Al2O3-water nanofluids, Appl. Nanosci 2 (2012) 325–331, 10.1007/s13204-012-0082-z.

[243]. Utomo AT, Poth H, Robbins PT, Pacek AW, Experimental and theoretical studies of thermal conductivity, viscosity and heat transfer coefficient of titania and alumina nanofluids, Int. J. Heat Mass Transf 55 (2012) 7772–7781, 10.1016/j.ijheatmasstransfer.2012.08.003.

[244]. Pang C, Lee JW, Kang YT, Enhanced thermal conductivity of nanofluids by nano-convection and percolation network, Heat Mass Transf 52 (2016) 511–520, 10.1007/s00231-015-1569-4.

[245]. Hong K, Hong TK, Yang HS, Thermal conductivity of Fe nanofluids depending on the cluster size of nanoparticles, Appl. Phys. Lett 88 (2006), 031901, 10.1063/1.2166199.

[246]. Karthikeyan N, Philip J, Raj B, Effect of clustering on the thermal conductivity of nanofluids, Mater. Chem. Phys 109 (2008) 50–55, 10.1016/j.matchemphys.2007.10.029.

[247]. Eapen J, Li J, Yip S, Beyond the maxwell limit: thermal conduction in nanofluids with percolating fluid structures, Phys. Rev. E 76 (2007b), 062501, 10.1103/PhysRevE.76.062501.

[248]. Philip J, Shima P, Raj B, Enhancement of thermal conductivity in magnetite based nanofluid due to chainlike structures, Appl. Phys. Lett 91 (2007) 203108, 10.1063/1.2812699.

[249]. Gharagozloo PE, Eaton JK, Goodson KE, Diffusion, aggregation, and the thermal conductivity of nanofluids, Appl. Phys. Lett 93 (2008) 103110, 10.1063/1.2977868.

[250]. Philip J, Shima P, Raj B, Evidence for enhanced thermal conduction through percolating structures in nanofluids, Nanotechnology 19 (2008) 305706, 10.1088/0957-4484/19/30/305706. [PubMed: 21828773]

[251]. Shalkevich N, Shalkevich A, Burgi T, Thermal conductivity of concentrated colloids in different states, J. Phys. Chem. C 114 (2009) 9568–9572, 10.1021/jp910722j.

[252]. Gao J, Zheng R, Ohtani H, Zhu D, Chen G, Experimental investigation of heat conduction mechanisms in nanofluids, Nano Lett 9 (2009) 4128–4132, 10.1021/nl902358m. [PubMed: 19995084]

[253]. Hong J, Kim D, Effects of aggregation on the thermal conductivity of alumina/water nanofluids, Thermochim. Acta 542 (2012) 28–32, 10.1016/j.tca.2011.12.019.

[254]. Vladkov M, Barrat JL, Modeling thermal conductivity and collective effects in a simple nanofluid, J. Comput. Theor. Nanosci 5 (2008) 187–193, 10.1166/jctn.2008.2459.

[255]. Shima P, Philip J, Raj B, Influence of aggregation on thermal conductivity in stable and unstable nanofluids, Appl. Phys. Lett 97 (2010) 153113, 10.1063/1.3497280.

[256]. Angayarkanni S, Philip J, Effect of nanoparticles aggregation on thermal and electrical conductivities of nanofluids, Journal of Nanofluids 3 (2014) 17–25, 10.1166/jon.2014.1083.

[257]. Uma B, Swaminathan TN, Radhakrishnan R, Eckmann DM, Ayyaswamy PS, Nanoparticle Brownian motion and hydrodynamic interactions in the presence of flow fields, Phys. Fluids 23 (7) (2011a), 073602.

[258]. Ramakrishnan N, Wang Y, Eckmann DM, Ayyaswamy PS, Radhakrishnan R, Motion of a nano-spheroid in a cylindrical vessel flow: brownian and hydrodynamic interactions, J. Fluid Mech 821 (6 2017) 117–152. [PubMed: 29109590]

[259]. Einstein A, On the molecular-kinetic theory of the movement by heat of particles suspended in liquids at rest, Ann. Phys 17 (8) (1905) 549–560, 10.1002/andp.19053220806. ISSN 1521–3889.

[260]. Zwanzig R, Nonequilibrium Statistical Mechanics, Oxford University Press, New York, 2001.

[261]. Heyes DM, Nuevo MJ, Morales JJ, Branka AC, Translational and rotational diffusion of model nanocolloidal dispersions studied by molecular dynamics simulations, J. Phys. Condens. Matter 10 (45) (1998) 10159–10178, 10.1088/0953-8984/10/45/005.

[262]. Gotoh T, Kaneda Y, Effect of an infinite plane wall on the motion of a spherical brownian particle, J. Chem. Phys 76 (1982) 3193–3197, 10.1063/1.443364.

[263]. Pagonabarraga I, Hagen MHJ, Lowe CP, Frenkel D, Algebraic decay of velocity fluctuations near a wall, Phys. Rev. E 58 (1998a) 7288–7295, 10.1103/PhysRevE.58.7288.

[264]. Hagen MHJ, Pagonabarraga I, Lowe CP, Frenkel D, Algebraic decay of velocity fluctuations in a confined fluid, Phys. Rev. Lett 78 (1997) 3785–3788, 10.1103/PhysRevLett.78.3785.

[265]. Felderhof BU, Effect of the wall on the velocity autocorrelation function and longtime tail of brownian motion, J. Phys. Chem. B 109 (2005) 21406–21412, 10.1063/1.2084948. [PubMed: 16853777]

[266]. Franosch T, Jeney S, Persistent correlation of constrained colloidal motion, Phys. Rev. E 79 (2009), 031402, 10.1103/PhysRevE.79.031402.

[267]. Vitoshkin H, Yu H-Y, Eckmann DM, Ayyaswamy PS, Radhakrishnan R, Nanoparticle stochastic motion in the inertial regime and hydrodynamic interactions close to a cylindrical wall, Phys. Rev. Fluids 1 (5) (2016), 054104, 10.1103/PhysRevFluids.1.054104. [PubMed: 27830213]

[268]. Español P, Zúñiga I, On the definition of discrete hydrodynamic variables, J. Chem. Phys 131 (2009) 164106, 10.1063/1.3247586. [PubMed: 19894926]

[269]. Donev A, Vanden-Eijnden E, Garcia A, Bell J, On the accuracy of finite-volume schemes for fluctuating hydrodynamics, Commun. Appl. Math. Comput. Sci 5 (2) (2010b) 149–197.

[270]. Iwashita T, Nakayama Y, Yamamoto R, Velocity autocorrelation function of fluctuating particles in incompressible fluids, Prog. Theor. Phys 178 (2009) 86–91, 10.1143/PTPS.178.86.

[271]. Iwashita T, Nakayama Y, Yamamoto R, A numerical model for Brownian particles fluctuating in incompressible fluids, J. Phys. Soc. Jpn 77 (7) (2008a), 074007, 10.1143/JPSJ.77.074007.

[272]. Atzberger PJ, Stochastic Eulerian Lagrangian methods for fluid-structure interactions with thermal fluctuations, J. Comput. Phys 230 (8) (2011) 2821–2837, 10.1016/j.jcp.2010.12.028.

[273]. Ermak DL, McCammon JA, Brownian dynamics with hydrodynamic interactions, J. Chem. Phys 69 (4) (1978) 1352–1360, 10.1063/1.436761.

[274]. Brady JF, Bossis G, Stokesian dynamics, Annu. Rev. Fluid Mech 20 (1) (1988) 111–157, 10.1146/annurev.fl.20.010188.000551.

[275]. Foss DR, Brady JF, Structure, diffusion and rheology of Brownian suspensions by Stokesian dynamics simulation, J. Fluid Mech 407 (2000) 167–200, 10.1017/S0022112099007557.

[276]. Banchio AJ, Brady JF, Accelerated Stokesian dynamics: brownian motion, J. Chem. Phys 118 (22) (2003) 10323–10332, 10.1063/1.1571819.

[277]. Iwashita T, Yamamoto R, Short-time motion of Brownian particles in a shear flow, Phys. Rev. E 79 (3) (3 2009), 031401, 10.1103/PhysRevE.79.031401.

[278]. Uma B, Swaminathan TN, Ayyaswamy PS, Eckmann DM, Radhakrishnan R, Generalized Langevin dynamics of a nanoparticle using a finite element approach: thermostating with correlated noise, J. Chem. Phys 135 (11) (2011b) 114104, 10.1063/1.3635776. [PubMed: 21950847]

[279]. Uma B, Eckmann DM, Ayyaswamy PS, Radhakrishnan R, A hybrid formalism combining fluctuating hydrodynamics and generalized Langevin dynamics for the simulation of nanoparticle thermal motion in an incompressible fluid medium, Mol. Phys 110 (11–12) (2012) 1057–1067, 10.1080/00268976.2012.663510. [PubMed: 22865935]

[280]. Kubo R, The fluctuation-dissipation theorem, Rep. Prog. Phys 29 (1) (1966b) 255–284, 10.1088/0034-4885/29/1/306.

[281]. Pagonabarraga I, Hagen MHJ, Lowe CP, Frenkel D, Algebraic decay of velocity fluctuations near a wall, Phys. Rev. E 58 (6) (1998b) 7288–7295, 10.1103/PhysRevE.58.7288.

[282]. Iwashita T, Nakayama Y, Yamamoto R, A numerical model for brownian particles fluctuating in incompressible fluids, J. Phys. Soc. Jpn (7) (2008b), 074007, 10.1143/JPSJ.77.074007.

[283]. Yu H-Y, Eckmann DM, Ayyaswamy PS, Radhakrishnan R, Composite generalized Langevin equation for Brownian motion in different hydrodynamic and adhesion regimes, Phys. Rev. E 91 (5) (2015), 052303, 10.1063/1.3635776.

[284]. Chandler D, Introduction to Modern Statistical Mechanics, Oxford University Press, New York, 1987b.

[285]. Shang BZ, Voulgarakis NK, Chu J-W, Fluctuating hydrodynamics for multiscale modeling and simulation: energy and heat transfer in molecular fluids, J. Chem. Phys 137 (4) (2012), 044117, 10.1063/1.4738763. URL, https://doi.org/10.1063/1.4738763. [PubMed: 22852607]

[286]. Voulgarakis NK, Satish S, Chu J-W, Modeling the nanoscale viscoelasticity of fluids by bridging non-markovian fluctuating hydrodynamics and molecular dynamics simulations, J. Chem. Phys 131 (23) (2009b) 234115, 10.1063/1.3273210. URL, https://doi.org/10.1063/1.3273210. [PubMed: 20025322]

[287]. Voulgarakis NK, Satish S, Chu J-W, Modelling the viscoelasticity and thermal fluctuations of fluids at the nanoscale, Mol. Simul 36 (7–8) (2010) 552–559, 10.1080/08927022.2010.486832. URL, 10.1080/08927022.2010.486832.

[288]. Kou S, Xie XS, Generalized Langevin equation with fractional Gaussian noise: Sub-diffusion within a single protein molecule, Phys. Rev. Lett 93 (18) (2004) 180603, 10.1103/PhysRevLett.93.180603. [PubMed: 15525146]

[289]. Min W, Luo G, Cherayil BJ, Kou SC, Xie XS, Observation of a power-law memory kernel for fluctuations within a single protein molecule, Phys. Rev. Lett 94 (19) (2005) 198302, 10.1103/PhysRevLett.94.198302. [PubMed: 16090221]

[290]. Yu HY, Jabeen Z, Eckmann DM, Ayyaswamy PS, Radhakrishnan R, Microstructure of flow-driven suspension of hardspheres in cylindrical confinement: a dynamical density functional theory and Monte Carlo study, Langmuir 33 (42) (2017) 11332–11344, 10.1021/acs.langmuir.7b01860. URL, http://pubs.acs.org/doi/abs/10.1021/acs.langmuir.7b01860. [PubMed: 28810736]

[291]. Jabeen Z, Yu HY, Eckmann DM, Ayyaswamy PS, Radhakrishnan R, Rheology of colloidal suspensions in confined flow: treatment of hydrodynamic interactions in particle-based simulations inspired by dynamical density functional theory, Phys. Rev. E 98 (2018), 042602, 10.1103/PhysRevE.98.042602. [PubMed: 30687804]

[292]. Wakiya A, Slow motions of a viscous fluid around two spheres, J. Phys. Soc. Japan 22 (4) (1967) 1101–1109, 10.1143/JPSJ.22.1101. ISSN 0031–9015, 1347–4073.

[293]. Peer D, Karp JM, Hong S, Farokhzad OC, Margalit R, Langer R, Nanocarriers as an emerging platform for cancer therapy, Nat. Nanotechnol 2 (12) (12 2007) 751–760. [PubMed: 18654426]

[294]. Muzykantov V, Targeted drug delivery to endothelial adhesion molecules, ISRN Vascular Medicine 2013 (916254) (1 2013) 1–27.

[295]. Goldberg M, Mahon K, Anderson D, Combinatorial and rational approaches to polymer synthesis for medicine, Adv. Drug Deliv. Rev 60 (9) (2008) 971–978. [PubMed: 18423930]

[296]. Schroeder A, Heller DA, Winslow MM, Dahlman JE, Pratt GW, Langer R, Tyler J, Anderson DG, Treating metastatic cancer with nanotechnology, Nat. Rev. Cancer 12 (1) (1 2012) 39–50.

[297]. Mitragotri S, Anderson DG, Chen X, Chow EK, Ho D, Kabanov AV, Karp JM, Kataoka K, Mirkin CA, Petrosko SH, Shi J, Stevens MM, Sun S, Teoh S, Venkatraman SS, Xia Y, Wang S, Gu Z, Xu C, Accelerating the translation of nanomaterials in biomedicine, ACS Nano 9 (7) (7 2015) 6644–6654. [PubMed: 26115196]

[298]. Mitragotri S, Burke PA, Langer R, Overcoming the challenges in administering biopharmaceuticals: formulation and delivery strategies, Nat. Rev. Drug Discov 13 (9) (8 2014) 655–672. [PubMed: 25103255]

[299]. Brenner JS, et al., Mechanisms that determine nanocarrier targeting to healthy versus inflamed lung regions, Nanomedicine 13 (4) (2017) 1495–1506. [PubMed: 28065731]

[300]. Ayyaswamy PS, Muzykantov V, Eckmann DM, Radhakrishnan R, Nanocarrier hydrodynamics and binding in targeted drug delivery: challenges in numerical modeling and experimental validation, J. Nanotechnol. Eng. Med 4 (1) (2013) 101011–1010115, 10.1115/1.4024004. ISSN 1949–2944 (Print). URL, http://www.ncbi.nlm.nih.gov/pubmed/23917383. [PubMed: 23917383]

[301]. Ding HM, Ma YQ, Theoretical and computational investigations of nanoparticle-biomembrane interactions in cellular delivery, Small 11 (2015) 1055–1071. [PubMed: 25387905]

[302]. Vácha R, Martinez-Veracoechea FJ, Frenkel D, Intracellular release of endocytosed nanoparticles upon a change of ligand-receptor interaction, ACS Nano 6 (12) (12 2012) 10598–10605. [PubMed: 23148579]

[303]. Martinez-Veracoechea FJ, Frenkel D, Designing super selectivity in multivalent nanoparticle binding, Proc. Natl. Acad. Sci. U.S.A 108 (27) (7 2011) 10963–10968. [PubMed: 21690358]

[304]. V Dubacheva G, Curk T, Auzély-Velty R, Frenkel D, Richter RP, Designing multivalent probes for tunable superselective targeting, Proc. Natl. Acad. Sci. U.S.A 112 (18) (5 2015) 5579–5584. [PubMed: 25901321]

[305]. Gonzalez-Rodriguez D, I Barakat A, Dynamics of receptor-mediated nanoparticle internalization into endothelial cells, PLoS One 10 (4) (4 2015), e0122097. [PubMed: 25901833]

[306]. Liu J, Weller GER, Zern B, Ayyaswamy PS, Eckmann DM, Muzykantov VR, Radhakrishnan R, Computational model for nanocarrier binding to endothelium validated using in vivo, in vitro, and atomic force microscopy experiments, Proc. Natl. Acad. Sci 107 (38) (2010) 16530–16535, 10.1073/pnas.1006611107. URL, http://www.pnas.org/content/107/38/16530.abstract. [PubMed: 20823256]

[307]. Liu J, Agrawal NJ, Calderon A, Ayyaswamy PS, Eckmann DM, Radhakrishnan R, Multivalent binding of nanocarrier to endothelial cells under shear flow, Biophys. J 101 (2) (7 2011) 319–326. [PubMed: 21767483]

[308]. Ramakrishnan N, Tourdot RW, Eckmann DM, Ayyaswamy PS, Muzykantov V, Radhakrishnan R, Biophysically inspired model for functionalized nanocarrier adhesion to cell surface: roles of protein expression and mechanical factors, Journal of Royal Society Open Science 3 (6) (2016b) 160260, 10.1098/rsos.160260. [PubMed: 27429783]

[309]. McKenzie M, Ha SM, Rammohan A, Radhakrishnan R, Ramakrishnan N, Multivalent binding of a ligand-coated particle: role of shape, size, and ligand heterogeneity, Biophys. J 114 (8) (2018) 1830–1840. [PubMed: 29694862]

[310]. Zern BJ, Chacko A-M, Liu J, Greineder CF, Blankemeyer ER, Radhakrishnan R, Muzykantov V, Reduction of nanoparticle avidity enhances the selectivity of vascular targeting and PET detection of pulmonary inflammation, ACS Nano 7 (3) (3 2013) 2461–2469. [PubMed: 23383962]

[311]. Tan J, Thomas A, Liu Y, Influence of red blood cells on nanoparticle targeted delivery in microcirculation, Soft Matter 8 (2012) 1934–1946.

[312]. Muller K, Fedosov DA, Gompper G, Margination of micro- and nano-particles in blood flow and its effect on drug delivery, Sci. Rep 4 (4871) (2014) 1–8.

[313]. Fish MB, Fromen CA, Lopez-Cazares G, Golinski AW, Scott TF, Adili R, Holinstat M, Eniola-Adefeso O, Exploring deformable particles in vascular-targeted drug delivery: Softer is only sometimes better, Biomaterials 124 (2017) 169–179. [PubMed: 28209527]

[314]. Rosensweig RE, Heating magnetic fluid with alternating magnetic field, J. Magn. Magn. Mater 252 (2002) 370, 10.1016/S0304-8853(02)00706-0.

[315]. Li CH, Hodgins P, Peterson GP, Experimental study of fundamental mechanisms in inductive heating of ferromagnetic nanoparticles suspension (Fe3O4 iron oxide ferrofluid), J. Appl. Phys 110 (2011), 054303, 10.1063/1.3626049.

[316]. Gilchrist RK, Medal R, Shorey WD, Hanselman RC, Parrott JC, Taylor CB, Selective inductive heating of lymph nodes, Ann. Surg 146 (1957) 596, 10.1097/00000658-195710000-00007. [PubMed: 13470751]

[317]. Wust P, Gneveckow U, Johannsen M, Böhmer D, Henkel T, Kahmann F, Sehouli J, Felix R, Ricke J, Jordan A, Magnetic nanoparticles for interstitial thermotherapy - feasibility, tolerance and achieved temperatures, Int. J. Hyperth 22 (2006) 673, 10.1080/02656730601106037.

[318]. O'Handley RC, Modern Magnetic Materials: Principles and Applications, first ed., John Wiley and Sons, Inc., New York, 2000.

[319]. Deatsch AE, Evans BA, Heating efficiency in magnetic nanoparticle hyperthermia, J. Magn. Magn. Mater 354 (2014) 163–172, 10.1016/j.jmmm.2013.11.006.

[320]. Hergt R, Dutz S, Magnetic particle hyperthermia-biophysical limitations of a visionary tumour therapy, J. Magn. Magn. Mater 311 (2007) 187–192, 10.1016/j.jmmm.2006.10.1156.

[321]. Etheridge ML, Bischof JC, Optimizing magnetic nanoparticle based thermal therapies within the physical limits of heating, Ann. Biomed. Eng 41 (2013) 78–88, 10.1007/s10439-012-0633-1. [PubMed: 22855120]

[322]. Cantillon-Murphy P, Wald LL, Adalsteinsson E, Zahn M, Heating in the MRI environment due to superparamagnetic fluid suspensions in a rotating magnetic field, J. Magn. Magn. Mater 322 (2010) 727–733, 10.1016/j.jmmm.2009.10.050. [PubMed: 20161608]

[323]. Tsafnat N, Tsafnat G, Lambert TD, Jones SK, Modelling heating of liver tumors with heterogeneous magnetic microsphere deposition, Phys. Med. Biol 50 (2005) 2937–2953, 10.1088/0031-9155/50/12/014. [PubMed: 15930612]

[324]. Staruch RM, Ganguly M, Tannock IF, Hynynen K, Chopra R, Enhanced drug delivery in rabbit VX2 tumours using thermosensitive liposomes and MRI controlled focused ultrasound hyperthermia, Int. J. Hyperth 28 (2012) 776–787, 10.3109/02656736.2012.736670.

[325]. Cressman ENK, Geeslin MG, Shenoi MM, Hennings LJ, Zhang Y, Iaizzo PA, Bischof JC, Concentration and volume effects in thermochemical ablation in vivo: results in a porcine model, Int. J. Hyperth 28 (2012) 113–121, 10.3109/02656736.2011.644621.

[326]. Pennes HH, Analysis of tissue and arterial blood temperatures in resting human forearm, J. Appl. Physiol 1 (1948) 93–122, 10.1152/jappl.1948.1.2.93. [PubMed: 18887578]

[327]. Arkin H, Xu L, Holmes KR, Recent developments in modeling heat transfer in blood perfused tissues, IEEE Trans. Biomed. Eng 41 (1994) 97–107, 10.1109/10.284920. [PubMed: 8026856]

[328]. Bagaria HG, Johnson DT, Transient solution to the bioheat equation and optimization for magnetic fluid hyperthermia treatment, Int. J. Hyperth 21 (2005) 57, 10.1080/02656730410001726956.

[329]. Bagaria HG, Johnson DT, Transient solution to the bioheat equation and optimization for magnetic fluid hyperthermia treatment, Int. J. Hyperth 21 (2009) 57, 10.1080/02656730410001726956.

[330]. Serantes D, Baldomir D, Martinez-Boubeta C, Simeonidis K, Angelakeris M, Natividad E, Castro M, Mediano A, Chen DX, Sanchez A, Balcells LI, Martínez B, Influence of dipolar interactions on hyperthermia properties of ferromagnetic particles, J. Appl. Phys 108 (2010), 073918, 10.1063/1.3488881.

[331]. Kaddi CD, Phan JH, Wang MD, Computational nanomedicine: modeling of nanoparticle-mediated hyperthermia cancer therapy, Nanomedicine 8 (2013) 1323–1333, 10.2217/nnm.13.117. [PubMed: 23914967]

[332]. Suriyanto EYN, Kumar SD, Physical mechanism and modeling of heat generation and transfer in magnetic fluid hyperthermia through néelian and brownian relaxation: a review, Biomed. Eng. Online 16 (2017) 36, 10.1186/s12938-017-0327-x. [PubMed: 28335790]

[333]. Surry KJM, Austin HJB, Fenster A, Peters TM, Poly(vinyl alcohol) cryogel phantoms for use in ultrasound and MR imaging, Phys. Med. Biol 49 (2004) 5529–5546, 10.1088/0031-9155/49/24/009. [PubMed: 15724540]

[334]. Lazebnik M, Madsen EL, Frank GR, Hagness SC, Tissue-mimicking phantom materials for narrowband and ultrawideband microwave applications, Phys. Med. Biol 50 (2005) 4245–4258, 10.1088/0031-9155/50/18/001. [PubMed: 16148391]

[335]. Divkovic GW, Liebler M, Braun K, Dreyer T, Huber PE, Jenne JW, Thermal properties and changes of acoustic parameters in an egg white phantom during heating and coagulation by high intensity focused ultrasound, Ultrasound Med. Biol 33 (2007) 981–986, 10.1016/j.ultrasmedbio. 2006.11.021. [PubMed: 17434665]

[336]. Yella A, Li BQ, Mohanty P, Liu C, Measurement of temperature distribution and evolution during surface plasma resonance heating of gold nanoshells-embedded phantom tissue, Exp. Therm. Fluid Sci 47 (2013) 34–39, 10.1016/j.ultrasmedbio.2006.11.021.

[337]. Searles DJ, Evans DJ, The fluctuation theorem and green-kubo relations, J. Chem. Phys 112 (22) (2000) 9727–9735, 10.1063/1.481610. URL, https://doi.org/10.1063/1.481610.

[338]. Ratanapisit J, Isbister DJ, Ely J, Transport properties of fluids: Symplectic integrators and their usefulness, Fluid Phase Equilib 183–184 (07 2001) 351–361, 10.1016/S0378-3812(01)00447-2.

[339]. Henry AS, Chen G, Spectral phonon transport properties of silicon based on molecular dynamics simulations and lattice dynamics, J. Comput. Theor. Nanosci 5 (2) (2008) 141–152, 10.1166/jctn.2008.2454. URL, https://www.ingentaconnect.com/content/asp/jctn/2008/00000005/00000002/art00002.

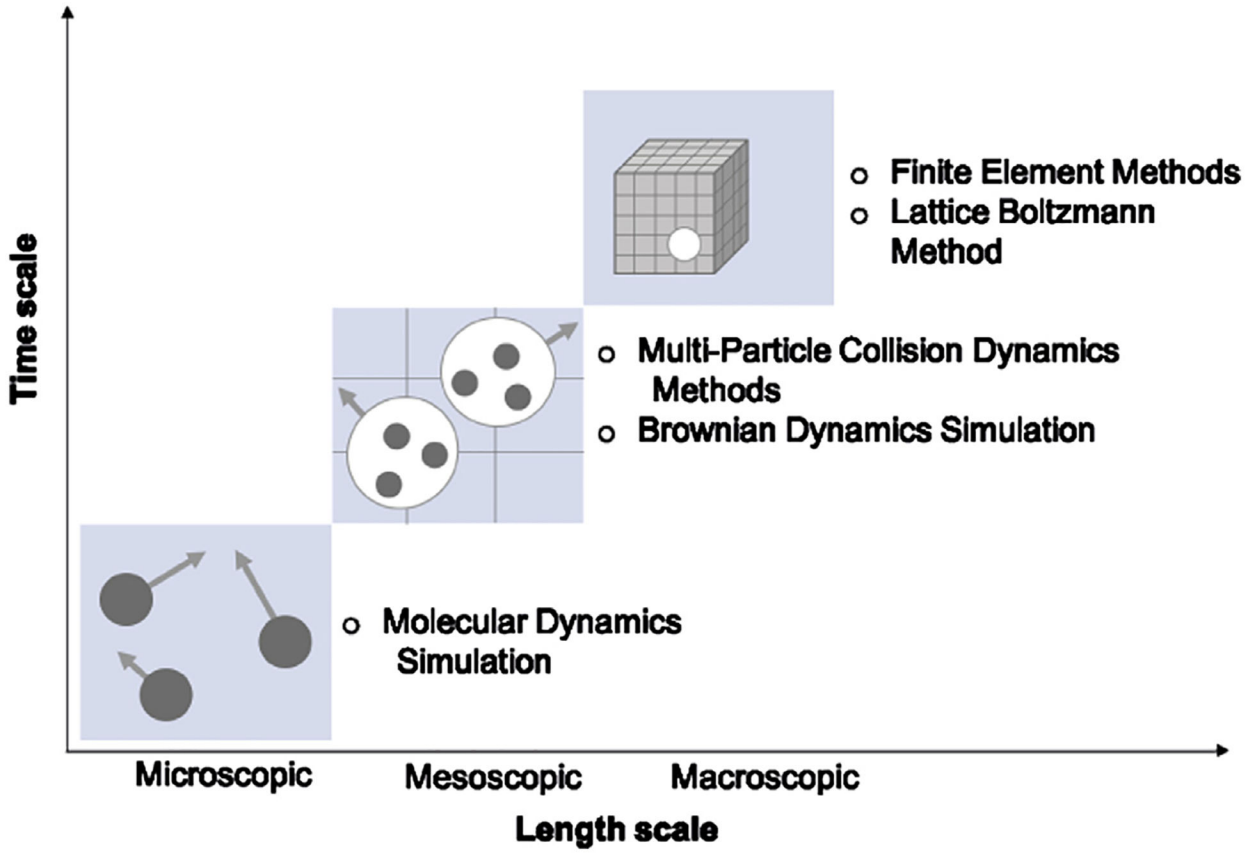


**Fig. 1.**
Computational models in micro, meso and macroscale for solution of nanofluids flows.

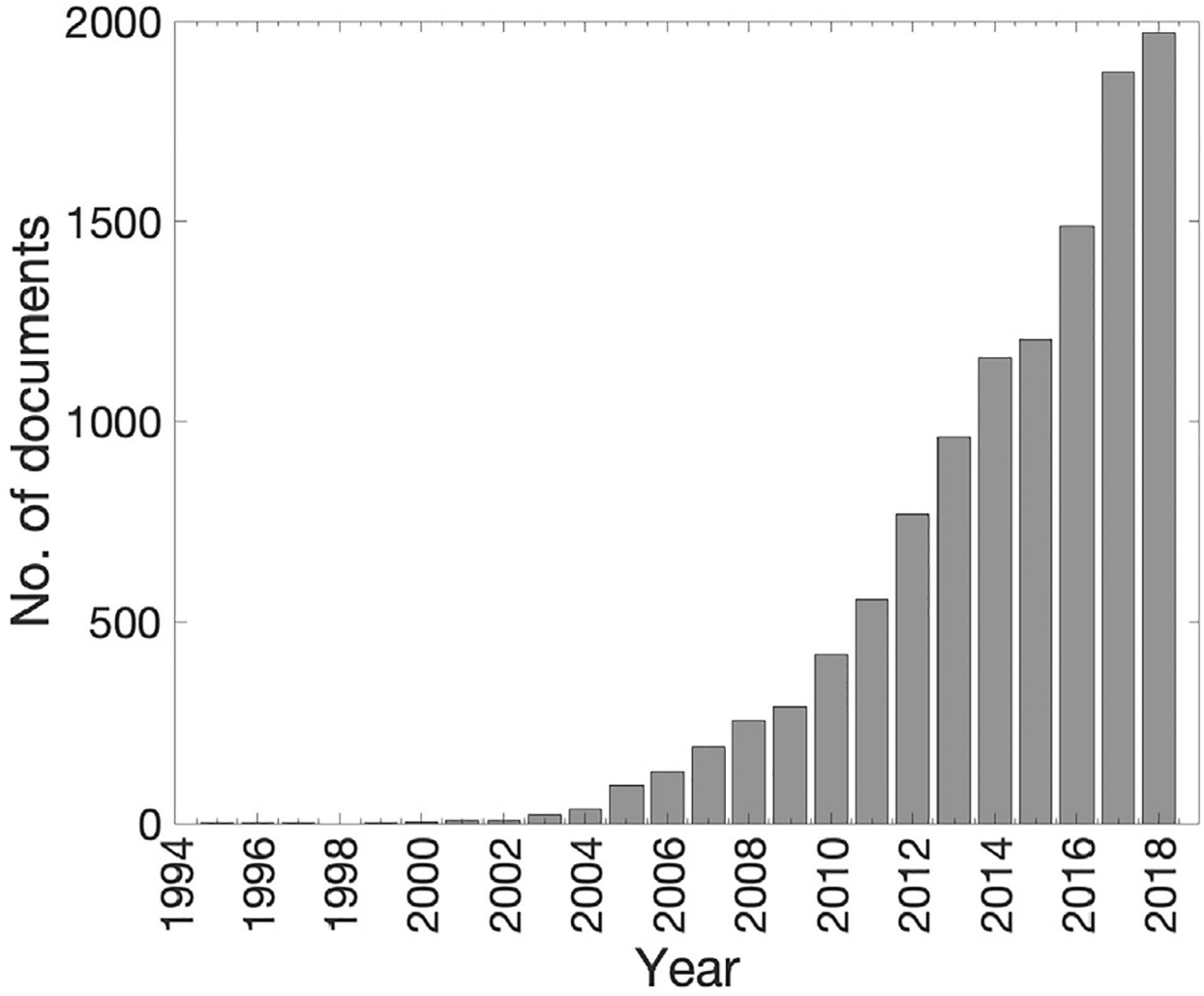


**Fig. 2.**
Annual Scopus publications on nanofluids.

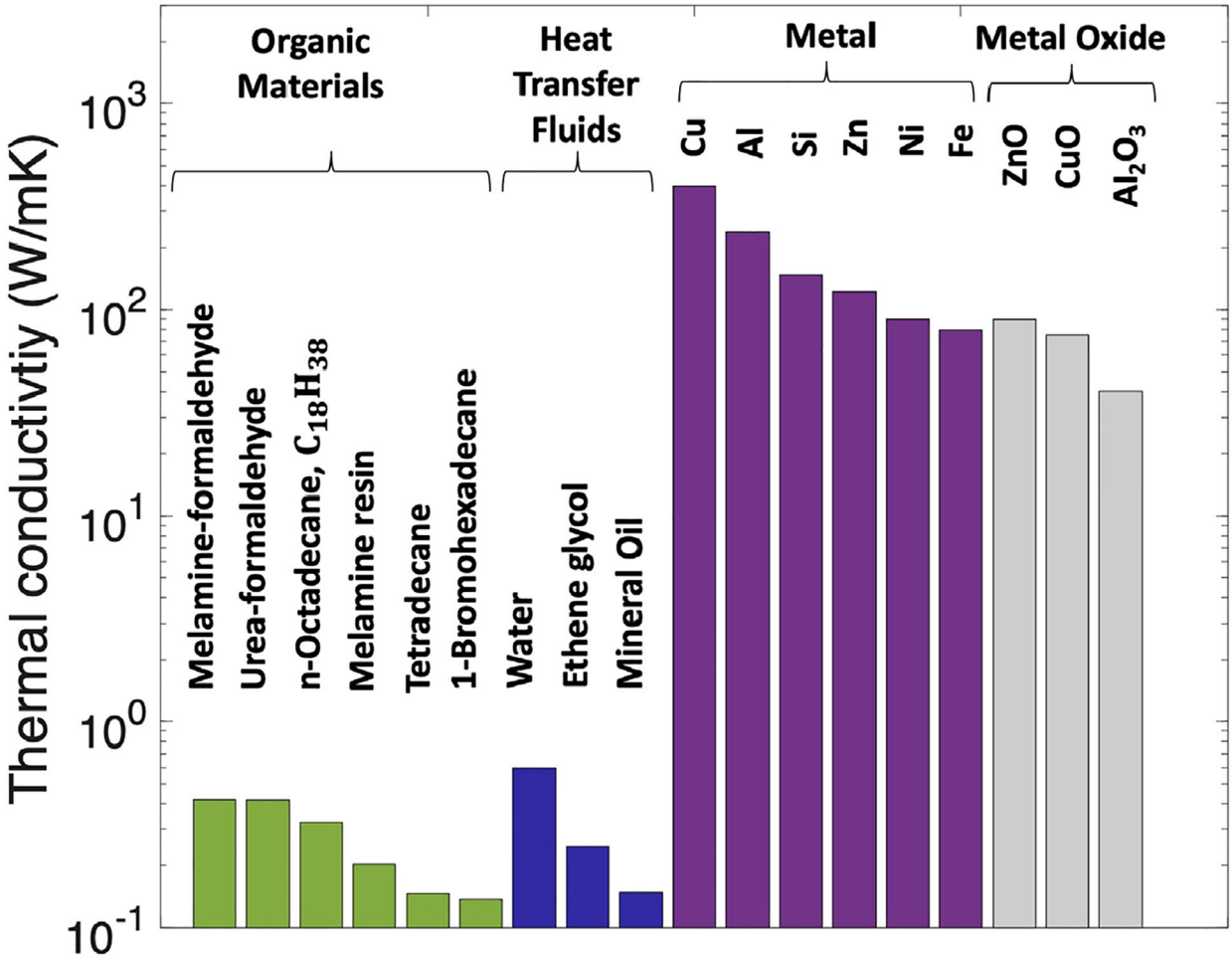


**Fig. 3.**

Thermal conductivity comparison of common polymers, liquids, and solids, redrawn from Ref. [115].

| Nanofluid | Particle size (nm) | Particle volume Fraction (%) | Viscosity enhancement (%) | Reference |
|---|---|---|---|---|
| Al2O3-DW | 28 | 1-6 | 9-86 | Wang et al [1999] |
| Al2O3-DIW | 80 | 1-5 | 4-82 | Murshed et al [2008] |
| Al2O3-Water | 13 | 1-3 | 60-300 | Pak et al [1998] |
| Al2O3-Water | 36 | 2.1-12 | 10-210 | Nguyen et al [2007], Nguyen et al [2008] |
| Al2O3-Water | 45 | 2-8 | 1-6 | Anoop et al [2009b] |
| Al2O3-Water | 150 | 2-8 | 1-3 | Anoop et al [2009] |
| Al2O3-Water | 95 | 0.5-6 | 3-77 | Anoop et al [2009] |
| Al2O3-Water | 100 | 0.5-6 | 3-57 | Anoop et al [2009a] |
| Al2O3-Water | 43 | 1-5 | 14-136 | Chandrasekar et al [2010] |
| Al2O3-EG | 28 | 1.2-3.5 | 7-39 | Wang et al [1999] |
| Al2O3-EG | 100 | 0.5-6 | 5.5-30 | Anoop et al [2009a] |
| Al2O3-PG | 27 | 0.5-3 | 7-29 | Prasher et al [2006d] |
| Al2O3-PG | 40 | 0.5-3 | 6-36 | Prasher et al [2006d] |
| CuO-EG | 152 | 0.5-6 | 8-32 | Anoop et al [2009a] |
| TiO2-Water | 27 | 1-43 | 11-60 | Masuda et al [1993] |
| TiO2-Water | 25 | 0.25-1.2 | 3-11 | Chen et al [2009b] |
| TiO2-Water | 21 | 0.2-2 | 4-15 | Duangthongsuk et al [2009] |
| TiO2-DW | 15 | 1-5 | 24-86 | Masuda et al [1993] |
| TiO2-DW | 95, 145, 210 | 0.024-1.18 | 4-11 | He et al [2007] |
| TiO2-DW | 21 | 0.2-3 | 4-135 | Turgut et al [2009] |
| CuO-water | 23-37 | 1-10 | 0.5-11.5 | Pastoriza-Gallego et al [2011a] |
| CuO-water | 11±3 | 1-10 | 2.5-73 | Pastoriza-Gallego et al [2011a] |
| Cu-EG | 200 | 0.4-2 | 5-24 | Garg et al [2008] |
| CaCO3-DW | 20-50 | 0.12-4.22 | 1-69 | Zhu et al [2010] |
| SiO2-Ethanol | 35 | 1.2-5 | 15-95 | Chevalier et al [2007] |
| SiO2-Ethanol | 94 | 1.4-7 | 12-85 | Chevalier et al [2007] |
| SiO2-Ethanol | 190 | 1.5-6 | 5-44 | Chen et al [2009a] - Chen et al [2009b] |
| SiC-DW | <100 | 0.001-3 | 1-102 | Lee et al [2011] |

**Remarks: DW-distilled water; EG- ethylene glycol; PG- propylene glycol; DIW-deionised water**

**Fig. 4.**

Experimental measurements on the viscosity enhancement of nanofluids based on the particle volume fraction; redrawn from Ref. [224].

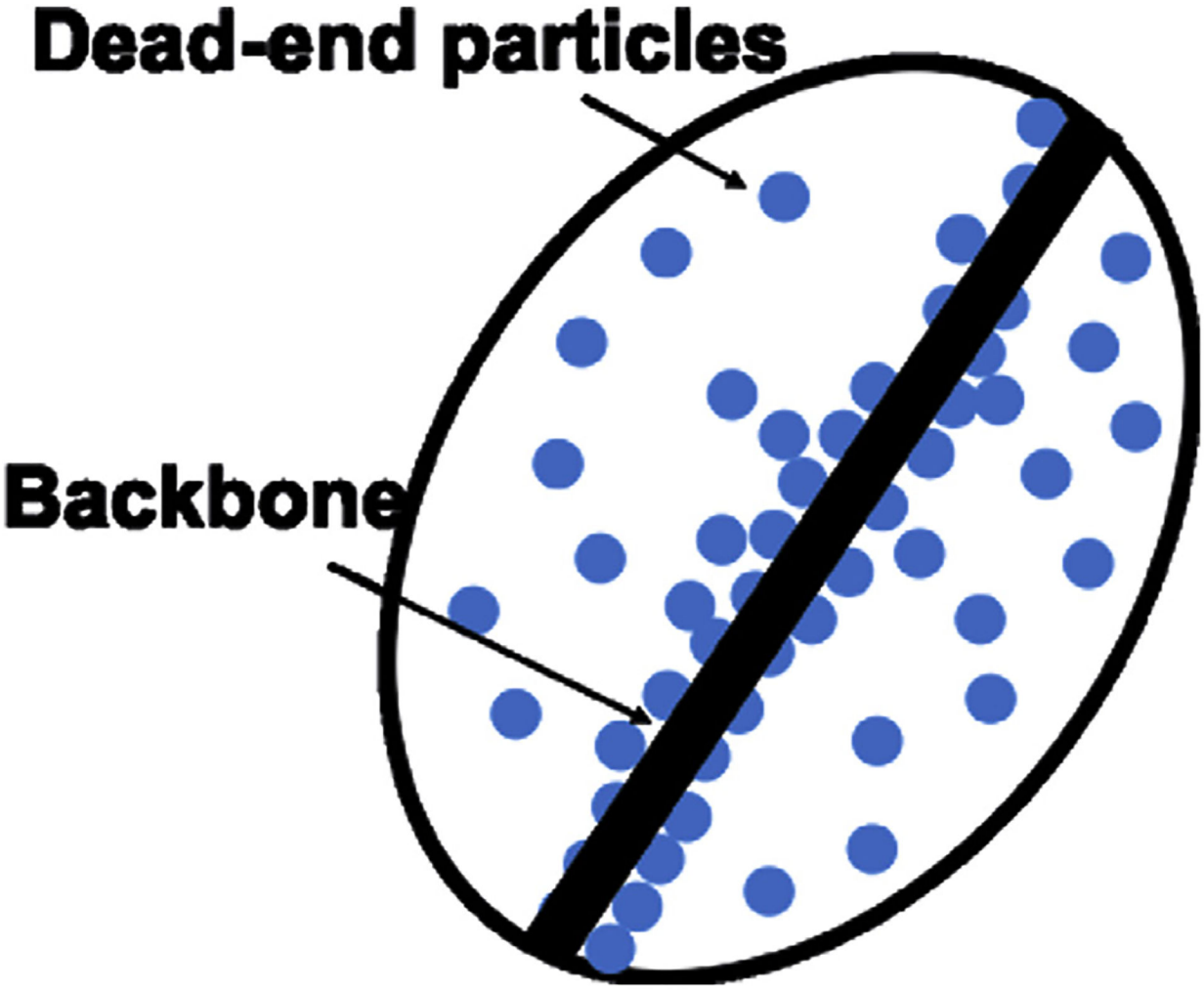


**Fig. 5.**
Schematic of aggregated nanoparticles consisting of the backbone and dead-ends with the fluid [169].

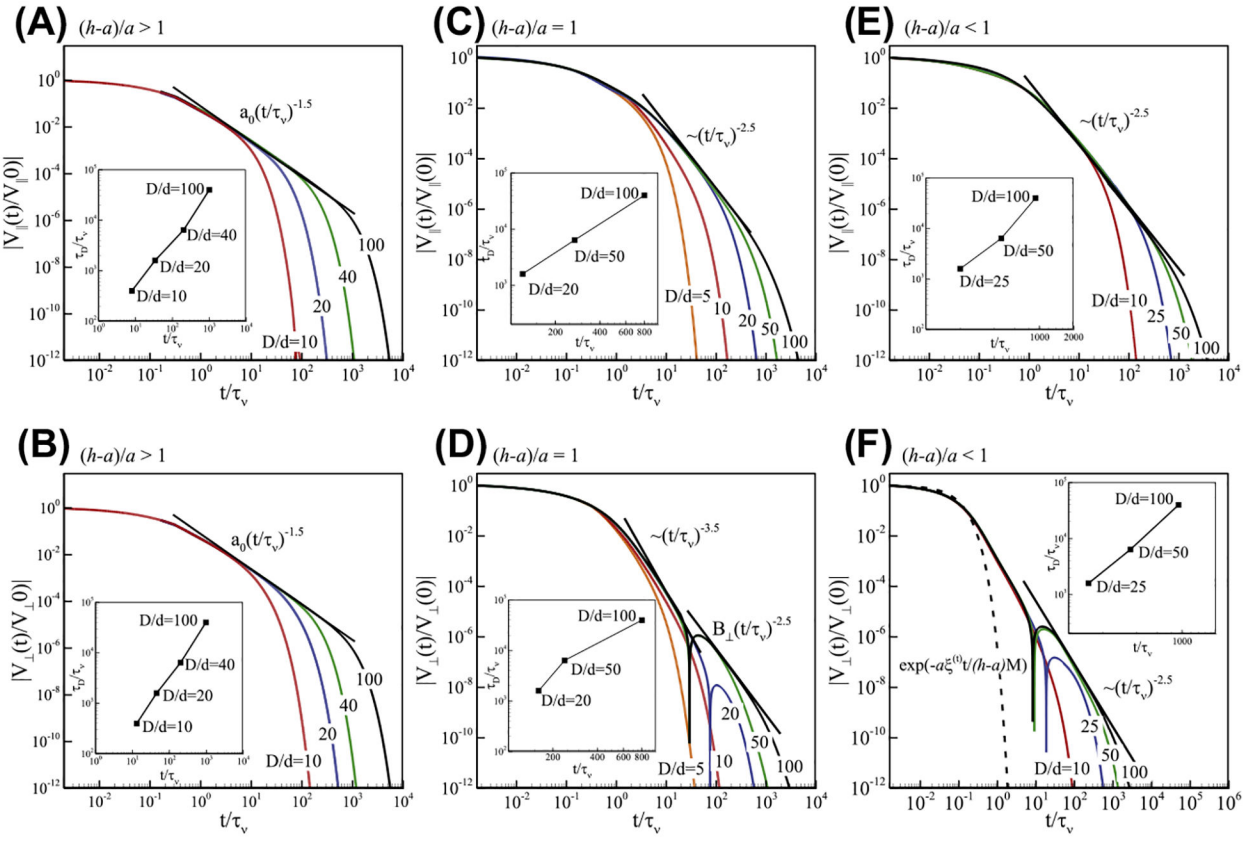


**Fig. 6.**

The effect of confinement and curvature of the cylindrical wall on the translational velocity of a 500 nm-diameter particle in a stationary fluid (calculated by the deterministic method), located in the center of the vessel with (a) parallel $(h - a)/a > 1$ (axial) and (b) perpendicular $(h - a)/a > 1$ (radial) directions; near wall in a direction (c) parallel $(h - a)/a = 1$ and (d) perpendicular $(h - a)/a = 1$ to the wall, and in the lubrication zone (e) parallel $(h - a)/a < 1$ and (f) perpendicular $(h - a)/a < 1$. (see section A1) and $B_{\perp} = \left(h^2/a^2 - 5/9\right)/4\sqrt{\pi}$. The inset in each panel shows the corresponding comparison between $\tau_D$ and the time at which the second exponential decay appears $C_1^{tr}\tau_D$. The coefficient $C_1^{tr}$ is approximately 0.025, 0.017, and 0.019 for bulk, near-wall, and lubrication regimes, respectively. These coefficients have been determined by plotting the axes in a semi-log scale and then fitting the data.

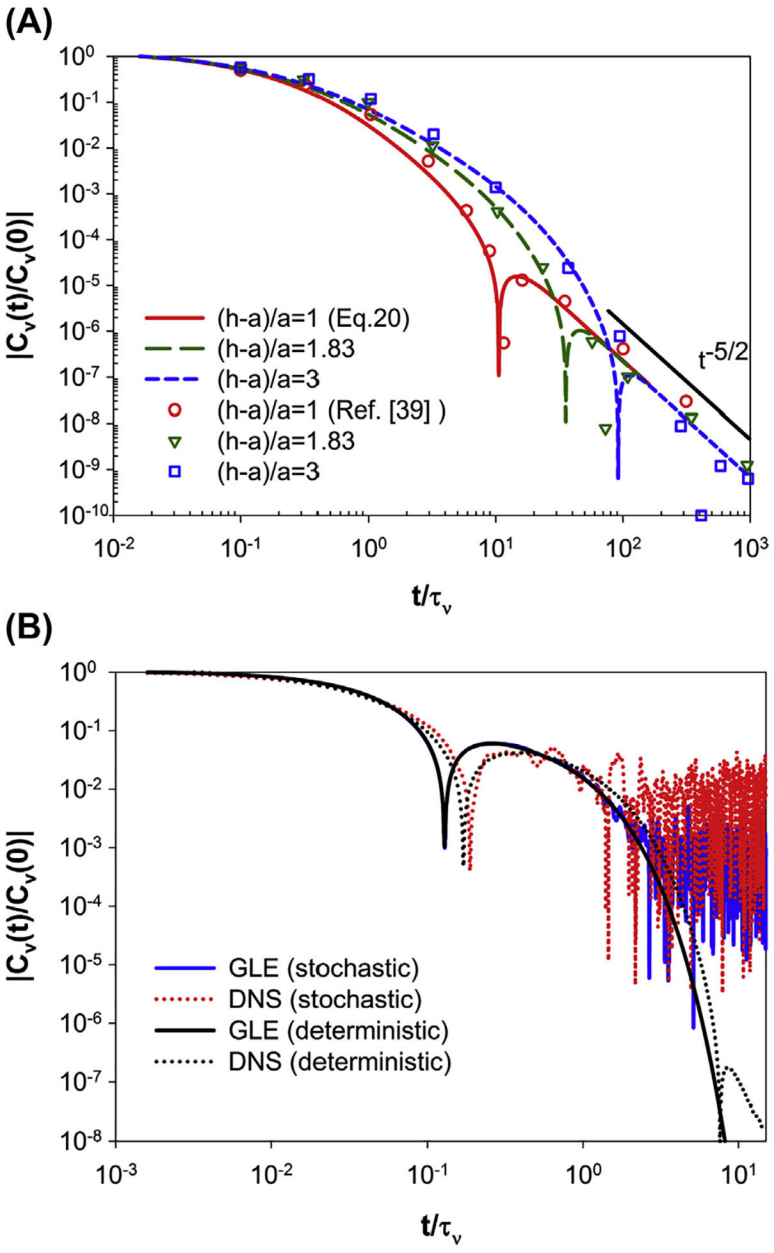


**Fig. 7.**

(A) Normalized VACF of a non-neutrally-buoyant Brownian particle near an infinite plane wall in an incompressible, quiescent fluid medium for different separations from the wall. The symbols are the corresponding results from Ref. [266] and the lines are the predictions from the composite GLE simulations reported by Ref. [283]; here $\rho_p/\rho = 2.25$ with $\rho_p$ being the density of the particle. (B) Normalized VACF of a neutrally-buoyant Brownian particle in the lubrication regime with $h/a = 1.14$ in the presence of a harmonic spring (representing strong adhesion with $k = 1$ N/m) and comparison with DNS and FHD simulations.